Addis Ababa University

Addis Ababa Institute of Technology

School of Electrical and Computer Engineering

Twisting Sliding Mode Control Design with Particle Swarm Optimization for Fixed Wing UAV

A thesis submitted to School of Graduate Studies, Addis Ababa Institute of Technology, Addis Ababa University in partial fulfillment of the requirement for the Degree of Master of Science in Electrical Engineering (Control Engineering)

By

Haileleul Biazn

Advisor

Lebsework Negash (PhD)

November 14, 2023

Addis Ababa, Ethiopia

Addis Ababa University

Addis Ababa Institute of Technology

School of Electrical and Computer Engineering

Twisting Sliding Mode Control Design with Particle Swarm Optimization for Fixed Wing UAV

By

Haileleul Biazn

Approved by Examining Board

Dean, School of Graduate Committee	Signature	Date
Dr. Bisrat Derebssa	_____	Nov 14, 2023
Advisor	Signature	Date
Dr. Lebsework Negash	_____	Nov 14, 2023
Internal Examiner	Signature	Date
Ms. Bethlehem Aberra	_____	Nov 14, 2023
External Examiner	Signature	Date
Dr. Dereje Shiferaw	_____	Nov 14, 2023

Declaration

I, the undersigned, declare that this MSc thesis is my original work, has not been presented for fulfillment of any degree in this or any other university and all sources and materials used for the thesis are acknowledged.

Author

Haileleul Biazn

Signature

_____

Place:

Addis Ababa Institute of Technology, AAiT
Addis Ababa University, AAU
Addis Ababa, Ethiopia.
Submitted by: November 14, 2023.

This thesis has been submitted for examination with my approval under university advisor Lebsework Negash (PhD).

Dedication

Dedicated to my mother, Azeneg Y. and brother Daniel for their eternal love and support, and families who back me throughout my life.

Acknowledgment

First, and foremost, praises and thanks to GOD, the Almighty, for all the showers of blessings bestowed in my life.

I would like to express my deep and sincere gratitude to my advisor, Dr. Lebsework Negash, Assistant Professor, School of Electrical and Computer Engineering, Addis Ababa Institute of Technology (AAiT), Addis Ababa University (AAU). Dr. Lebsework's unwavering support, guidance, and expertise were instrumental in the successful completion of this thesis. His dedication to my academic and professional growth, as well as his insightful feedback and encouragement, played a pivotal role in shaping the direction of my research. I am truly fortunate to have had the opportunity to work with Dr. Lebsework. I am deeply thankful for the valuable knowledge and skills I have acquired under his mentorship.

I am equally grateful and lots of thanks to whom, present themselves to hand for me throughout my journey.

Abstract

Control of fixed wing unmanned aerial vehicles (FW-UAVs) is challenging due to their highly coupled, complex, nonlinear, and uncertain mathematical model, and under-actuated dynamics. To overcome this difficulty a nonlinear robust twisting sliding mode control (SMC) was designed for inertial positions, attitudes and airspeed control to track the desired trajectories. Fuzzy based switching for inertial positions, and airspeed control was applied to overcome the trade-off between chattering and robustness. Where as, quasi-static saturation switching was used for attitude control. Particle swarm optimization (PSO) was used for optimizing the gain parameters of the designed controllers.

Different set of trajectories; bow-tie, helical, and real data minimum snap polynomial paths were prepared for guiding the FW-UAV. The required real data way-points were taken manually using 'Google Earth Pro' as latitudes and longitudes in units of degree. These data points converted into coordinates in earth-centered-earth-fixed frame, and then to the north-east down frame. Using these sample points minimum snap polynomial trajectories developed through minimizing snap as a quadratic programming. The overall mathematical model has been prepared in MATLAB Simulink for simulation.

Finally, the performance of controllers was evaluated against disturbances, model uncertainty, parameter variation, and including actuator dynamics. Integral-time-absolute-error (ITAE) has been used as performance index and in all trajectories the controllers were robust within 93% accuracy about the nominal value. The control was achieved within practically accepted ranges of control effort. Nominal deflection angles of aileron (14°), elevator (34°), and rudder (22°) were required, which are in the working ranges of practical control, unity rad. The thrust force generated by the propeller has an average value of 133 N, which is nearly equivalent to the weight of UAV, 132.5 N. The propeller engine acceleration had maximum values of 10 m/s (376 revolutions per minute) and 30 m/s (1128 revolutions per minute) in helical and level flights respectively.

Keywords: FW-UAV, coupled, twisting SMC, MATLAB Simulink, PSO, ITAE

Contents

List of Figures

List of Tables

List of Acronyms

3D three dimensional

AC actuator dynamics

ADRC active disturbance rejection control

ANFIS artificial neural fuzzy inference system

argmin argument that minimizes a function

ASTA adaptive super twisting algorithm

BF body frame

BIF body inertial Frame

COG center of gravity

DOF degree of freedom

ECEF earth centered earth fixed

FSMC fuzzy sliding mode control

FWUAV fixed wing unmanned aerial vehicle

GCS ground control station

GIF ground inertial Frame

GPS ground position system

HILS hardware in loop simulation

ID input disturbance

IF inertial frame

IMU inertial measurement unit

ITAE integral time absolute error

LQG linear quadratic Gaussian

LQR linear quadratic regulator

MDP markov decision process

MU matched uncertainity

NED north east down

NMPC nonlinear model predictive control

PID proportional integral and derivative

PSO particle swarm optimization

PV parameter variation

QP quadratic programming

RF reference frame

RMS root mean square

SF stability Frame

SMC sliding mode control

UAV unmanned aerial vehicle

vs. versus

WF wind frame

List of Symbols

$*$ - scalar multiplier from the left

$\circledast$ - matrix multiplication

$\otimes$ - vector cross product multiplier

$\downarrow$ - decrement sign

$\uparrow$ - increment sign

α - angle of attack

β - angle of side-slip

ϕ - roll angle about x-axis

θ - pitch angle about y-axis

ψ - yaw angle about z-axis

ξ - sliding surface

i^B - unit vector along x-axis in BF

j^B - unit vector along y-axis in BF

k^B - unit vector along z-axis in BF

F - force

J - moment of inertia

m - take-off mass

M - moment

g - acceleration due to gravity

p - body rate about x-axis

q - body rate about y-axis

r - body rate about z-axis

V_a - airspeed magnitude

V^T - Transpose of matrix or vector

x - inertial position along x-axis

y - inertial position along y-axis

z - inertial position along z-axis

$R_B{}^S(\alpha)$ - BF to SF rotation

$R_B{}^W(\beta, \alpha)$ - BF to WF rotation

$R_S{}^W(\beta)$ - SF to WF rotation

$R_I{}^B(\phi, \theta, \psi)$ - IF to BF rotation

$T_I{}^B(\phi, \theta)$ - rate transformation

$s_{(.)}$ - sine of the argument

$c_{(.)}$ - cosine of the argument

$t_{(.)}$ - tangent of the argument

$S_{(.)}$ - secant of the argument

Chapter 1

Introduction

1.1 General Background

Nowadays the need of unmanned aerial vehicles (UAV) for border patrolling, surveillance, searching, and rescue places, and assessing damaged areas which are too dangerous for human beings is increasing. There are different types of UAV depending on their wing construction fixed-wing, rotary-wing and hybrid each have their own field of application, [11]. Fixed wing unmanned aerial vehicles (FW-UAV) are good in longer distance flight, increased speed, larger area coverage, and or remote mapping, reduced labor cost, increased flight safety and payload capability. Fixed wing UAVs are used in high endurance flight and need advanced control systems but rotating ones are easily controlled and used for smaller flight duration.

Furthermore, there is difficulty in developing FW-UAVs model, by taking into account the real environment, and control effectively. Lots of research have been done on establishing acceptable modeling techniques and controller design for FW-UAVs. From these literatures it is evident that FW-UAVs suffer with highly coupled, nonlinear, complex, and uncertainty in model approximations to the real situations. Every complete mathematical model of the FW-UAVs is under-actuated. In most real flight situations controllers are designed based on linear, decoupled, and simple models. But due to natural complexity these methods don't perform well as expected for handling disturbed environment and uncertainties.

Fixed wing unmanned aerial vehicles can be autonomously controlled through complete analysis about guidance, trajectory development, controller design for attitude and speed tracking and stabilization, [21]. Guidance is the high level part and it is the position control of the UAV for paths or trajectory following. This level needs trajectory generation from ground position system (GPS) sensor; signal sensing, receiving, processing and sending. Guidance can be done in two methods of operation, using remote control and ground control station (GCS) systems, [30]. GCS based control uses a computer to connect the software with the UAV, which then carries out the user uploaded mission commands.

The information from various sensors installed on board of the UAV collected, and GCS monitors, control, and made decisions on the status of UAV, like current altitude, distance, map location, and actual mission status. The GPS information in UAV processed and used for identifying the desired target and path. Based on the desired trajectory the UAV can be guided with the mission planned based on the GPS and returns to the control station guided through preinstalled mission commands. In the case of remote control the guiding person involved in the overall process and it is actually applicable in small distance within line of sight.

Low level flight controllers of fixed wing unmanned aerial vehicles are traditionally designed based on the small perturbation theory, assuming that flight dynamics are linear and time invariant at many trimmed flight states, [12]. With this assumption the longitudinal and lateral motions are independent of each other. This helps the equations of motion to be able decoupled, treated independently, and controlled using linear conventional controllers around the trim points. However, the performance of these control systems deteriorates with time due to unmodelled effects of the strong inherent nonlinearities in the dynamics and coupling effects between the longitudinal and lateral motions, [12]. Then after, to overcome these problems nonlinear control methods, [21], of H-infinity, H-2 loop-shaping, adaptive, nonlinear model predictive (NMPC), [17] and sliding mode control (SMC) have been developed, [8, 11, 28].

The sliding mode control is robust in the case of fixed wing UAV control that handles system complexity which results from inherent system non-linearity especially in longi-

tudinal flight, coupling between state variables, actuator saturation, double integrator characteristics and under-actuated system, [21]. SMC is not robust against unmodelled uncertainty or no bound on the uncertainty and there exists also a problem of chattering i.e high frequency gain, so the modified higher order sliding modes, fuzzy and adaptive controllers are recommended to overcome these problems.

1.2 Statement of Problem

The application of UAVs for border patrol is becoming the norm of many nations; United States and Europeans are the main leading users in the world. In large covered areas for patrolling borders; medium and large sized fixed wing UAVs come to application for their endurance, high flight speed, and low operational cost. Autonomous control of FW-UAVs is very recursive method that comprises desired trajectory generation and controller setups for guiding the FW-UAV along the desired paths. However, their effective control in dynamic and uncertain environments remains a complex challenge.

This thesis proposes a control approach that combines twisting sliding mode control with particle swarm optimization to tackle the control challenge. The use of twisting SMC offers a robust method to handle nonlinearities and uncertainties, while PSO optimizes control parameters for enhanced performance. Hence, the proposed control is expected to deal with the nonlinear dynamics of FW-UAVs, robustness, and optimization of the control parameters.

The FW-UAV is used in patrolling borders, where some geographical lines of paths are followed. To such a highly dynamic system smooth and continuous motion is required for flight. Therefore, polynomial path planning is proposed for generating polynomial trajectories along different selected flight lines. The real data for path planning are used as GPS information and extracted from the real environment using "Google Earth Pro". The path planning is proposed to ensure precise control of FW-UAV. The FW-UAV is expected to precisely follow desired way-points for border patrolling. The thesis is expected to contribute to the advancement of FW-UAV control for capable and efficient control in various applications.

1.3 Objective of the Thesis

1.3.1 General Objective

The general objective of the thesis is to develop and evaluate a twisting sliding mode control design optimized through particle swarm optimization for enhancing the stability, robustness, and maneuverability of a fixed wing unmanned aerial vehicle.

1.3.2 Specific Objectives

The specific objective of the thesis are:

- To model mathematically a fixed wing UAV that can be used for border patrolling.
- To design twisting SMC with fuzzy switching for fixed wing UAV.
- To simulate the designed model with controllers in MATLAB Simulink.
- To validate the performance of designed controllers in the presence of actuator dynamics, external disturbances, parameter variation, and matched uncertainty.

1.4 Significance of the Thesis

FW-UAV's construction, controller design and monitoring have very detailed analysis and done in secrecy. The security behind secrecy is crucial. Therefore, the details in modeling, controlling and manufacturing FW-UAV within the country guarantee the issue of secrecy and security. In recent years, there is an increasing conflict in the border areas of Ethiopia-Sudan and Ethiopia-Eritrea and even in the regional states within the country. To control and reduce these types of security issues, FW-UAVs provide significant role in patrolling and monitoring every location on the border areas which are risky, expensive, inaccessible to patrol agents and hardly possible task.

This study adds the overall general purpose of the FW-UAV's control design that can be used for searching, observation, target identification, material delivery and emergency in rescue places. The viability of discontinuous and robust controllers makes the fixed wing unmanned aerial vehicles effort-fully available for the present and futures uses.

1.5 Methodology

The basic procedures to complete the thesis and meet specified objectives of research are shown in the following flowchart, 1.1.

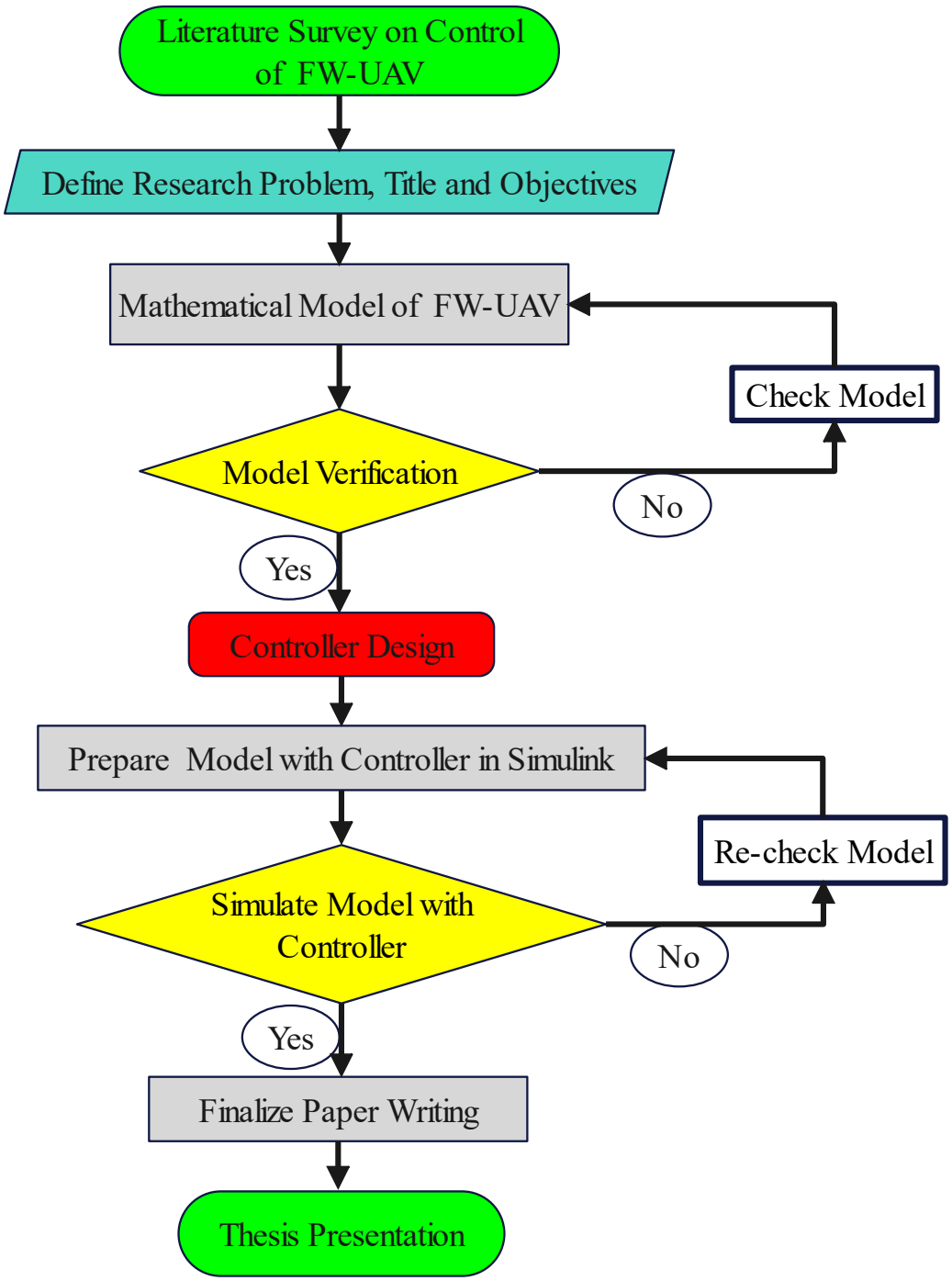

Figure 1.1: Methodology Flowchart

1.6 Scope and Limitation of Research

The thesis focuses on twisting SMC design for a FW-UAV which can be used for border patrol. The problem of trajectory generation has been approached from considering the existing GPS data. The developed system wasn't designed full autonomous, it needed higher level path planner algorithm implementation, which is one limitation to this thesis.

In this thesis modeling and controller designs were acted on simulation environment only, MATLAB Simulink to achieve desired trajectory tracking. Furthermore, even though there are lots of policies from national agents about the application and usage of UAVs in borders control, they are not discussed in this aspect; only the Engineering aspect designs are presented. The controller parameters are tuned and selected statically for each desired, and developed trajectory. For autonomous control dynamic gain scheduling is required between different flight zones, which is out of this scope.

1.7 Thesis Outline

The overall thesis research structure is organized by six chapters as follows.

Chapter 1 presents the general introduction about FW-UAV and their control system.

Chapter 2 discusses review of various research papers which were significant and used as background concepts for this research to-be done.

Chapter 3 presents the Newton-Euler modeling of fixed wing UAVs. The principles of operation of the FW-UAV is discussed with the help of state variables inertial positions, attitudes and speed using reference frames.

Chapter 4 presents the overall control scheme design using twisting sliding mode control principles. The controllers designed for positions, attitudes, and airspeed of FW-UAV. PSO algorithm is also presented thoroughly.

Chapter 5 basic principles of trajectory generation for semi-autonomous control of FW-UAV. Discusses the simulation results, trajectory tracking, and some analysis is done based on the results.

Chapter 6 conclusion is drawn from the overall analysis performed and recommendation for future work are presented.

Chapter 2

Literature Review

In this thesis the border patrolling FW-UAV modeling and control is discussed. Border patrol is the act of controlling the terrorists, weapons, and illegal immigrants entering and or leaving the borders of the country. This task is the most challenging problem, due to different reasons. Countries with hundreds of kilometer border have difficulties to allocate board patrolling units for a complete 24/7 surveillance. The application of FW-UAVs for this purpose have been the focus of many researches in the past recent years, [6, 30]. UAVs are used in border control by a number of nations with differing motives, based on their national security, policy, and government issues and agendas.

The use of FW-UAVs in border areas has particular risks as it can be seen in many research findings. There is the risk of using FW-UAVs for surveillance of the wider population which isn't just the geographically-defined border itself that may affect the privacy of individuals. The use of UAV primarily for military technology can make dehumanization of those attempting to cross borders, and information from unrelated surveillance activities is passed on to border control. UAV deployment in a zone of border tensions between two nations results a blurring between military roles leading tension, [6]. So the use of these FW-UAVs must be in the way that they have to align with the basics of accepting these national issues.

The ability of FW-UAVs to provide surveillance for extended periods, monitor remote and inaccessible areas, and relative ease of deployment makes them attractive tools for agencies responsible for border control.

2.1 Fixed Wing UAVs and Border Patrolling

Among the different UAV types the fixed wing unmanned aerial vehicles are highly used in long flight applications due to the increased flight speed, high load capacity, high range of flight areas, endurance, reduced noise, reduced labor work and reduced operating cost.

Border control is effectively done by guiding the UAV about some specified paths. The specified path generation depends on the border line of the country. A border is a thin line on a map which precisely defines the territory of a state, for security purposes its definition is much more complex. Government agencies have sweeping powers to enforce border security across the whole nation in terms of tackling border crime, identifying irregular migrants, and imposing security requirements upon travelers and goods crossing borders, [6]. The purpose of the path generation is to develop trajectories that best close the look alike of the border. Therefore, FW-UAVs can be guided along the predefined border lines as a trajectory tracking for patrolling that specified border line.

2.2 Fixed Wing UAV Control Problem

Control of fixed wing unmanned aerial vehicles is very difficult due to complexity of the model. The complex model results from the multiple state variables which are coupled, nonlinear, under-actuated, complex nature of system development, and description. Different control methods have been under research from the conventional to robust for many years, discussed in the following sections.

The model of fixed wing UAV brought in two forms, linear vs. nonlinear for controller design. The linearized models around the trim points of equilibrium are used for controller designs of proportional integral and derivative (PID), linear quadratic regulator (LQR), linear quadratic Gaussian (LQG), and H-infinity. Nonlinear model based controllers; sliding mode (SMC), artificial neural with fuzzy inference system (ANFIS), nonlinear model predictive (NMPC), artificial neural network and others are better than the linear classes of controllers interms of robustness, speed of response, and handling model uncertainty.

2.2.1 Conventional Controllers for Fixed Wing UAV

Conventional controllers are proportional, integral, derivative and the combination of these three controllers. Controller which has fast response with reduced overshoot and steady state error is good for FW-UAV control.

In 2019, a research entitled "control of longitudinal flight dynamics of a FW-UAV using linear quadratic regulator, linear quadratic Gaussian and nonlinear control" was under study, [15]. Comparative study between the three controllers for pitch control of Ultra-Stick 25e FW-UAV was done. LQG controller shows good disturbance rejection ability and the FW-UAV moves smoothly and responds faster than LQR controller without disturbance. Ordinary differential equations method of nonlinear controller shows faster response, smooth, more stable, reliable and more robust than the LQR and LQG. In this paper only pitch control was developed for small sized FW-UAV. They weren't able to fully control the other state variables.

Amber Israr et al. (2021), proposed guidance, navigation, and neural network based PID control for a FW-UAV, [16]. The researchers designed PID control which allows to enable feedback and use control action for fixed wing aircraft that has the abilities of both vertical take-off. They have developed a prototype of aircraft. They were able to design controller for attitude, speed, altitude, turn, and take-off using the mathematical model and a GPS module.

2.2.2 Adaptive Controllers for Fixed Wing UAV

Adaptive controller design methods extract knowledge of the plant parameters online and redesigns the control law in repetitive manner. This method doesn't need a priori information about the bounds on the uncertain and or time-varying parameters.

Herman Castañeda et al. (2013), proposed adaptive super twisting observer based flight control of inertial attitude and estimated airspeed for a FW-UAV (B-25 Mitchell), [8]. The performance of the adaptive super-twisting sliding mode (ASTA) controller compared with the active disturbance rejection control (ADRC) incorporated with a PID. The results showed that the ASTA results less tracking error in all control problems in

the presence of noisy measurements, uncertainties and external perturbations, seen from the graphical plot of trajectory tracking.

Yang Han et al. (2019), proposed a non-decoupled back stepping control for FW-UAV (B-25 Mitchell) with multi variable fixed time sliding mode disturbance observer, [12]. The paper addressed the issue of controlling the attitude together with the airspeed of FW-UAV in a vector manner. They were able to estimate the disturbances in very close approximation to the real. They assured stability of the full closed loop system and a multi variable is incorporated at the design stages of both observer and back-stepping to provide a more elegant solution.

Yeonsik Kang et al. (2009) designed a nonlinear model predictive control (NMPC) to a small FW-UAV for linear tracking, [17]. The online (steepest descent method) and offline optimal problems were successfully solved and the real implementation of the designed model tested. The controller was tested through hardware in the loop simulations (HILSs) in-order to see NMPC algorithm performance in real-time on a real UAV system. They have checked the controller against different trajectories; linear and square desired paths in HILS. Tracking best seen in the linear path and the square path tracking gives emphasis on the possibility of using NMPC for multiple line segment following tasks.

2.2.3 Robust Controllers for Fixed Wing UAV

Robust control is an approach for controller design that explicitly deals with uncertainty. Robust controllers are designed to function properly provided that uncertain parameters or disturbances are found within some set i.e control law need not be changed. FW-UAVs are highly affected by input and output disturbances due to wind, aerodynamics and model uncertainty during the process of mathematical modeling. To overcome these types of problems the need of robust controllers for fixed wing unmanned aerial vehicles have been the focus of many researchers, discussed in the following sections.

Yufei Guo et al. (2022), suggested a combination of three adaptive, fuzzy and sliding mode controllers to stabilize and control a FW-UAV, [11]. They were able to control the five state variables, attitudes, altitude and airspeed based on the decoupled state

space models. The developed algorithm shows better performances like fast response speed, small steady-state error, and strong robustness compared to the traditional sliding mode control. But during decoupling the model, they have taken external sinusoidal disturbances of known magnitude in place of matched uncertainties, which isn't justified properly how it's determined. Traditional SMC shows faster response in the absence of model uncertainties and this isn't also explained with proper reasoning.

Abid Raza et al. (2017), designed sampled data sliding mode control of FW-UAV for altitude, yaw and roll angle control, [25]. They designed sampled data SMC based on continuous and discrete time system and super twisting algorithm based on continuous time model. The speed of response and robustness to wind gust increases as we go from sampled data SMC on continuous model (5 seconds) to sampled data super twisting SMC on continuous model (4 seconds) and discrete data SMC on discrete model (3 seconds).

Andra Saicharan et al. (2016), have designed a method for controlling the attitude of a fixed wing aircraft in the presence of uncertainties, [28]. They have proposed inertial delay controller in the framework of multiple sliding surfaces. The effectiveness of proposed algorithm and robustness was checked with half of parametric uncertainty and sinusoidal disturbances in simulation. It has been able to track the desired angles (within 0.5 seconds) and mitigate the effects of uncertainty but there was no aerodynamic analysis for the coefficients and adverse disturbance effects.

Yu-Xin Zhao et al. (2013), designed a second order sliding mode controller for spacecraft, [34]. They have designed exponential second order sliding mode controller for decoupled attitude control. Tracking was achieved for constant reference attitudes (within 6 seconds) with sinusoidal external disturbance taken as the coupling within the model. They lacked testing the controller against internal matched uncertainty and parameter variation for robustness.

Myung Hwangbo et al. (2013), tried to address the problem of achieving autonomous navigation of a small fixed-wing UAV (SuperCub) using low-cost sensors GPS, IMU and camera, [14]. The authors claimed level flight, constant altitude turn and turn with a constant climb rate as the three primitive motions used to formulate the planning problem with a Markov Decision Process (MDP) based on the three factors; an uncertainty

motion model using probability distributions, efficient discretization of the state space, and infinite horizon. Desired attitudes provided by MDP planner. Altitude tracking and trajectory completion done within a range of 15 meters, which is the application of small FW-UAV.

Dynamic modeling of a lightweight model airplane (FW-UAV) using the Lagrange-Euler formalism presented in [23]. The derived model of the aircraft is used for system analysis, control-law design and simulation. They have tried to show the open-loop responses as model verification for further analysis.

According to the existing research, for this type of complex nonlinear FW-UAV model, sliding mode control is becoming a more popular control method. However, there are two main problems to overcome when using the SMC method to control FW-UAV. The first problem is dealing the effects of unknown internal and external disturbances on the system, which can be solved using adaptive and SMC control respectively. The second problem is the chattering and it can be solved through the fuzzy, and twisting SMC, [11]. Therefore, fuzzy twisting SMC is developed for seven state control of FW-UAV that handles both disturbance and chattering.

Chapter 3

Fixed Wing UAV Modeling

3.1 Working Principle

Fixed-wing UAVs are capable of controlling and make use of air for generating forces that allow them to stay in the air by taking advantage of their aerodynamics. The high fluid pressure difference between the bottom and top of the wing foils and the propeller itself is used to generate an upward force also called a lift for flight. This force is responsible for lifting the weight of fixed wing UAV. The level of this lift force depends on the angle of inclination of the aero-foil and or propeller.

Fixed wing UAVs configuration depends on the application area of desire, i.e the dimensions, aerodynamics, propulsion system and controls, are very different from one model to another. Irrespective of their difference in design all of them have similar principle of flight. UAVs are classified based on different standards by different agencies. They are classified by size (length, mass, wing span), wing type, range of flight distance, payload capacity and endurance.

UAVs classified as in table 3.1 based on the range of flight distance and time. From the classification high endurance FW-UAV types of long range are more of efficient in border patrolling purposes. So the developed models simulated using Aerosonde, a kind of UAV with an ability to fly in the long distance over 30 hours.

Aerosonde UAV has well known properties and open loop dynamics which is used in most literatures to test fixed wing UAV control performances. It has wing span of 2.8956

meters and can fly at a maximum speed of 40 m/sec. It's dimension able for flying for longer ranges and can be used for patrolling large sized areas like borders, river basin surveillance and material delivery for long rural areas. It can take-off way with a car-roof-rack method and has ability to land on its belly. It can operate autonomously and navigate through GPS. It can fly about 150 kilometers under UHF radio communication with the ground stationed control.

Table 3.1: Classification of UAVs Based on Range, [22]

UAV Range	**Distance(km)**	**Time(hr)**	**Application**
Very close	5	1	Recreation
Close	5 - 50	1-6	Surveillance, Photography
Short	50 - 150	8-12	Utility inspection
Mid	644	24	Military combat
Long	≥644	≥24	Military surveillance, mapping

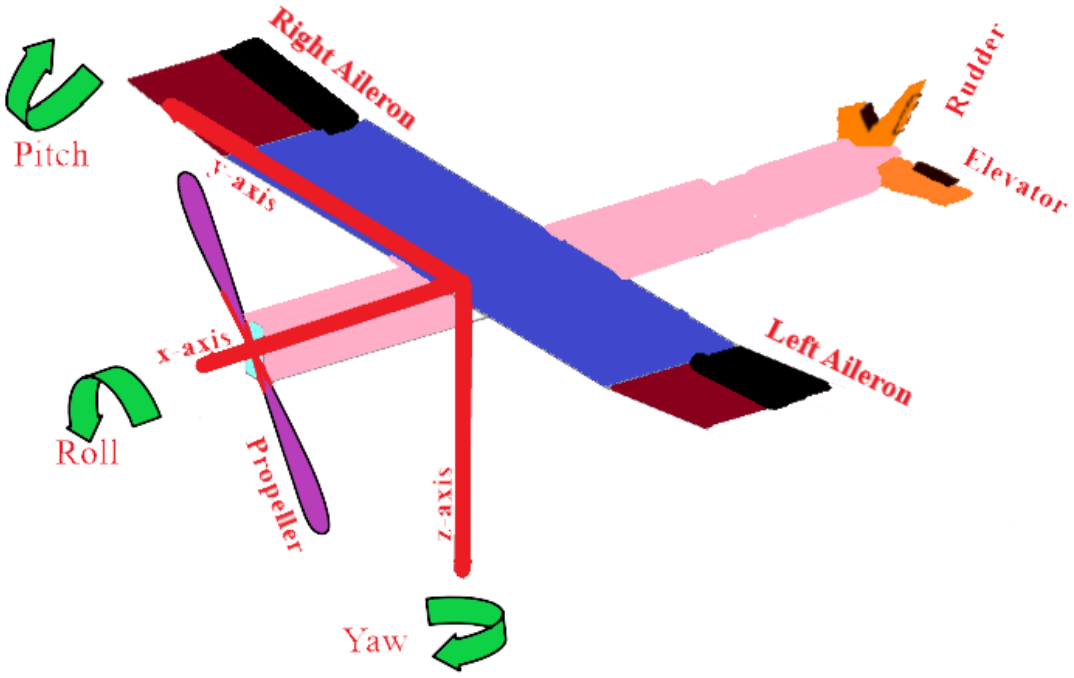

Figure 3.1: FW-UAV Structural Setup

3.2 FW-UAV Modeling

In any engineering, physical systems are modelled and analysed for control system design, verification, simulation and validation in the working environment before their real implementation. Any plant needs its model to be developed for control system design and development. In control engineering, mathematical modeling can be in the form of differential equation, transfer function or state space.

Mathematical models are expected to resemble the actual plants (physical system) in their behavior and operation. Models of FW-UAVs highly rely on the physical system, their working area and purpose. In this thesis, a more conventional mathematical modeling for FW-UAV called state-space is developed and presented in the following sections. In literature, there are two types of modeling approaches; Quaternion and Newton-Euler. However, Newton-Euler is approached to derive the equations of motion that describe the dynamics of the FW-UAV.

Modeling assumptions are made based on some reference existing plants, and listed across different literatures for model simplification of FW-UAV. Assumptions are taken carefully and necessarily from literature, [21, 23], not to miss any significant characteristics of the FW-UAV.

- The earth is considered fixed and flat in space.
- The FW-UAV structure is assumed rigid and symmetric about the (x-z) plane.
- The mass of the FW-UAV body assumed to be constant (time-invariant).
- Center of mass and the body frame origins coincide.
- Drag force of the fuselage is neglected.
- The propeller of the FW-UAV assumed to be rigid.
- The wind speed included in the kinematics.

3.3 Reference Frames

In order to study about the kinematics, dynamics and aerodynamics of FW-UAV in different flight regions, coordinate frames rigidly attached to each point, and then the geometric relationships between these coordinate frames is specified. The understanding of reference frames helps to describe the full degree of equation of motion in FW-UAV control and analysis. Almost all FW-UAV motions described and defined using five reference frames namely; ground inertial frame (GIF), body inertial frame (BIF), body frame (BF), stability frame (SF) and wind frame (WF).

In defining these reference frames two center of points are used; center of mass and gravity. Center of mass is the point at which the distribution of mass is equal in all directions and does not depend on gravitational field. Center of gravity is the point at which the distribution of weight is equal in all directions, depends on gravitational field.

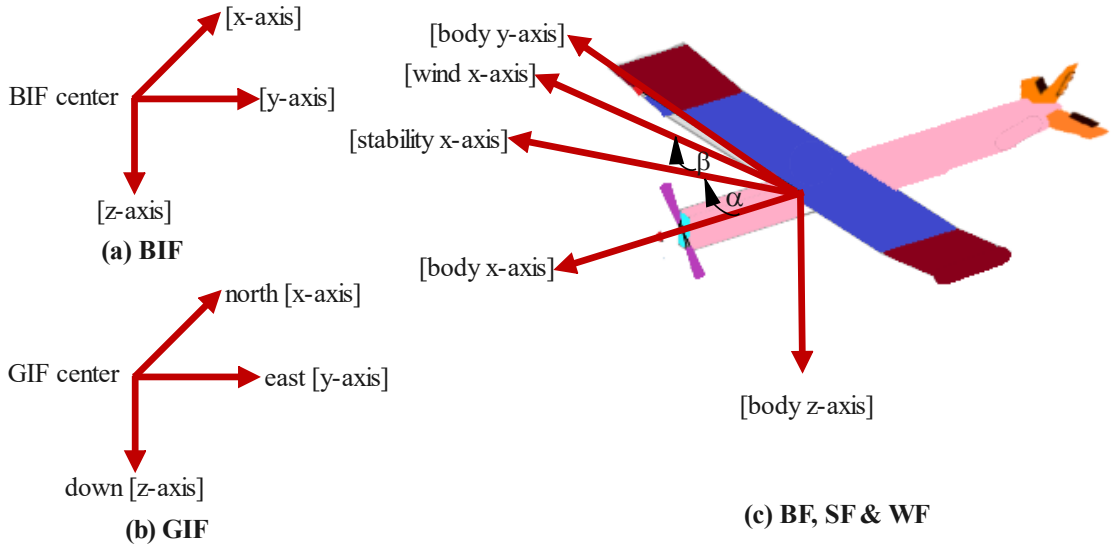

Figure 3.2: Definition of Reference Frames

3.3.1 Ground Inertial Frame (GIF)

It's defined with the origin at takeoff point of the UAV (earth centered), x_G-axis points due north from the origin, and y_G-axis points due east from the origin, see fig 3.2, mostly known as North-East-Down (NED) frame. It doesn't involve acceleration with respect to the earth and Newton's first law of motion applied for system analysis. The inertial positions of x, y, and z are described with this reference frame.

3.3.2 Body Inertial Frame (BIF)

BIF is defined with the origin at center of mass of the UAV and axes (x_I,y_I,z_I) are parallel to the GIF, fig 3.2. System of 3D lines attached to the center of mass of a FW-UAV that are used to describe the relative linear and angular velocities of FW-UAV.

3.3.3 Body Frame (BF)

This frame is defined with the origin at UAV's center of mass, x_B-axis pointing to the nose from the origin, y_B-axis pointing out from the origin towards right wing and z_B-axis out to the abdomen of UAV body. It's always attached to a moving aircraft, see fig 3.2.

3.3.4 Stability Frame (SF)

The origin is at UAV's center of mass, x_S-axis points from the origin to the direction of projection of the UAV motion direction in the longitudinal plane of symmetry, and z_S-axis points to the right wing from the origin, see fig 3.2.

3.3.5 Airflow (Wind) Frame (WF)

It's origin is at center of gravity of the UAV, x_A-axis points from the origin to the direction in which the UAV is moving, and z_A-axis points downward vertically with x_A-axis in the longitudinal symmetry plane of UAV, fig 3.2.

3.3.6 Why Different Reference Frames

- Newton's equations of motion are derived relative to IRF, and used for model dev't.
- Aerodynamic forces and moments act on FW-UAV body and described in a BF.
- GPS information (position, ground speed and course angle), flight trajectories and map information are given in an IF.
- IMU, accelerometers and rate gyros measure information with respect to BF and control surface deflections and thrust are manipulated on BF.

3.4 Coordinate Transformation

Coordinate transformation is defined as the introduction of a new set of mathematical coordinates which are distinctly stated functions of the original coordinates of the FW-UAV position and orientation. It gives the capability to move position information from one coordinate reference system to another. Different set of variables are transformed from one coordinate frame to another through two basic operations: rotation and translation. There are two types, methods of coordinate transformation from literature [4], namely Euler, and Quaternion. In this research only the Euler approach technique is used and adopted.

3.4.1 Rotational Transformations

Euler states that "any rotation can be described by three successive rotations about linearly independent primary axes". Euler uses three rotation angles: roll (ϕ), pitch (θ), and yaw (ψ) to describe orientation in 3D space about x-y-z axes respectively. There are 12 possible combination of rotation sequences and the yaw-pitch-roll angle combinations is adopted in this thesis for rotation matrix development.

Rotation matrices give description of frame orientation, which are characterized by nine elements which are not independent but related by six constraints due to the orthogonality conditions.This leads to three independent parameters are sufficient to describe orientation of a rigid body in space, minimal representation.

Let's consider the rotation matrix expressing the elementary rotation about one of the coordinate axes as a function of a single angle and then, a generic rotation matrix can be obtained by composing a suitable sequence of three elementary rotations while guaranteeing that two successive rotations are not made about parallel axes.

Using Euler's principle starting from the inertial frame we can end-up on another frame through the different rotation sequences. Let's start with the ground inertial frame of reference and pass through body, stability and wind frames in sequences for complete kinematic and dynamic model development of the FW-UAV.

3.4.2 Inertial to Body Frame Rotation

The angles about axes z-y-x defined as yaw-pitch-roll to denote the typical changes of attitude of FW-UAV, respectively. The rotation from GIF to BIF computed in the following sequences. First, rotate right-handed about z-axis through angle ψ to go to intermediate RF (x_1, y_1, z_1), with rotation matrix $R(\psi)$. Secondly, take right-handed rotation about y-axis by angle θ to move to the intermediate RF (x_2, y_2, z_2), gives rotation matrix $R(\theta)$. Finally, right-handed rotation about x-axis through angle ϕ results RF (x, y, z), with the rotation matrix $R(\phi)$, illustrated in appendix B with fig. B.1.

The overall rotation matrix expressed as the product of these three rotation matrices in respective sequences because Euler angles preserve linearity in three independent axes.

$$R_I{}^B(\phi,\theta,\psi) = R(\phi) \circledast R(\theta) \circledast R(\psi) \quad = \begin{pmatrix} c_\psi c_\theta & s_\psi c_\theta & -s_\theta \\ c_\psi s_\theta s_\phi - s_\psi c_\phi & s_\psi s_\theta s_\phi + c_\psi c_\phi & c_\theta s_\phi \\ c_\psi s_\theta c_\phi + s_\psi s_\phi & s_\psi s_\theta c_\phi - c_\psi s_\phi & c_\theta c_\phi \end{pmatrix} \tag{3.1}$$

3.4.3 Body to Stability Frame Rotation

The fixed wing UAV fly in the forward direction with a velocity, V_a with respect to the surrounding air. The UAV moves by generating the lift force and making pitching up by an angle of attack, α from the (x, z)-plane, which leads that the UAV leaves its previous stable region and goes to the new body frame region. So the stability frame is found through the left hand rotation of body frame by angle α about the (x, z)-plane or y-axis.

$$R_B{}^S(\alpha) = \begin{pmatrix} c_\alpha & 0 & s_\alpha \\ 0 & 1 & 0 \\ -s_\alpha & 0 & c_\alpha \end{pmatrix} \tag{3.2}$$

The rotation matrix $R_B{}^S(\alpha)$ is used for transforming vectors from the body to stability frame; whereas the inverse transformation matrix is just the transpose of $R_B{}^S(\alpha)$. This is proved by multiplying the matrix with it's transpose resulting an identity matrix.

3.4.4 Stability to Wind Frame Rotation

As the aircraft flies it leaves it's stable region of motion the (x, z) plane by angle of slide say β in the z - direction due to wind disturbance, so the wind frame can be found through right-handed transformation of the stable frame in z - axis.

$$R_S{}^W(\beta) = \begin{pmatrix} c_\beta & s_\beta & 0 \\ -s_\beta & c_\beta & 0 \\ 0 & 0 & 1 \end{pmatrix} \tag{3.3}$$

The total transformation from the body frame to the wind frame is calculated through multiplying the rotation matrices i.e $R_B{}^W = R_S{}^W \circledast R_B{}^S$.

$$R_B{}^W(\beta, \alpha) = \begin{pmatrix} c_\beta c_\alpha & s_\beta & c_\beta s_\alpha \\ -s_\beta c_\alpha & c_\beta & -s_\beta s_\alpha \\ -s_\alpha & 0 & c_\alpha \end{pmatrix} \tag{3.4}$$

3.4.5 Rotation Sequence Between Angular Velocities

In this section the transformation matrix between body angular rates (p, q, r) and Euler rates ($\dot{\phi}$, $\dot{\theta}$, $\dot{\psi}$) is developed, because Euler rates are defined in their respective axes, not on specified frame. In transforming we need the following sequences;

1. $\dot{\phi}$ directly transformed to p because both are defined in the same frame, BF.
2. $\dot{\theta}$ transformed to q proceeded by rotation about x-axis, R_ϕ.
3. $\dot{\psi}$ transformed to r proceeded by rotation about x, and y -axis, $R_\phi R_\theta$.

The matrix that transforms Euler rates to body rates can be denoted with $T_I{}^B(\phi, \theta)$ and expressed by equ. 3.5 with it's inverse given in B.4, see the derivation in appendix B.

$$T_I{}^B(\phi, \theta) = \begin{pmatrix} 1 & 0 & -s_\theta \\ 0 & c_\phi & s_\phi c_\theta \\ 0 & -s_\phi & c_\phi c_\theta \end{pmatrix} \tag{3.5}$$

3.5 FW-UAV Mathematical Modeling

Mathematical model of FW-UAV is analysed and developed in two ways namely the kinematics and dynamics.

3.5.1 FW-UAV Kinematics

Kinematics is the description of geometric characteristics of the FW-UAV's motion specifically position, velocity, and acceleration without considering the forces and or moments that cause the motion. The state variables in this analysis are defined in different RF.

- Three linear positions (x,y,z) defined in IF.
- Three angular positions (ϕ, θ, ψ) defined in BF, intermediate1 and intermediate2 frames respectively.
- Three linear velocities (u,v,w) defined in BF.
- Three body angular rates or velocities (p,q,r) defined in BF.

Now the body frame velocities are projected onto the inertial frame by the equ. 3.6:

$$\begin{aligned} \frac{d}{dt}(x,y,z)^T &= R_B^I(\phi,\theta,\psi) \circledast (u,v,w)^T \\ \frac{d}{dt}(\phi,\theta,\psi)^T &= T_B{}^I(\phi,\theta) \circledast (p,q,r)^T \end{aligned} \tag{3.6}$$

Equ. 3.6 is simplified using the previous rotation matrices and given by equ. 3.7, [1].

$$\begin{aligned} \dot{x} &= uc_\psi c_\theta + v(c_\psi s_\theta s_\phi - s_\psi c_\phi) + w(c_\psi s_\theta c_\phi + s_\psi s_\phi) \\ \dot{y} &= us_\psi c_\theta + v(s_\psi s_\theta s_\phi + c_\psi c_\phi) + w(s_\psi s_\theta c_\phi - c_\psi s_\phi) \\ \dot{z} &= -us_\theta + vc_\theta s_\phi + wc_\theta c_\phi \\ \dot{\phi} &= p + qs_\phi t_\theta + rc_\phi t_\theta \\ \dot{\theta} &= qc_\phi - rs_\phi \\ \dot{\psi} &= qs_\phi S_\theta + rc_\phi S_\theta \end{aligned} \tag{3.7}$$

[1] $s_.$ = sine, $c_.$ = cosine, $t_.$ = tangent and $S_.$ = secant

3.5.2 FW-UAV Rigid Body Dynamics

FW-UAV dynamics is the study of the relation between the applied forces and or torques and the resulting motion. The dynamic response of the time rate of change of FW-UAV configuration to input forces and torques can be expressed by a differential equation. The dynamics study is needed for simulation and animation (test desired motions without resorting to real experimentation), analysis and synthesis of suitable control algorithms. Therefore, dynamic modeling is vital for model development and control system design i.e. simulate and tune a controller.

There are different approaches to formulate the dynamics of a FW-UAV; Euler-Lagrange and Newton-Euler are basic ones. Lagrangian formulation treats the FW-UAV as a whole and perform the analysis using Lagrangian function.

Where as, Newton-Euler formulation treats FW-UAV in each reference frame separately, and write down the equations describing its linear and angular motion. This formulation is used in this thesis research. Newton's second law is utilized in IF for translational motion and Euler's equation discussed for rotational motions considering flat earth surface and rigid body FW-UAV.

3.5.2.1 Translational Motion of FW-UAV

Translational motion of the FW-UAV is the motion in which all the points of a moving aircraft move uniformly in the same line of direction. All the points on the FW-UAV move the same distance in the same amount of time. There is no changes in orientation of aircraft relative to the fixed reference frames we have attached to the UAV.

A rigid body is assumed to have constant mass even if it varies continuously due-to different reasons. Newton's second law in IF for deriving translational equations of motion is written by equ. 3.8;

$$\sum F_{ext}^{I} = ma = m\frac{d}{dt}V_{g}^{I} \tag{3.8}$$

This time derivative is in IF, so now let's recall the vector differentiation rule from

equation C.1 and project equ. 3.8 onto the BF [2] .

$$\begin{aligned}\sum F_{ext}^{B} &= (F_x^B, F_y^B, F_z^B)^T = m * (\frac{d}{dt} V_g^B + \omega_{B/I} \otimes V_g^B) \\ &= m * ((\dot{u}, \dot{v}, \dot{w})^T + (p, q, r)^T \otimes (u, v, w)^T)\end{aligned} \tag{3.9}$$

Computing the mathematical computation and simplification the translational state space model in BF is written in equ. 3.10, where: [3].

$$\begin{aligned}\dot{u} &= \frac{1}{m} F_x^B + (rv - qw) \\ \dot{v} &= \frac{1}{m} F_y^B + (pw - ru) \\ \dot{w} &= \frac{1}{m} F_z^B + (qu - pv)\end{aligned} \tag{3.10}$$

3.5.2.2 Rotational Motion of FW-UAV

Euler's equation of motion stated as, the sum of all external moments about the center of mass of FW-UAV translated at the ground is defined as the time rate of angular momentum in ground IF.

$$\sum M_{ext}^{I} = \frac{d}{dt} H^I \tag{3.11}$$

now let's recall vector differentiation from equ. C.1 and project equ. 3.11 onto the BF.

$$\sum M_{ext}^{B} = \frac{d}{dt} H^B + \omega_{B/I} \otimes H^B \tag{3.12}$$

The angular momentum in BF is expressed by basic formula of equ. 3.13, [4]

$$H^B = J \circledast \omega_{B/I} \tag{3.13}$$

[2] F_{ext}^{I} = all external forces in IF, F_{ext}^{B} = all external forces in BF, m = rigid body mass and a = translational acceleration.

[3] F_x^B = all external forces along x-axis in BF, F_y^B = all external forces along y-axis in BF and F_z^B = all external forces along z-axis in BF

[4] Note that: J = Inertia matrix can be numerically computed from CAD model or experimentally using Bifilar pendulum.

Moment of inertia denoted by J, measures the extent to which a FW-UAV resists rotational acceleration about a particular axis in IRF. Where it's components can be calculated through equ. [5], and $\omega^B_{B/I}$ is defined as the body angular velocity in the BF as seen from the IF. Considering rough engineering approximation the aircraft is assumed to be aligned in the (x,z) plane of geometry and leaving $J_{xy} = J_{yz} = 0$ the inertia J and it's inverse J^{-1} given by equ. 3.14.

$$J = \begin{pmatrix} J_x & -J_{xy} & -J_{xz} \\ -J_{xy} & J_y & -J_{yz} \\ -J_{xz} & -J_{yz} & J_z \end{pmatrix}, \quad J^{-1} = \begin{pmatrix} \frac{J_z}{(J_xJ_z - J_{xz}^2)} & 0 & \frac{J_{xz}}{(J_xJ_z - J_{xz}^2)} \\ 0 & \frac{1}{J_y} & 0 \\ \frac{J_{xz}}{(J_xJ_z - J_{xz}^2)} & 0 & \frac{J_x}{(J_xJ_z - J_{xz}^2)} \end{pmatrix} \tag{3.14}$$

Now let's rewrite the BF rotational equations of motion, equ. 3.12 using inertia matrices.

$$\begin{aligned} \sum M^B_{ext} = (M^B_x, M^B_y, M^B_z)^T &= \frac{d}{dt}(J \circledast \omega_{B/I}) + \omega_{B/I} \otimes (J \circledast \omega_{B/I}) \\ &= J \circledast \dot{\omega}_{B/I} + \omega_{B/I} \otimes (J \circledast \omega_{B/I}) \\ &= J \circledast (\dot{p}, \dot{q}, \dot{r})^T + (p, q, r)^T \otimes (J \circledast (p, q, r)^T) \\ (\dot{p}, \dot{q}, \dot{r})^T &= J^{-1} \circledast ((M^B_x, M^B_y, M^B_z)^T - (p, q, r)^T \otimes (J \circledast (p, q, r)^T)) \end{aligned} \tag{3.15}$$

Finally, the rotational equations of motion in state space is expressed by equ. 3.16, [6]

$$\begin{aligned} \dot{p} &= \frac{1}{J_xJ_z - J_{xz}^2}(J_zM^B_x + J_{xz}M^B_z + pqJ_{xz}(J_x - J_y + J_z) + qr(J_yJ_z - J_z^2 - J_{xz}^2)) \\ \dot{q} &= \frac{1}{J_y}(M^B_y + pr(J_z - J_x) + J_{xz}(p^2 - r^2)) \\ \dot{r} &= \frac{1}{J_xJ_z - J_{xz}^2}(J_{xz}M^B_x + J_xM^B_z + pq(J_{xz}^2 + J_x^2 - J_xJ_y) + qrJ_{xz}(J_y - J_x - J_z)) \end{aligned} \tag{3.16}$$

[5] Component inertia's

$$J_x = \int (y^2+z^2)dm, J_y = \int (x^2+z^2)dm, J_z = \int (x^2+y^2)dm, J_{xy} = \int (xy)dm, J_{xz} = \int (xz)dm, J_{yz} = \int (yz)dm$$

[6] Where:
M^I_{ext} = all external moments in IF, M^B_{ext} = all external moments in BF, J = inertia matrix, H = angular momentum and
M^B_x = all external moments about x-axis in BF, M^B_y = all external moments about y-axis in BF and M^B_z = all external moments about z-axis in BF

3.5.3 External Forces and Moments on FW-UAV

The FW-UAV is a highly complex nonlinear system, works under various external forces and moments. The external forces are due to gravity, aerodynamics and propulsive. Moments are resulted from the aerodynamic and propeller effects, note that the plane is symmetrical and aligned about the (x, z) plane (the effect of gravity is neglected).

$$\begin{aligned} F_{ext} &= F_g + F_a + F_p \\ M_{ext} &= M_a + M_p \end{aligned} \tag{3.17}$$

Where: g - gravity, a - aerodynamics, and p - propeller

3.5.3.1 Gravitational Force

The force due to gravity is analyzed by newton's second law in the IF, so it must be projected onto body frame for dynamic analysis.

$$\begin{aligned} F_g^I &= (0, 0, mg)^T \\ F_g^B &= R_I^B \circledast (0, 0, mg)^T \\ &= mg * (-s_\theta, c_\theta s_\phi, c_\theta c_\phi)^T \end{aligned} \tag{3.18}$$

3.5.3.2 Aerodynamic Forces and Moments

The main source of force and moment in aerodynamics is air pressure strength and distribution which depends on the airspeed, air density, shape and altitude of UAV. So the expression for dynamic pressure combining Pascal's law and work-energy theorem is given by equ. 3.19, where the variables are defined in [7] .

$$P_D = \frac{F}{A} = \frac{W/d}{A} = \frac{E}{A.d} = \frac{E}{V} = \frac{KE}{V} = \frac{\frac{1}{2}mV_a^2}{V} = \frac{1}{2}\frac{m}{V}V_a^2 = \frac{1}{2}\rho V_a^2 \tag{3.19}$$

[7] P_D= dynamic pressure, F= force, W= work done, d= displacement, A= area, V= volume, E= energy, KE= kinetic energy, m= mass of air, V_a= magnitude of airspeed, and ρ= density of air

3.5.3.3 Fixed Wing UAV Control Surfaces

In this thesis, the FW-UAV has seven degrees of freedom inertial positions (x, y, z), attitudes (ϕ, θ, ψ), and airspeed (V_a). However, the aircraft has only four control inputs applied at different control surfaces. FW-UAV's mostly have three flight control surfaces aileron, elevator, and rudder; which are attached to the air-frame on hinges. These are the aerodynamic devices which are used to adjust and control the UAV's flight condition in response to external forces and moments.

Hence, it isn't possible to control all the state variables explicitly, due to under actuated nature of the system. However, intermediate controllable variables associated to the FW-UAV are selected as (x, y, z) positions and the rest are controlled explicitly through decoupling, which makes the control design easier and handy. The three control inputs and surfaces are illustrated with figures in 3.3.

(a) Aileron, [2] **(b)** Elevator, [1] **(c)** Rudder, [27]

Figure 3.3: Three Control Surfaces in FW-UAV

Ailerons are mounted on the rear edge of each wing near the wingtips and move in opposite directions. The left and right ailerons work oppositely, one increases lift the other decreases, [2]. This way it's possible to turn about the longitudinal axis, roll (ϕ) left-to-right about x-axis. The net aileron control signal deflection command is denoted with γ_a and calculated by the formula; $\gamma_a = \frac{1}{2}(\gamma_{a_l} - \gamma_{a_r})$, where [8]. From this formula turning the FW-UAV left is considered as positive turn.

Elevators joined to the back of the fixed part of the horizontal tail. It's part of horizontal flight stabilizer by generating downward force on the tail to lift the heavy

[8] γ_{a_l}-left aileron command and - γ_{a_r}-right aileron command

nose body of UAV, which makes the wings to fly at a higher angle of attack (α). It's also necessary for pitching (θ) up and down the nose of FW-UAV about the y-axis. The elevator command signal denoted by γ_e.

Rudder mounted on the trailing edge of the vertical tail. Rudder deflected left-to-right and vice-versa through respective commands and causes the nose to yaw left-to-right about the z-axis. Centering the rudder pedals returns the rudder to neutral and stops the yaw. The rudder deflection angle denoted by γ_r. The main purpose of γ_r is to counteract the drag caused by the lowered aileron during a turn.

Flight in air is performed in every axis (x, y, z) of imaginary line around which an aircraft can turn. There are three axes up on which it can move; left-right, forward-rearward and up-down. Most commonly known with technical names of longitudinal, lateral, and vertical flights.

1. Longitudinal Flight: it's most commonly known as level flight along longitudinal axis (x-axis) runs in the nose-to-tail direction.
2. Lateral Flight: it's a flight along lateral axis (y-axis) running in the wing-to-wing direction. It's the turning effect of left and right from the level flight.
3. Vertical Flight: this is the motion of UAV up and down in the z-direction.

Now let's examine the aerodynamic forces and moments during two flight phases, longitudinal and lateral aerodynamics.

3.5.3.4 Longitudinal Aerodynamics

Longitudinal flight is under (x, z) plane in which the forces and moments are defined in SF, [4] and they are the result of dynamic pressure computed at equ. 3.19 . Recalling basic fluid dynamics we have the relations between force and pressure in equ. 3.20:

$$\begin{aligned} F_D &= P_D * area * C_{F_P} \\ M_D &= F_D * C \end{aligned} \tag{3.20}$$

Where; F_D and M_D are aerodynamic forces and moments respectively. C_{F_P} is the proportionality constant between force and pressure which is nonlinear function depends on

angle of attack, body angular rate about y-axis, and elevator deflection angle. It differs from axis to axis, so the lift and drag forces along x and z-axis respectively and moment bout the y-axis in stability frame expressed with equ. 3.21.

$$\begin{aligned} f_{lift}^{S} &= \frac{1}{2}\rho V_a^2 S C_l(\alpha, q, \gamma_e) \\ f_{drag}^{S} &= \frac{1}{2}\rho V_a^2 S C_d(\alpha, q, \gamma_e) \\ M_y^{S} &= \frac{1}{2}\rho V_a^2 C S C_y(\alpha, q, \gamma_e) \end{aligned} \tag{3.21}$$

The lift force is applied along the negative z-axis as it's defined from NED frame. The drag force is always in opposite direction to the forward velocity of the aircraft (it's in the negative x-axis) and independent of the sign of angle of attack α.

The constants and variables are defined in [9]. The nondimensional physical constants can be calculated using Taylor series based linear equations 3.22, [4].

$$\begin{aligned} C_l(\alpha, q, \gamma_e) &= C_{l_0} + \frac{\partial C_l}{\partial \alpha}\alpha + \frac{\partial C_l}{\partial q}q + \frac{\partial C_l}{\partial \gamma_e}\gamma_e \\ C_d(\alpha, q, \gamma_e) &= C_{d_0} + \frac{\partial C_d}{\partial \alpha}\alpha + \frac{\partial C_d}{\partial q}q + \frac{\partial C_d}{\partial \gamma_e}\gamma_e \\ C_y(\alpha, q, \gamma_e) &= C_{y_0} + \frac{\partial C_y}{\partial \alpha}\alpha + \frac{\partial C_y}{\partial q}q + \frac{\partial C_y}{\partial \gamma_e}\gamma_e \end{aligned} \tag{3.22}$$

The partial derivatives in linear equ. 3.22 are commonly non-dimensionalized. Since C_l, C_d, C_y, α and γ_e expressed in radians are dimensionless, the only partial requiring non-dimensionalization is q, a standard factor to use is $C/(2V_a)$. We can then rewrite as:

$$\begin{aligned} C_l(\alpha, q, \gamma_e) &= C_{l_0} + C_{l_\alpha}\alpha + C_{l_q}\frac{C}{2V_a}q + C_{l_{\gamma_e}}\gamma_e \\ C_d(\alpha, q, \gamma_e) &= C_{d_0} + C_{d_\alpha}\alpha + C_{d_q}\frac{C}{2V_a}q + C_{d_{\gamma_e}}\gamma_e \\ C_y(\alpha, q, \gamma_e) &= C_{y_0} + C_{y_\alpha}\alpha + C_{y_q}\frac{C}{2V_a}q + C_{y_{\gamma_e}}\gamma_e \end{aligned} \tag{3.23}$$

But note that to incorporate wing stall into longitudinal aerodynamic model the forces

[9] S=surface area swept by plane wing, C=mean chord length from aerodynamic center, α=the angle of attack from the (x,z) plane, q=BF linear velocity along y axis, γ_e=pitching angle from elevator and C_l, C_d and C_y are nondimensional coefficients of lift (F_{lift}^{S}), drag (F_{drag}^{S}) and moment (M_y^{S}) respectively.

and moment must be nonlinear functions of angle of attack α. The lift and drag forces must be projected onto BF for aerodynamic analysis and computed with equ. 3.24.

$$\begin{aligned}(f_x^B, 0, f_z^B)^T &= R_S^B(\alpha) \circledast (-f_{drag}^S, 0, -f_{lift}^S)^T \\ f_x^B &= \frac{1}{2}\rho V_a^2 S(C_l(\alpha, q, \gamma_e) * s_\alpha - C_d(\alpha, q, \gamma_e) * c_\alpha) \\ f_z^B &= -\frac{1}{2}\rho V_a^2 S(C_l(\alpha, q, \gamma_e) * c_\alpha + C_d(\alpha, q, \gamma_e) * s_\alpha)\end{aligned} \tag{3.24}$$

The moment about the y-axis due-to the rotational effect of the longitudinal aerodynamic forces is projected on the BF from SF using equ. 3.25.

$$\begin{aligned}(0, M_y^B, 0)^T &= R_S^B(\alpha) \circledast (0, m_y^S, 0)^T \\ M_y^S &\approxeq M_y^B\end{aligned} \tag{3.25}$$

3.5.3.5 Lateral Aerodynamics

Lateral flight is a condition in which translational motion along y-axis and rotational motion about (x, z) stable plane is performed in the presence of disturbances in WF, [4].

$$\begin{aligned}f_y^W &= \frac{1}{2}\rho V_a^2 S C_Y(\beta, p, r, \gamma_a, \gamma_r) \\ M_x^W &= \frac{1}{2}\rho V_a^2 S B C_x(\beta, p, r, \gamma_a, \gamma_r) \\ M_z^W &= \frac{1}{2}\rho V_a^2 S B C_z(\beta, p, r, \gamma_a, \gamma_r)\end{aligned} \tag{3.26}$$

Where the constants and variables are defined in [10]. Lateral flight highly influenced by p, r, β, γ_a and γ_r. Recalling Taylor series lateral constants are given by equ. 3.27, [4].

$$\begin{aligned}C_Y(\beta, p, r, \gamma_a, \gamma_r) &= C_{Y_0} + \frac{\partial C_Y}{\partial \beta}\beta + \frac{\partial C_Y}{\partial p}p + \frac{\partial C_Y}{\partial r}r + \frac{\partial C_Y}{\partial \gamma_a}\gamma_a + \frac{\partial C_Y}{\partial \gamma_r}\gamma_r \\ C_x(\beta, p, r, \gamma_a, \gamma_r) &= C_{x_0} + \frac{\partial C_x}{\partial \beta}\beta + \frac{\partial C_x}{\partial p}p + \frac{\partial C_x}{\partial r}r + \frac{\partial C_x}{\partial \gamma_a}\gamma_a + \frac{\partial C_x}{\partial \gamma_r}\gamma_r \\ C_z(\beta, p, r, \gamma_a, \gamma_r) &= C_{z_0} + \frac{\partial C_z}{\partial \beta}\beta + \frac{\partial C_z}{\partial p}p + \frac{\partial C_z}{\partial r}r + \frac{\partial C_z}{\partial \gamma_a}\gamma_a + \frac{\partial C_z}{\partial \gamma_r}\gamma_r\end{aligned} \tag{3.27}$$

[10] B=wing span, β=angle of side-slip from (x, z) plane, p=BF linear velocity along x-axis, r=BF linear velocity along z-axis, γ_a=rolling angle from aileron, γ_r=yawing angle from rudder, and C_Y, C_x and C_z are nondimensional coefficients of force (f_y^W), moments (M_x^W) and (M_z^W) respectively.

The partial derivatives in linear equ. 3.27 are non-dimensionalized. Since C_Y, C_x, C_z and the angles β, γ_a and γ_r expressed in radians are dimensionless, then the partial requiring non-dimensionalization are q and r, a standard factor to use is then $B/(2V_a)$.

$$\begin{aligned} C_Y(\beta,p,r,\gamma_a,\gamma_r) &= C_{Y_0} + C_{Y_\beta}\beta + C_{Y_p}\frac{B}{2V_a}p + C_{Y_r}\frac{B}{2V_a}r + C_{Y_{\gamma_a}}\gamma_a + C_{Y_{\gamma_r}}\gamma_r \\ C_x(\beta,p,r,\gamma_a,\gamma_r) &= C_{x_0} + C_{x_\beta}\beta + C_{x_p}\frac{B}{2V_a}p + C_{x_r}\frac{B}{2V_a}r + C_{x_{\gamma_a}}\gamma_a + C_{x_{\gamma_r}}\gamma_r \\ C_z(\beta,p,r,\gamma_a,\gamma_r) &= C_{z_0} + C_{z_\beta}\beta + C_{z_p}\frac{B}{2V_a}p + C_{z_r}\frac{B}{2V_a}r + C_{z_{\gamma_a}}\gamma_a + C_{z_{\gamma_r}}\gamma_r \end{aligned} \tag{3.28}$$

The force f_y^W must be projected onto BF for aerodynamic analysis through equ. 3.29.

$$\begin{aligned} (0, f_y^B, 0)^T &= R_W^B(\alpha,\beta) \circledast (0, f_y^W, 0)^T \\ f_y^B &= \frac{1}{2}\rho V_a^2 S C_Y(\beta,p,r,\gamma_a,\gamma_r) * c_\beta \end{aligned} \tag{3.29}$$

Since the only additional nonlinear term exists as a multiplier in equ. 3.29 from equ. 3.26 is cosine function of β, c(β) it's value can be taken as unity through small angle approximation (small β is desired), resulting force in BF expressed through equ. 3.30.

$$f_y^B \approxeq \frac{1}{2}\rho V_a^2 S C_Y(\beta,p,r,\gamma_a,\gamma_r) \tag{3.30}$$

Now let's transform lateral moments from WF onto BF using $R_W^B(\alpha,\beta)$ and equ. 3.31.

$$\begin{aligned} (M_x^B, 0, M_z^B)^T &= R_W^B(\alpha,\beta) \circledast (M_x^W, 0, M_z^W)^T \\ M_x^B &= M_x^W c_\beta c_\alpha - M_z^W s_\alpha \\ M_z^B &= M_x^W c_\beta s_\alpha + M_z^W c_\alpha \end{aligned} \tag{3.31}$$

In lateral flight it's desired that the attack and side-slip angles to be as small as possible (≤ 0.262 rad), because angle of attack is highly incorporated at longitudinal flight dynamics and side-slip is needed to be minimal. Applying small angle approximation the lateral moments in BF can be described by simplified equ. 3.32.

$$M_x^B \approxeq M_x^W, and \quad M_z^B \approxeq M_z^W \tag{3.32}$$

3.5.3.6 Force and Moment from Propeller

Bernoulli's equation of fluid dynamics states that for an ideal fluid i.e. no viscosity, constant density, and steady flow; the sum of its kinetic, potential, and thermal energy must be conserved. This statement is used for establishing a relationship between the velocity of fluid, its pressure, and its relative height. There are two pressures developed for generating thrust in the forward flight direction; pressure ahead of and behind the propeller.

$$\begin{aligned} P_{ahead} &= P_0 + \frac{1}{2}\rho V_a^2 \\ P_{behind} &= P_0 + \frac{1}{2}\rho V_{exit}^2 \end{aligned} \tag{3.33}$$

The difference in these pressures develops thrust force. V_{exit} is the speed of air as it leaves propeller, there is a linear relationship between the PWM command signal δ_t and the angular velocity of the propeller if no transients in the motor. The propeller in turn creates an exit air speed of $(k_m\delta_t)^2$. The force generated along the x-axis in BF can be calculated through equ. 3.34 applying pressure difference in the forward flight direction, with the variables defined in [11] .

$$f_{p_x} = S_P C_P(P_{behind} - P_{ahead}) = \frac{1}{2}\rho S_P C_P(V_{exit}^2 - V_a^2) = \frac{1}{2}\rho S_P C_P(k_m^2\delta_t^2 - V_a^2) \tag{3.34}$$

As propeller spins, it applies force to the air that passes through the propeller, while the air applies a reaction force on the propeller. The net effect of these forces generates a torque about x-axis. This torque is opposite to the direction of the propeller rotation and proportional to the square of the propeller's angular velocity, given by equ. 3.35 [12].

$$M_P = -K_M\Omega^2 = -K_M k_\Omega^2 \delta_t^2 \tag{3.35}$$

[11] f_{p_x} - thrust force along x-axis, P_{ahead} - developed due to propeller's ahead velocity, P_{behind} - developed due to the air velocity behind the propeller, P_0 - static pressure, ρ - air density, V_a - airspeed, V_{exit} - speed of air leaving propeller, k_m - motor linear speed constant(engine parameter), δ_t - engine acceleration, S_P - area swept by air leaving propeller and C_P - the proportionality constant between pressure difference and force

[12] K_M - engine torque constant, Ω - propeller angular speed, M_P - reactive torque on propeller and k_Ω - angular speed constant

3.5.3.7 External Disturbances on FW-UAV Dynamics

The wind disturbance in aerodynamic analysis has two components, steady and transient (stochastic). Wind disturbance comes into the aerodynamic analysis in the form of velocity vector components, so let's define them by equ. 3.36.

$$\begin{aligned} V_{S_W}^I &= (V_{S_x}, V_{S_y}, V_{S_z})^T \\ V_{T_W}^B &= (V_{T_x}, V_{T_y}, V_{T_z})^T \end{aligned} \tag{3.36}$$

Where the stochastic wind components are defined by [13]. The stochastic wind modeled through two ways, experimentally using wind gust generation and LTI system transfer function of Dryden or Von Karmen spectrum methods. Dryden model transfer functions in (x, y, z) axes as in equ. 3.37, [14].

$$H_x(s)^B = \mu_x\sqrt{\frac{2V_a}{L_x}}\frac{1}{s+\frac{V_a}{L_x}}, \quad H_y(s)^B = \mu_y\sqrt{\frac{3V_a}{L_y}}\frac{s+\frac{V_a}{\sqrt{3}L_y}}{(s+\frac{V_a}{L_y})^2}, \quad H_z(s)^B = \mu_z\sqrt{\frac{3V_a}{L_z}}\frac{s+\frac{V_a}{\sqrt{3}L_z}}{(s+\frac{V_a}{L_z})^2} \tag{3.37}$$

The total wind velocity in BF can be computed by equ. 3.38:

$$V_W^B = (u_w, v_w, w_w)^T = R_I^B(\phi, \theta, \psi) \circledast V_{S_W}^I + V_{T_W}^B \tag{3.38}$$

Simplifying the above expression we have:

$$\begin{aligned} u_w &= V_{S_x}c_\theta c_\psi + V_{S_y}c_\theta s_\psi - V_{S_z}s_\theta + V_{T_x} \\ v_w &= V_{S_x}(s_\phi s_\theta c_\psi - c_\phi s_\psi) + V_{S_y}(s_\phi s_\theta s_\psi + c_\phi c_\psi) + V_{S_z}s_\phi s_\theta + V_{T_y} \\ w_w &= V_{S_x}(c_\phi s_\theta c_\psi + s_\phi s_\psi) + V_{S_y}(c_\phi s_\theta s_\psi - s_\phi c_\psi) + V_{S_z}c_\phi c_\theta + V_{T_z} \end{aligned} \tag{3.39}$$

[13] $V_{S_W}^I$ = steady wind, is typically expressed in the GIF and $V_{T_W}^B$ = stochastic component expressed in the aircraft BF because the atmospheric effects experienced by the aircraft in the direction of its forward motion occur at a higher frequency than in the lateral and down directions. V_{S_x}, V_{S_y}, V_{S_z} steady state wind velocities and V_{T_x}, V_{T_y}, V_{T_z} transient wind velocities along x, y and z-axis respectively.

[14] Where: $H_x(s)^B$, $H_y(s)^B$, $H_z(s)^B$ transfer functions in BF, μ_x, μ_y, μ_z turbulence intensity and L_x, L_y, L_z spectral wavelength along x, y, z-axis respectively, V_a = airspeed magnitude.

3.6 Airspeed in the Presence of Wind Disturbance

From the components of wind velocity V_W^B and ground velocity V_g^B in BF, we can calculate the BF components of the airspeed vector denoted by $V_a^B = (V_{a_x}, V_{a_y}, V_{a_z})^T$ and calculated through equ. 3.40.

$$\begin{aligned} V_a^B &= (V_{a_x}, V_{a_y}, V_{a_z})^T = V_g^B - V_W^B \\ &= (u, v, w)^T - (u_w, v_w, w_w)^T \\ &= (u - u_w, v - v_w, w - w_w)^T \end{aligned} \tag{3.40}$$

The aircraft in the presence of wind is assumed to be moving in forward direction in WF, so let's define airspeed in WF as $V_a^W = (V_a, 0, 0)^T$ where V_a is the magnitude of resultant airspeed vector. And then project V_a^W on BF using equ. 3.41.

$$\begin{aligned} V_a^B &= R_W^B \circledast (V_a, 0, 0)^T \\ &= (V_a c_\alpha c_\beta, V_a s_\beta, V_a s_\alpha c_\beta)^T \end{aligned} \tag{3.41}$$

Now we can equate the final results of equ. 3.40 and 3.41 and calculate the airspeed magnitude (V_a), angle of attack (α), and side-slip (β) using the equ. 3.42 [15].

$$\begin{aligned} V_a &= \sqrt{V_{a_x}^2 + V_{a_y}^2 + V_{a_z}^2} \\ \alpha &= \arctan(\frac{V_{a_z}}{V_{a_x}}) \\ \beta &= \arcsin(\frac{V_{a_y}}{V_a}) \end{aligned} \tag{3.42}$$

[15] Where:
V_a - airspeed magnitude
$c_.$ - cosine
$s_.$ - sine
$S_.$ - secant
$t_.$ - tangent
arcsin and *arctan* are inverse of sine and tangent trigonometric functions respectively.

3.7 State Space Model of FW-UAV

From the previous sections the overall external force and moment equations combined and written in BF with equ. C.2, and C.3 respectively. The coupled and nonlinear state space model of a FW-UAV in the BF and IF is given by 3.43, developed through combining the equations 3.7, 3.10, 3.16, 3.42, C.2 and C.3, where:[16].

$$
\begin{aligned}
\dot{x} &= uc_\psi c_\theta + v(c_\psi s_\theta s_\phi - s_\psi c_\phi) + w(c_\psi s_\theta c_\phi + s_\psi s_\phi) \\
\dot{y} &= us_\psi c_\theta + v(s_\psi s_\theta s_\phi + c_\psi c_\phi) + w(s_\psi s_\theta c_\phi - c_\psi s_\phi) \\
\dot{z} &= -us_\theta + vc_\theta s_\phi + wc_\theta c_\phi \\
\dot{\phi} &= p + qs_\phi t_\theta + rc_\phi t_\theta \\
\dot{\theta} &= qc_\phi - rs_\phi \\
\dot{\psi} &= qs_\phi S_\theta + rc_\phi S_\theta \\
\dot{u} &= \frac{1}{2m}\rho V_a^2 S(C_l s_\alpha - C_d c_\alpha) + \frac{1}{2m}\rho S_P C_P(k_m^2 U_4^2 - V_a^2) - gs_\theta + (rv - qw) \\
\dot{v} &= \frac{1}{2m}\rho V_a^2 S C_Y + gs_\phi c_\theta + (pw - ru) \\
\dot{w} &= -\frac{1}{2m}\rho V_a^2 S(C_l c_\alpha + C_d s_\alpha) + gc_\phi c_\theta + (qu - pv) \\
\dot{p} &= J_0 J_z(\frac{1}{2}\rho V_a^2 S B C_x - K_M k_\Omega^2 U_4^2) + J_0 J_{xz}(\frac{1}{2}\rho V_a^2 S B C_z) \\
&\quad + J_0 pq J_{xz}(J_x - J_y + J_z) + J_0 qr(J_y J_z - J_z^2 - J_{xz}^2) \\
\dot{q} &= \frac{1}{J_y}(\frac{1}{2}\rho V_a^2 C S C_y + pr(J_z - J_x) + J_{xz}(r^2 - p^2)) \\
\dot{r} &= J_0(\frac{J_{xz}}{2}\rho V_a^2 S B C_x - J_{xz} K_M k_\Omega^2 U_4^2) + J_0(\frac{J_x}{2}\rho V_a^2 S B C_z) \\
&\quad + J_0 pq(J_{xz}^2 + J_x^2 - J_x J_y) + J_0 qr J_{xz}(J_y - J_x - J_z) \\
V_a &= \sqrt{(u - u_w)^2 + (v - v_w)^2 + (w - w_w)^2}
\end{aligned}
\tag{3.43}
$$

[16] Aerodynamic constants are symbolized in short as:
$C_Y = C_Y(\beta, p, r, \gamma_a, \gamma_r)$
$C_l = C_l(\alpha, q, \gamma_e)$
$C_d = C_d(\alpha, q, \gamma_e)c_\alpha$
$C_x = C_x(\beta, p, r, \gamma_a, \gamma_r)$
$C_y = C_y(\alpha, q, \gamma_e)$
$C_z = C_z(\beta, p, r, \gamma_a, \gamma_r)$
$U_1 = \gamma_a$, $U_2 = \gamma_e$, $U_3 = \gamma_r$, $U_4 = \delta_t$
$J_0 = \frac{1}{J_x J_z - J_{xz}^2}$

3.8 FW-UAV Model Open-loop Simulation

In open loop simulation of the FW-UAV, the model should be stabilized to it's equilibrium value with time if the control surface deflection inputs are null. The natural stabilization is needed for the FW-UAV model before any further controller design. The verification was done on MATLAB Simulink R2022b, taking the physical parameters and coefficients from [4] for Aerosonde UAV, appendix A. The natural stability of the model is elaborated as follows with $u_0 = 12$ m/s and $\delta_t = 0.0437$ m/s. In all cases asymptotic stability of states have been seen.

Case 1: Aileron kick of 0.25 rad have been introduced and stabilizes roll angle to zero within 20 seconds.

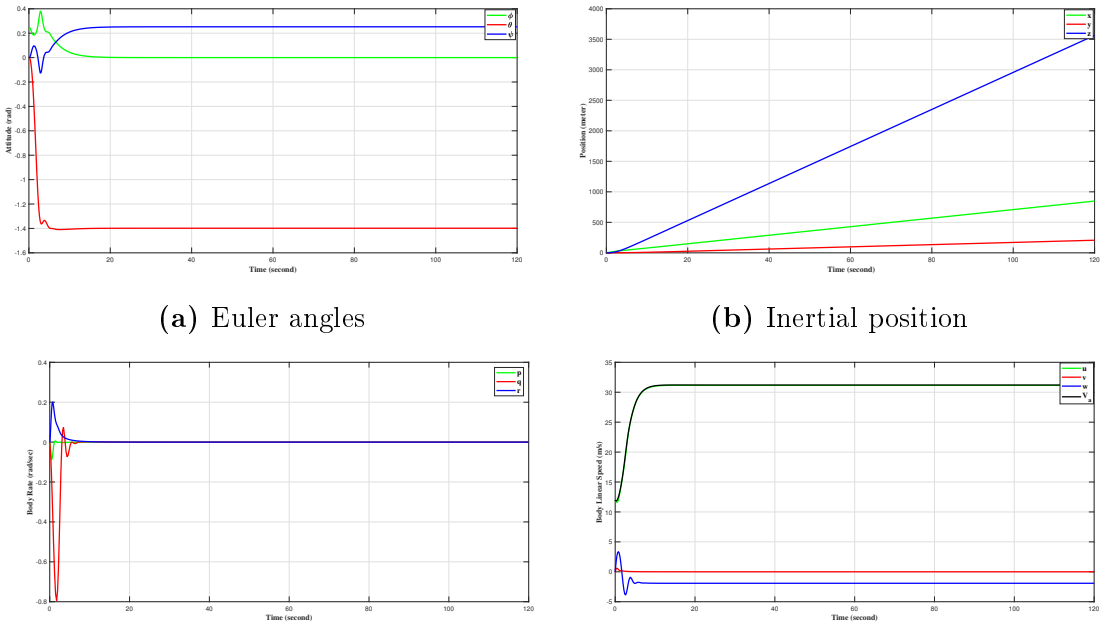

(a) Euler angles

(b) Inertial position

(c) Body angular rates

(d) Body linear speed

Figure 3.4: Open-loop Simulation in Roll Stabilization

Case 2: Elevator kick of 0.25 rad have been introduced and the pitch angle was marginally asymptotically stabilized.

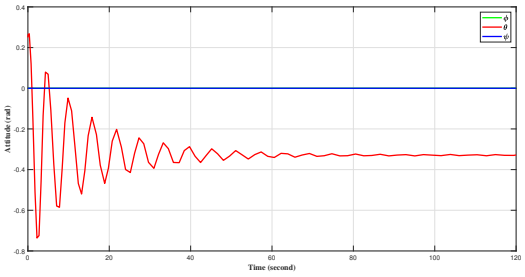

(a) Euler angles

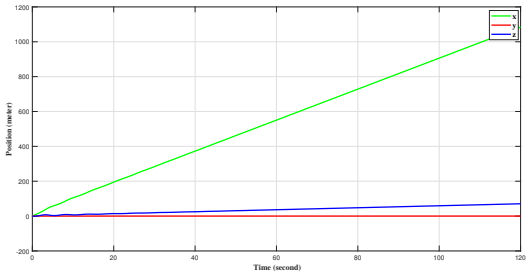

(b) Inertial position

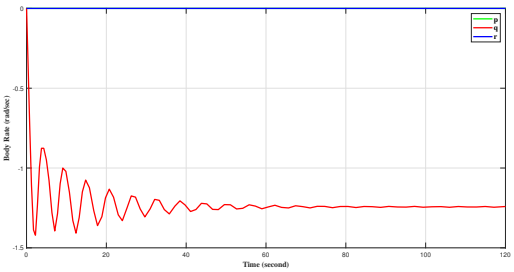

(c) Body angular rates

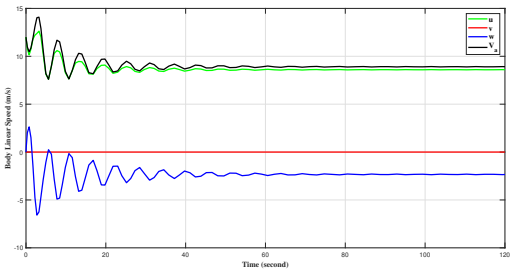

(d) Body linear speed

Figure 3.5: Open-loop Simulation in Pitch Stabilization

Case 3: Rudder kick of -0.00025 rad was introduced for stabilizing the yaw angle and the following results found.

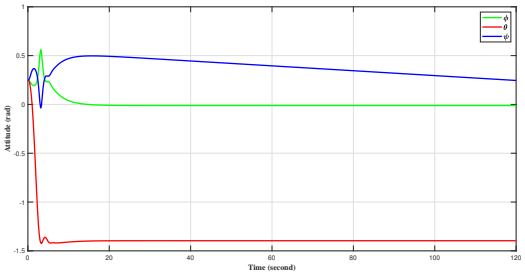

(a) Euler angles

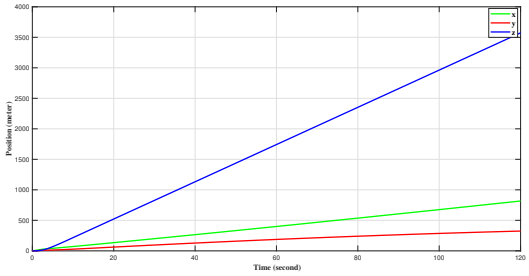

(b) Inertial position

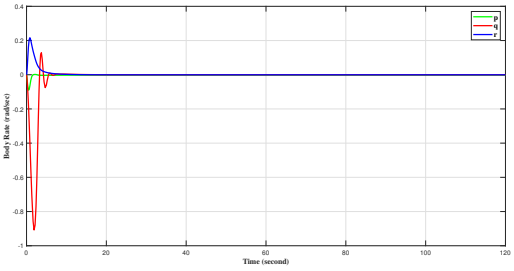

(c) Body angular rates

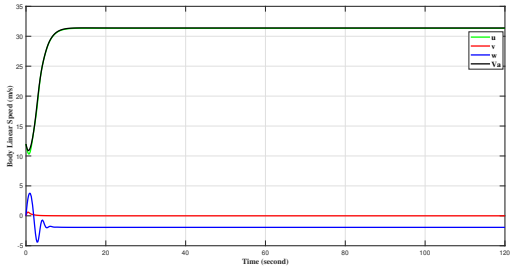

(d) Body linear speed

Figure 3.6: Open-loop Simulation in Yaw Stabilization

Case 4: Setting control surface deflections to zero the natural stability of the system have been achieved, fig. 3.7.

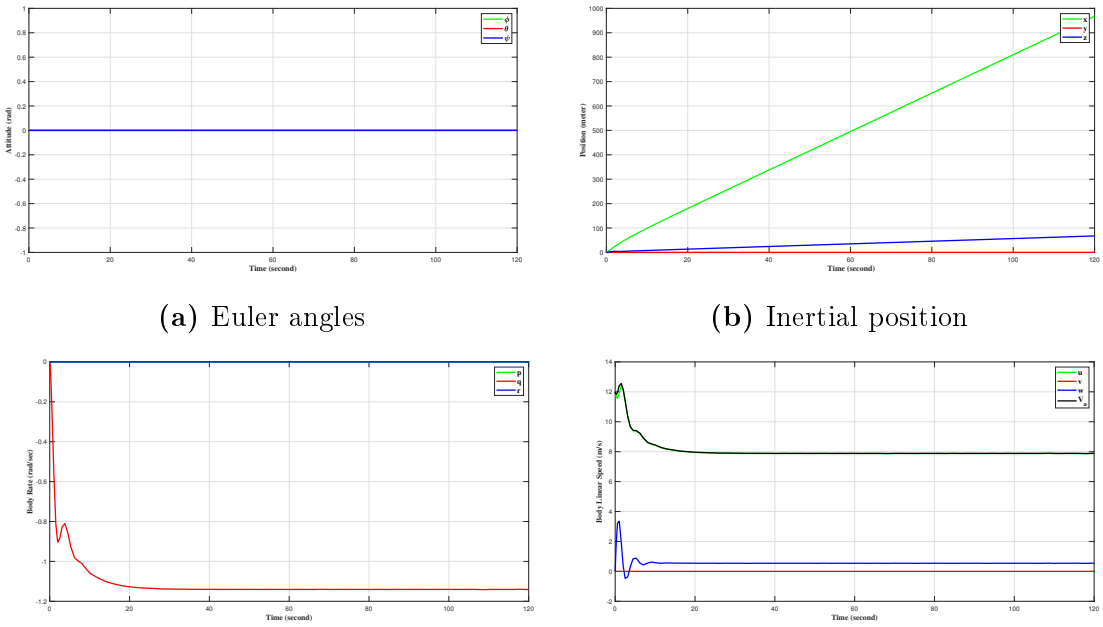

(a) Euler angles

(b) Inertial position

(c) Body angular rates

(d) Body linear speed

Figure 3.7: Open-loop Simulation in Null Control Surface Deflections

Chapter 4

Fixed Wing UAV Controller Design and Optimization Algorithms

FW-UAV model is a nonlinear system which is characterized by multiple inputs-outputs, strong coupling, and under actuation. To overcome these characteristics fuzzy switching twisting SMC method is studied in this paper. The SMC is mainly used to deal with the control problem of highly coupled non-linearity, and disturbance factors. Twisting method and fuzzy switching control are used to tackle the chattering.

FW-UAV has 12 states and it is very complicated to control and track all states simultaneously, because it's in a state of high speed movement under working conditions. In this study, seven degree of freedom (DOF) are selected for tracking and control to meet the desired characteristics. These seven state variables are namely three inertial positions (x, y, z), attitudes (ϕ, θ, ψ), and airspeed (V_a).

There are three control surface deflections $(\gamma_a, \gamma_e, \gamma_r)$ and engine acceleration (δ_t), which are denoted as control commands of $U_1 = \gamma_a$, $U_2 = \gamma_e$, $U_3 = \gamma_r$ and $U_4 = \delta_t$. These are the means for manipulating the states of a FW-UAV through the force which in-turn must be related to the output of the control surface of the FW-UAV. As it can be seen from the model in equ. 3.43, it's highly coupled system, changing one of the control parameters affects all the state variables. So the control system is designed with decoupling the dynamics of attitudes, airspeed and inertial positions separately. Finally the controllers implemented on the overall coupled mathematical model of the FW-UAV.

4.1 Fixed Wing UAV Control and Guidance

FW-UAVs autonomously controlled by using the two layers of control loops called the cascaded control loops namely; low level and high level. Low level control includes the attitude and speed tracking , regulation, and stabilization where as high level control is about position control, guidance, and trajectory tracking. The overall control architecture layout is presented with fig. 4.1.

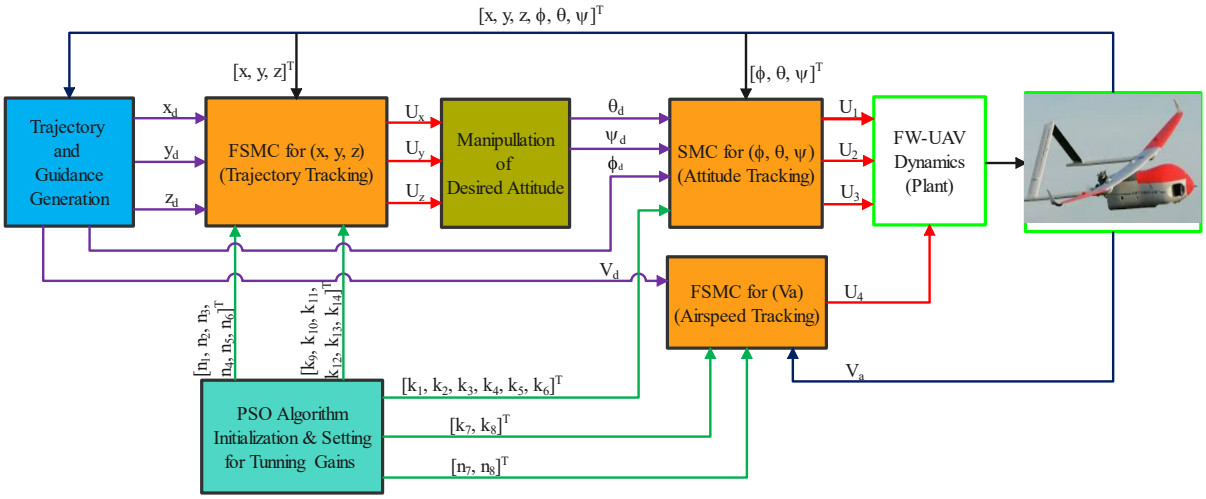

Figure 4.1: Cascade Control Structure for FW-UAV

The first block in the figure is used for guidance and trajectory generation. The real data is collected from sensor measurements or GPS data and based on the mission of FW-UAV desired trajectories are developed as (x_d, y_d, z_d) along x-y-z axes. Then the virtual controllers, (U_x, U_y, U_z) are designed for inertial positions along x-y-z axes respectively for tracking the desired position trajectories. From system modeling, inertial positions are manipulated through the attitudes of the system, so based on the virtual control signals the desired attitudes, $(\phi_d, \theta_d, \psi_d)$ are computed. After generating $(\phi_d, \theta_d, \psi_d)$, the attitude controllers are developed which tries to make the actual attitudes track desired angles. Finally, the command signals, (U_1, U_2, U_3, U_4) are given to the plant dynamic model for manipulation and control of output variables. Based on this control architecture the twisting sliding mode controllers are designed starting from low level (attitude and airspeed) to high level (position) in the proceeding sections.

4.2 Sliding Mode Controller (SMC)

There are lots of discrepancies between the actual FW-UAV plant and the mathematical model developed for controller design. The mismatch results from different sources unmodelled dynamics, variation in system parameters or the approximation of complex behaviors by a straightforward model. It must be ensured that the designed controller to have the ability to produce the required performance levels in practice despite model mismatches, [20]. This leads to the intense interest in the development of robust control methods that seek to solve this type of problem, SMC is one of these methodologies.

SMC is a class of variable structure system that targets decreasing the complexity of high-order systems to reduced-order state variables, defined as a sliding function and its derivative. It's advantageous for order reduction, disturbance rejection, insensitivity to parameter variations, decoupling design parameters and hence robust and handles all system non-linearity. It utilizes high speed switching feedback control. This process has two stages: sliding surface and control action design.

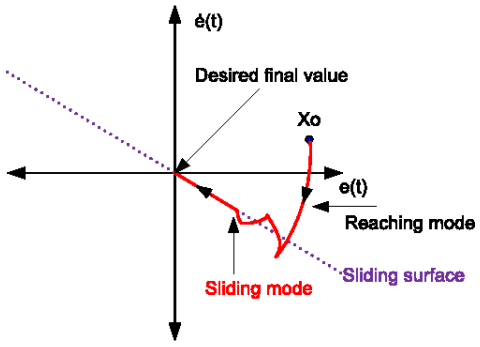

Figure 4.2: Reaching and Sliding Phases of SMC, [13]

Sliding surface design is performed to achieve the characteristics required from the system when sliding, [18]. It can be linear or nonlinear function of the states or error.

Control law design has the purpose of driving the system trajectories into the sliding manifold, and thereafter to maintain them within the sliding manifold despite uncertainties being present, [18]. It involves setting of conditions on the control law to make the sliding surface attractive. This is developed in two parts: reaching and sliding modes.

4.2.1 Switching Controller Design

Switching control denoted with, $U_{switching}$ and it tries to maintain system trajectories to approach the sliding manifold. It's used to make the sliding surface attractive. The time in reaching mode should be minimized as robustness to matched uncertainties isn't present. In this phase the system dynamics governs the control.

Switching control is designed based on reaching law method using Lyapunove's direct method for stability analysis without solving the differential equations. Lyapunove states that if a positive definite function, V is taken, its time derivative along system trajectories must be negative to-be stable. This is achieved by designing a control, $U_{switching}$ on one of the following: constant rate, exponential or power rate reaching laws.

4.2.2 Equivalent Controller Design

The control law which maintains the sliding motion is called equivalent controller denoted with $U_{equivalent}$. Sliding motion is the motion when the system trajectories are confined within the sliding manifold. It's calculated from equating the r^{th} order derivative of the sliding variable to zero for an r^{th} order sliding mode control design. This isn't the actual control applied but represents the average sense of the applied control.

4.2.3 Twisting Sliding Mode Control

The existence of chattering, due to the discontinuous control action affect the stability of the control system and even lead to system oscillation, instability, and other serious consequences. It is needed to optimize the traditional SMC to reduce the chattering problem. The commonly used methods to suppress chattering include quasi-sliding mode, filtering, and higher-order sliding mode methods, [31].

In quasi-sliding mode and filtering the main idea is to change the state dynamics in a small vicinity of the discontinuity surface in order to avoid real discontinuity and at the same time to preserve the main properties of the whole system, [24]. However,the ultimate accuracy and robustness of the sliding mode are partially lost, [24]. Saturation, relay and tan-hyperbolic are recommended quasi-SMC algorithms, [31].

The higher-order sliding mode is improved on the basis of the traditional sliding mode, which makes the r-order sliding surface converge in finite time for $r \geq 2$. Therefore, the higher order SMC can't only keep the advantages of simple and strong robustness of the traditional SMC but also greatly reduce the chattering of the system and improve the control accuracy. Twisting, super-twisting and dynamic SMC are some of higher order.

In this thesis the twisting SMC was developed for inertial position, attitude and air-speed control. Since the chattering is not completely removed by the twisting algorithm, saturation was also applied in attitude. Let the sliding surface be denoted with variable ξ, then the overall proposition set by equ. 4.1, where: i=1,...,13 and k_i-switching gain.

$$\begin{aligned} e_{(t)} &= r_{(t)} - y_{(t)} \\ \xi_{(t)} &= k_p e_{(t)} \\ U_{switching} &= k_i sgn(\xi) + k_{i+1} sgn(\dot{\xi}) \end{aligned} \tag{4.1}$$

4.2.4 Fuzzy Switching Surface

The twisting and saturation approaches in the switching items have trade-off between chattering and robustness in large mathematical computing system models. So to tackle this trade-off fuzzy based switching items developed for inertial positions, and airspeed control of FW-UAV, due to its inherent advantages of good robustness. This approach reduces the effect of wind gust disturbances, which come into effect across the speed and position model of most FW-UAVs. Where: i=7,...,13.

$$U_{switching} = k_i Fuzzy(n_{i-6}\xi) + k_{i+1} Fuzzy(n_{i-5}\dot{\xi}) \tag{4.2}$$

The same membership functions are selected for the switching items of position (x, y, z) and airspeed (V_a) controllers. The fuzzy outputs are determined by the normalized surface 'ξ' and '$\dot{\xi}$', see equ. 4.2, [1]. In fuzzy setting there are two main process; fuzzification and defuzzification.

[1] Where;
k_i=switching gain for ξ, k_{i+1}=switching gain for $\dot{\xi}$, n_{i-6}=normalizing gain for ξ, n_{i-5}=normalizing gain for $\dot{\xi}$, ξ=sliding surface, k_p=proportional gain of sliding surface, $e_{(t)}$=error dynamics, $r_{(t)}$=reference and $y_{(t)}$=output

Fuzzification is the process of transforming the real values of the variables ξ and $\dot{\xi}$ into defined fuzzy set membership values. Both ξ and $\dot{\xi}$ are fuzzified with the same type of seven membership functions, single input-output, triangular fuzzy rules, fig. 4.3. Mamdani is the inference method that relates the conditional statements in fuzzy rules. Input-output fuzzy rules are defined in tab. 4.1, 4.2, where [2].

Table 4.1: Fuzzy Rule Bases for ξ

ξ :	NB	NM	NS	Z	PS	PM	PB
$Fuzzy(n_{i-6}\xi)$:	NB	NM	NS	Z	PS	PM	PB

Table 4.2: Fuzzy Rule Bases for $\dot{\xi}$

$\dot{\xi}$:	NB	NM	NS	Z	PS	PM	PB
$Fuzzy(n_{i-5}\dot{\xi})$:	NB	NM	NS	Z	PS	PM	PB

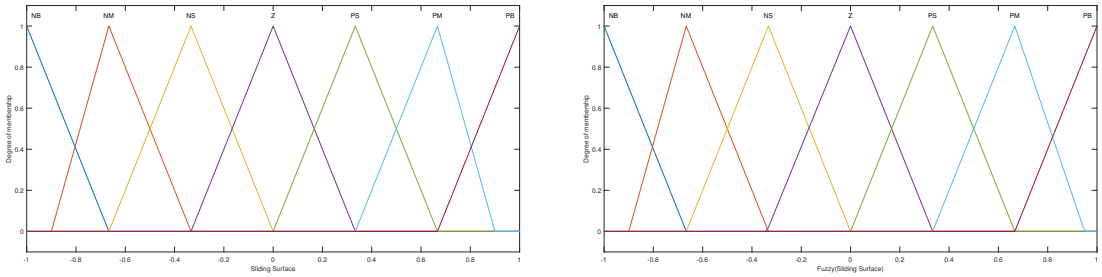

(a) Input membership functions **(b)** Output membership functions

Figure 4.3: Graphical plot of triangular membership functions

De-fuzzification is the process of obtaining a single number from the output of the aggregated fuzzy set. It's a decision-making algorithm that selects the best crisp value (human readable language) based on a fuzzy set. "Centroid" defuzzification method was adopted in both 'ξ' and '$\dot{\xi}$' fuzzy inferences. Note that both normalized 'ξ' and '$\dot{\xi}$' fuzzy settings are performed on similar functions, throughout all switching of respective states. i.e. The membership functions in fig. 4.3 are for both 'ξ' and '$\dot{\xi}$'.

[2] Fuzzy Rule Nomenclatures are: NB= negative big, NM= negative medium, NS= negative small Z= zero, PS= positive small, PM= positive medium, PB= positive big

4.3 Attitude Controller Design

The three attitudes angles are the main state variables which are going to-be discussed. The desire is to control each state explicitly i.e ϕ with U_1, θ with U_2, and ψ with U_3.

$$\begin{aligned}\dot{\phi} &= p + qs_\phi t_\theta + rc_\phi t_\theta \\ \dot{\theta} &= qc_\phi - rs_\phi \\ \dot{\psi} &= qs_\phi S_\theta + rc_\phi S_\theta\end{aligned} \tag{4.3}$$

To find the control commands U_1, U_2 and U_3 for explicit control in the attitude model of the equations above let's find the time derivative of equ. 4.3 using, Chain rule;

$$\begin{aligned}\ddot{\phi} &= \dot{p} + \dot{q}s_\phi t_\theta + \dot{r}c_\phi c_\theta + (qc_\phi t_\theta - rs_\phi c_\theta)\dot{\phi} + (qs_\phi + rc_\phi)S_\theta^2\dot{\theta} \\ \ddot{\theta} &= \dot{q}c_\phi - \dot{r}s_\phi - (qs_\phi + rc_\phi)\dot{\phi} \\ \ddot{\psi} &= \dot{q}s_\phi S_\theta + \dot{r}c_\phi S_\theta + (qc_\phi - rs_\phi)S_\theta\dot{\phi} + (qs_\phi + rc_\phi)S_\theta t_\theta\dot{\theta}\end{aligned} \tag{4.4}$$

As it's seen from equ. 4.3 and 4.4, all kinematic and dynamic models of the attitudes are very complex. To simplify the control process, it is necessary to decouple the mathematical models before designing the attitude controllers [3]. Decoupling is the process that mainly extracts the dominant state quantity and control signal in the control process and treat the remaining control quantities as uncertainty [12]. Note that decoupling is done to find the second order time derivative of the interest state variable, ($\phi^{(2)}$, $\theta^{(2)}$, $\psi^{(2)}$).

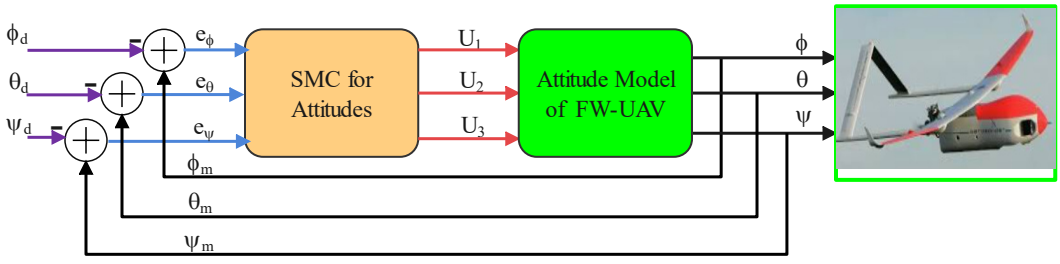

Figure 4.4: Attitude Controller Diagram

[3] Aerodynamic constants are
$C_l = C_{l_0} + C_{l_\alpha}\alpha + C_{l_q}\frac{C}{2V_a}q + C_{l_{\gamma_e}}U_2, C_d = C_{d_0} + C_{d_\alpha}\alpha + C_{d_q}\frac{C}{2V_a}q + C_{d_{\gamma_e}}U_2, C_y = C_{y_0} + C_{y_\alpha}\alpha + C_{y_q}\frac{C}{2V_a}q + C_{y_{\gamma_e}}U_2, C_Y = C_{Y_0} + C_{Y_\beta}\beta + C_{Y_p}\frac{B}{2V_a}p + C_{Y_r}\frac{B}{2V_a}r + C_{Y_{\gamma_a}}U_1 + C_{Y_{\gamma_r}}U_3, C_x = C_{x_0} + C_{x_\beta}\beta + C_{x_p}\frac{B}{2V_a}p + C_{x_r}\frac{B}{2V_a}r + C_{x_{\gamma_a}}U_1 + C_{x_{\gamma_r}}U_3, C_z = C_{z_0} + C_{z_\beta}\beta + C_{z_p}\frac{B}{2V_a}p + C_{z_r}\frac{B}{2V_a}r + C_{z_{\gamma_a}}U_1 + C_{z_{\gamma_r}}U_3$

4.3.1 Twisting SMC Design for Roll Angle

The state variable ϕ is influenced by all the control signals as seen from it's state space model. The desire is to control ϕ with U_1 as the main controller and take the others effect as uncertainty, decoupling. Let's start from the following equation.

$$\dot{\phi} = p + qs_\phi t_\theta + rc_\phi t_\theta \tag{4.5}$$

In most flight conditions, θ is small [4], can be approximated as ($t_\theta \approxeq \theta \approxeq 0$). This leads that the primary influence on $\dot{\phi}$ can be taken as p, so others are considered as uncertainty, resulting the state space equ. 4.6.

$$\begin{aligned} \dot{\phi} &= p + qs_\phi t_\theta + rc_\phi t_\theta \approxeq p + d_\Phi \\ \ddot{\phi} &= \dot{p} + \dot{d}_\Phi \end{aligned} \tag{4.6}$$

Using the expression $p = \dot{\phi} - d_\Phi$, the second order differential equation for ϕ simplified as follows in equ. 4.7. The variables ϕ and U_1 will be the dominant state variables in roll angle control.

$$\begin{aligned} \ddot{\phi} &= \frac{1}{2}J_0\rho V_a^2 SB(J_z C_x + J_{xz}C_z) - J_0 J_z K_M k_\Omega^2 U_4^2 + J_0 pq J_{xz}(J_x - J_y + J_z) + \dot{d}_\Phi \\ &= \frac{1}{2}J_0\rho V_a^2 SB(c_1 + c_2(\dot{\phi} - d_\phi) + c_3 U_1) - J_0 J_z K_M k_\Omega^2 U_4^2 + J_0 pq J_{xz}(J_x - J_y + J_z) + \dot{d}_\Phi \\ &= \frac{1}{2}J_0\rho V_a^2 SBc_2\dot{\phi} + \frac{1}{2}J_0\rho V_a^2 SBc_3 U_1 + \frac{1}{2}J_0\rho V_a^2 SB(c_1 - c_2 d_\phi) + J_0 pq J_{xz}(J_x - J_y + J_z) \\ &- J_0 J_z K_M k_\Omega^2 U_4^2 + \dot{d}_\Phi \end{aligned} \tag{4.7}$$

Simplified decoupled state equation for ϕ using the constants defined in footnote [4].

$$\begin{aligned} \dot{x}_1 &= \dot{\phi} = x_2 \\ \dot{x}_2 &= \ddot{\phi} = c_4\dot{\phi} + c_5 U_1 + d_\phi = c_4 x_2 + c_5 U_1 + d_\phi \end{aligned} \tag{4.8}$$

[4] The constant symbols used in roll control are defined as;
$d_\Phi = qs_\phi t_\theta + rc_\phi t_\theta, J_1 = (J_z + J_{xz}), J_2 = (J_x + J_{xz})$
$c_1 = J_z(C_{x_0} + C_{x_\beta}\beta + C_{x_r}\frac{B}{2V_a}r + C_{x_{\gamma_r}}U_3) + J_{xz}(C_{z_0} + C_{z_\beta}\beta + C_{z_r}\frac{B}{2V_a}r + C_{z_{\gamma_r}}U_3)$
$c_2 = J_z C_{x_p}\frac{B}{2V_a} + J_{xz}C_{z_p}\frac{B}{2V_a}, c_3 = J_z C_{x_{\gamma_a}} + J_{xz}C_{z_{\gamma_a}}, c_4 = \frac{1}{2}J_0\rho V_a^2 SBc_2, c_5 = \frac{1}{2}J_0\rho V_a^2 SBc_3$
$d_\phi = \frac{1}{2}J_0\rho V_a^2 SB(c_1 - c_2 d_\Phi) - J_0 J_z K_M k_\Omega^2 U_4^2 + J_0 pq J_{xz}(J_x - J_y + J_z) + \dot{d}_\Phi$

Let us treat c_4x_2 and c_5 as known nonlinear functions, $x_1 \in R^n$, $x_2 \in R$, $U_1 \in R$ and d_ϕ unknown interference (until computed from the model) with magnitude $|d_\Phi| \leq D_\phi$, $c_5 > 0$. Defining the desired roll angle with ϕ_d, systematic error by $(e = \phi - \phi_d)$ and $(z_1 = e,\ z_2 = \dot{e})$, the error dynamics;

$$\begin{aligned} \dot{z}_1 &= \dot{\phi} - \dot{\phi}_d = z_2 \\ \dot{z}_2 &= \ddot{\phi} - \ddot{\phi}_d \end{aligned} \tag{4.9}$$

Using model of equ. 4.8 and 4.9, the sliding variable ξ_Φ and surface defined as $\xi_\Phi = z_1$. Apply the reaching law of SMC design at the sliding manifold to find $U_{switching}$.

$$\begin{aligned} \dot{\xi}_\Phi &= \dot{z}_1 = z_2 \\ \ddot{\xi}_\Phi &= \dot{z}_2 = \ddot{\phi} - \ddot{\phi}_d = c_4\dot{\phi} + c_5U_1 + d_\phi - \ddot{\phi}_d = c_4x_2 + c_5U_1 + d_\phi - \ddot{\phi}_d \end{aligned} \tag{4.10}$$

The switching controller, $U_{switching} = -k_1 sgn(\xi_\Phi) - k_2 sgn(\dot{\xi}_\Phi)$ with constant rate reaching law is developed based on the Lyapunove function $V_{\xi_\Phi} = \frac{\xi_\Phi^2 + \dot{\xi}_\Phi^2}{2}$ that satisfies the negative definiteness of the function.

$$\begin{aligned} \dot{V}_{\xi_\Phi} &= \xi_\Phi\dot{\xi}_\Phi + \dot{\xi}_\Phi\ddot{\xi}_\Phi = z_1z_2 + z_2(c_4x_2 + c_5(-k_1sgn(z_1) - k_2sgn(z_2)) + d_\phi - \ddot{\phi}_d) \\ &= z_1z_2 - k_1c_5z_2sgn(z_1) + (-k_2c_5z_2sgn(z_2) + c_4z_2x_2 + z_2d_\phi - z_2\ddot{\phi}_d) \\ &= z_1z_2 - k_1c_5|z_1| + (-k_2c_5|z_2| + c_4z_2x_2 + z_2d_\phi - z_2\ddot{\phi}_d) \end{aligned} \tag{4.11}$$

Apply small signal approximation around the origin $z_1 \approxeq z_2 \approxeq \dot{z}_1 \approxeq 0$ for simplification. Then for asymptotic stability the design parameters (gains) must satisfy the conditions $k_2 > |(c_4x_2 + d_\phi - \ddot{\phi}_d)z_2| > 0$ and $k_1 > k_2 + |z_1z_2|$, provided that c_5 is positive.
The equivalent controller from $\ddot{\xi}_\Phi = 0$ and complete twisting-SMC for ϕ become;

$$U_{equivalent} = \frac{1}{c_5}(\ddot{\phi}_d - c_4x_2 - d_\phi) \tag{4.12}$$

$$U_1 = U_{switching} + U_{equivalent} = -k_1sgn(\xi_\Phi) - k_2sgn(\dot{\xi}_\Phi) + \frac{1}{c_5}(\ddot{\phi}_d - c_4x_2 - d_\phi) \tag{4.13}$$

4.3.2 Twisting SMC Design for Pitch Angle

In longitudinal dynamics the main control signals that influence are U_2 and U_4. However U_2 will be used to directly influence the pitch angle, θ in this controller design.

$$\dot{\theta} = qc_\phi - rs_\phi \tag{4.14}$$

Pitch rate given by equ. 4.14 simplified using small angle assumption as in equ 4.15.

$$\dot{\theta} = q + q(c_\phi - 1) - rs_\phi = q + d_\Theta \tag{4.15}$$

In chapter 3 α was defined as the drift angle from the pitch plane by flight path angle, denote by ϵ, which is small deviation from SF. This results the expression $\alpha = \theta - \epsilon$. Using this assumption with $q = \dot{\theta} - d_\Theta$ time derivative of equ. 4.15 simplified as follows.

$$\begin{aligned}
\ddot{\theta} = \dot{q} + \dot{d}_\Theta &= \frac{1}{J_y}(\frac{1}{2}\rho V_a^2 CSC_y + pr(J_z - J_x) + J_{xz}(r^2 - p^2)) + \dot{d}_\Theta \\
&= \frac{1}{2J_y}\rho V_a^2 CS(C_{y_0} + C_{y_\alpha}\alpha + C_{y_q}\frac{C}{2V_a}q + C_{y_{\gamma_e}}U_2) + \frac{pr}{J_y}(J_z - J_x) + \frac{J_{xz}}{J_y}(r^2 - p^2) + \dot{d}_\Theta \\
&= \frac{1}{2J_y}\rho V_a^2 CS(C_{y_0} + C_{y_\alpha}(\theta - \epsilon) + C_{y_q}\frac{C}{2V_a}(\dot{\theta} - d_\Theta) + C_{y_{\gamma_e}}U_2) \\
&+ \frac{pr}{J_y}(J_z - J_x) + \frac{J_{xz}}{J_y}(r^2 - p^2) + \dot{d}_\Theta
\end{aligned} \tag{4.16}$$

$\ddot{\theta}$ described as a function of θ, $\dot{\theta}$ and U_2 with treating all the other components as uncertainty, d_θ and defining the constants, [5] .

$$\ddot{\phi} = c_6\theta + c_7\dot{\theta} + c_8U_2 + d_\theta \tag{4.17}$$

Simplified decoupled pitch state equation written in equ. 4.18 using, ($x_3 = \theta$, $x_4 = \dot{\theta}$).

$$\dot{x}_3 = x_4, \quad \dot{x}_4 = c_6\theta + c_7\dot{\theta} + c_8U_2 + d_\theta = c_6x_3 + c_7x_4 + c_8U_2 + d_\theta \tag{4.18}$$

[5] $d_\Theta = q(c_\phi - 1) - rs_\phi, c_6 = \frac{1}{2J_y}\rho V_a^2 CSC_{y_\alpha}, c_7 = \frac{1}{4J_y}\rho V_a C^2 SC_{y_q}, c_8 = \frac{1}{2J_y}\rho V_a^2 CSC_{y_{\gamma_e}}$
$d_\theta = \frac{1}{2J_y}\rho V_a^2 CS(C_{y_0} - C_{y_\alpha}\epsilon - C_{y_q}\frac{C}{2V_a}d_\Theta) + \frac{pr}{J_y}(J_z - J_x) + \frac{J_{xz}}{J_y}(r^2 - p^2) + \dot{d}_\Theta$

Let c_6x_3, c_7x_4 and c_8 be known nonlinear functions, $x_3 \in R^n$, $x_4 \in R$, $U_2 \in R$ and d_θ unknown interference (until computed from the model) with magnitude $|d_\theta| \leq D_\theta$, and $c_8 > 0$. Defining the desired pitch angle with θ_d, systematic error by $(e = \theta - \theta_d)$ and $(z_3 = e,\ z_4 = \dot{e})$, the error dynamics;

$$\begin{aligned} \dot{z}_3 &= z_4 \\ \dot{z}_4 &= \ddot{\theta} - \ddot{\theta}_d \end{aligned} \tag{4.19}$$

Using equ. 4.18 and 4.19, the sliding variable ξ_Θ and surface defined as $\xi_\Theta = z_3$. Apply the reaching law of SMC design at the sliding manifold to find $U_{switching}$.

$$\begin{aligned} \dot{\xi}_\Theta &= \dot{z}_3 = z_4 \\ \ddot{\xi}_\Theta &= \dot{z}_4 = \ddot{\theta} - \ddot{\theta}_d \ \ = c_6x_3 + c_7x_4 + c_8U_2 + d_\theta - \ddot{\theta}_d \end{aligned} \tag{4.20}$$

The discontinuous controller $U_{switching} = -k_3 sgn(\xi_\Theta) - k_4 sgn(\dot{\xi}_\Theta)$ is developed using Lyapunove function $V_{\xi_\Theta} = \frac{\xi_\Theta^2 + \dot{\xi}_\Theta^2}{2}$.

$$\begin{aligned} \dot{V}_{\xi_\Theta} &= \xi_\Theta\dot{\xi}_\Theta + \dot{\xi}_\Theta\ddot{\xi}_\Theta = z_3z_4 + z_4(c_6x_3 + c_7x_4 + c_8(-k_3 sgn(\xi_\Theta) - k_4 sgn(\dot{\xi}_\Theta)) + d_\theta - \ddot{\theta}_d) \\ &= z_3z_4 - k_3c_8z_4 sgn(\xi_\Theta) + (-k_4c_8 sgn(\dot{\xi}_\Theta) + c_6x_3 + c_7x_4 + d_\theta - \ddot{\theta}_d)z_4 \\ &= z_3z_4 - k_3c_8|z_3| + (-k_4c_8|z_4| + (c_6x_3 + c_7x_4 + d_\theta - \ddot{\theta}_d)z_4) \end{aligned} \tag{4.21}$$

For asymptotic stability, to make $\dot{V}_{\xi_\Theta}$ negative definite the design parameters must satisfy the conditions, $k_4 > |(c_6x_3 + c_7x_4 + d_\theta - \ddot{\theta}_d)z_4)| > 0$ and $k_3 > k_4 + |z_3z_4|$, provided that c_8 is positive. The equivalent controller $U_{equivalent}$ from $\ddot{\xi}_\Theta = 0$ for θ became:

$$U_{equivalent} = \frac{1}{c_8}(\ddot{\theta}_d - c_6x_3 - c_7x_4 - d_\theta) \tag{4.22}$$

The complete twisting-SMC for pitch will be;

$$U_2 = U_{switching} + U_{equivalent} = -k_3 sgn(\xi_\Theta) - k_4 sgn(\dot{\xi}_\Theta) + \frac{1}{c_8}(\ddot{\theta}_d - c_6x_3 - c_7x_4 - d_\theta) \tag{4.23}$$

4.3.3 Twisting SMC Design for Yaw Angle

Starting from equ. 4.24 decoupled state equation is developed using ψ and U_3.

$$\dot{\psi} = qs_{\phi}S_{\theta} + rc_{\phi}S_{\theta} \tag{4.24}$$

To remove the effect of coupling from roll and pitch angles let's rearrange the above equation with the possibility of canceling as disturbance through small angle approximation.

$$\dot{\psi} = r + r(c_{\phi}S_{\theta} - 1) + qs_{\phi}S_{\theta} = r + d_{\Psi} \tag{4.25}$$

Differentiating equ. 4.25 w.r.t time the 2nd order differential equation for ψ becomes;

$$\begin{aligned}
\ddot{\psi} = \dot{r} + \dot{d}_{\Psi} &= J_0(\frac{J_{xz}}{2}\rho V_a^2 SBC_x - J_{xz}K_M k_{\Omega}^2 U_4^2) + J_0(\frac{J_x}{2}\rho V_a^2 SBC_z) \\
&+ J_0 pq(J_{xz}^2 + J_x^2 - J_x J_y) + J_0 qr J_{xz}(J_y - J_x - J_z) + \dot{d}_{\Psi} \\
&= \frac{J_0}{2}\rho V_a^2 SB(J_{xz}C_x + J_x C_z) + J_0 pq(J_{xz}^2 + J_x^2 - J_x J_y) \\
&+ J_0 qr J_{xz}(J_y - J_x - J_z) - J_0 K_M k_{\Omega}^2 U_4^2 + \dot{d}_{\Psi} \\
&= \frac{J_0}{2}\rho V_a^2 SB(c_9 + c_{10}\dot{\psi} + c_{11}U_3) + J_0 pq(J_{xz}^2 + J_x^2 - J_x J_y) \\
&+ J_0 qr J_{xz}(J_y - J_x - J_z) - J_0 K_M k_{\Omega}^2 U_4^2 + \dot{d}_{\Psi}
\end{aligned} \tag{4.26}$$

For decoupled control of ψ through U_3 the variables C_x and C_z have to-be explicitly included in $\ddot{\psi}$ as in equ. 4.26. So $\ddot{\psi}$ can be described as a function of $\dot{\psi}$ and U_3 with treating all the other components by uncertainty d_{ψ} where the constants defined in [6] .

$$\dot{\psi} = c_{12}\dot{\psi} + c_{13}U_3 + d_{\psi} \tag{4.27}$$

Defining states ($x_5 = \psi$, $x_6 = \dot{\psi}$), the decoupled yaw state equation is expressed as;

$$\dot{x}_5 = x_6, \quad \dot{x}_6 = c_{12}x_6 + c_{13}U_3 + d_{\psi} \tag{4.28}$$

[6] The constant symbols used in yaw control are defined as;
$c_9 = J_{xz}(C_{x_0} + C_{x_\beta}\beta + C_{x_p}\frac{B}{2V_a}p - C_{x_r}\frac{B}{2V_a}d_{\Psi} + C_{x_{\gamma_a}}U_1) + J_x(C_{z_0} + C_{z_\beta}\beta + C_{z_p}\frac{B}{2V_a}p - C_{z_r}\frac{B}{2V_a}d_{\Psi} + C_{z_{\gamma_a}}U_1)$
$d_{\Psi} = r(c_{\phi}S_{\theta} - 1) + qs_{\phi}S_{\theta}, c_{10} = (J_{xz}C_{x_r}\frac{B}{2V_a} + J_x C_{z_r}\frac{B}{2V_a}), c_{11} = (J_{xz}C_{x_{\gamma_r}} + J_x C_{z_{\gamma_r}}), c_{12} = \frac{J_0}{2}\rho V_a^2 SBc_{10}$
$c_{13} = \frac{J_0}{2}\rho V_a^2 SBc_{11}, d_{\psi} = \frac{J_0}{2}\rho V_a^2 SBc_9 - J_0 K_M k_{\Omega}^2 U_4^2 + J_0 pq(J_{xz}^2 + J_x^2 - J_x J_y) + J_0 qr J_{xz}(J_y - J_x - J_z) + \dot{d}_{\Psi}$

Let $c_{12}x_6$ and c_{13} be known nonlinear functions, $x_5 \in R^n$, $x_6 \in R$, $U_3 \in R$ and d_ψ unknown interference (until computed from the model) with magnitude $|d_\psi| \leq D_\psi$, $c_{13} > 0$. For trajectory tracking let's transform equ. 4.28 into error dynamic state space form, by defining the desired yaw angle as ψ_d, systematic error by $(e = \psi - \psi_d)$ and $(z_5 = e,$ $z_6 = \dot{e})$.

$$\dot{z}_5 = z_6, \quad \dot{z}_6 = \ddot{\psi} - \ddot{\psi}_d \tag{4.29}$$

Using the equ. 4.28, and 4.29, the sliding variable ξ_Ψ and surface for SMC defined as:

$$\xi_\Psi = z_5 \tag{4.30}$$

Apply the reaching law of SMC design at the sliding manifold to find $U_{switching}$.

$$\begin{aligned} \dot{\xi}_\Psi &= \dot{z}_5 = z_6 \\ \ddot{\xi}_\Psi &= \dot{z}_6 = \ddot{\psi} - \ddot{\psi}_d \quad = c_{12}\dot{\psi} + c_{13}U_3 + d_\psi - \ddot{\psi}_d = c_{12}x_6 + c_{13}U_3 + d_\psi - \ddot{\psi}_d \end{aligned} \tag{4.31}$$

$U_{switching} = -k_5 sgn(\xi_\Psi) - k_6 sgn(\dot{\xi}_\Psi)$ is designed to make $V_{\xi_\Psi} = \frac{\xi_\Psi^2 + \dot{\xi}_\Psi^2}{2}$ negative definite.

$$\begin{aligned} \dot{V}_{\xi_\Psi} &= \xi_\Psi\dot{\xi}_\Psi + \dot{\xi}_\Psi\ddot{\xi}_\Psi = z_5 z_6 + z_6(c_{12}x_6 + c_{13}(-k_5 sgn(\xi_\Psi) - k_6 sgn(\dot{\xi}_\Psi)) + d_\psi - \ddot{\psi}_d) \\ &= z_5 z_6 - k_5 c_{13} z_6 sgn(z_5) + (-k_6 c_{13} z_6 sgn(z_6) + c_{12} z_6 x_6 + z_6 d_\psi - z_6\ddot{\psi}_d) \\ &= z_5 z_6 - k_5 c_{13}|z_5| + (-k_6 c_{13}|z_6| + (c_{12}x_6 + d_\psi - \ddot{\psi}_d)z_6) \end{aligned} \tag{4.32}$$

For asymptotic stability $k_6 > |(c_{12}x_6 + d_\psi - \ddot{\psi}_d)z_6| > 0$ and $k_5 > k_6 + |z_5 z_6|$ must be satisfied, provided that c_{13} is positive. Then the equivalent controller for ψ is solved from the equation $\ddot{\xi}_\Psi = 0$.

$$U_{equivalent} = \frac{1}{c_{13}}(\ddot{\psi}_d - c_{12}x_6 - d_\psi) \tag{4.33}$$

The complete twisting-SMC for yaw is given by;

$$U_3 = U_{switching} + U_{equivalent} = -k_5 sgn(\xi_\Psi) - k_6 sgn(\dot{\xi}_\Psi) + \frac{1}{c_{13}}(\ddot{\psi}_d - c_{12}x_6 - d_\psi) \tag{4.34}$$

4.4 Airspeed Controller Design

The airspeed is given by equ. 3.42 in the BF. The desire is designing airspeed controller which operates in such a way that velocities other than the x-axis are treated as disturbances, because it's in the longitudinal model. Owing this, V_a can be modelled as;

$$V_a = V_{a_x} + d_A = u - u_w + d_A \tag{4.35}$$

The time derivative of equ. 4.35 is given by;

$$\dot{V}_a = \dot{u} - \dot{u}_w + \dot{d}_A \tag{4.36}$$

This can be proved that for small angle approximation about deflection angle and side slip we can have reduced equations for real $\dot{V}_a = \dot{V}_{a_x} c_\alpha c_\beta + \dot{V}_{a_y} s_\beta + \dot{V}_{a_z} s_\alpha c_\beta$. Further simplified using the constants defined in [7] as below.

$$\begin{aligned}
\dot{V}_a &= \frac{1}{2m}\rho V_a^2 S(C_l s_\alpha - C_d c_\alpha) + \frac{1}{2m}\rho S_P C_P (k_m^2 U_4^2 - V_a^2) - g s_\theta + rv - qw - \dot{u}_w + \dot{d}_A \\
\ddot{V}_a &= c_{14} V_a \dot{V}_a + c_{15} \dot{V}_a + c_{16} U_4 \dot{U}_4 + d_{V_a}
\end{aligned} \tag{4.37}$$

Now it's time to find the second order differential equation for V_a, Where the total uncertainty in equ. 4.38 is defined by d_V.

$$\ddot{V}_a = c_{14} V_a + c_{15} \dot{V}_a + c_{16} U_4 + d_V \tag{4.38}$$

Defining the states by ($x_7 = V_a$, $x_8 = \dot{V}_a$), decoupled airspeed state equation expressed in simplified form given by equ. 4.39.

$$\begin{aligned}
\dot{x}_7 &= x_8 \\
\dot{x}_8 &= c_{14} x_7 + c_{15} x_8 + c_{16} U_4 + d_V
\end{aligned} \tag{4.39}$$

[7] $c_{14} = \frac{1}{2m}\rho V_a^2 S[(C_{l_0} s_\alpha - C_{d_0} c_\alpha) + (C_{l_\alpha} s_\alpha - C_{d_\alpha} c_\alpha)\alpha + (C_{l_{\gamma_e}} s_\alpha - C_{d_{\gamma_e}} c_\alpha) U_2] - \frac{1}{2m}\rho S_P C_P$
$c_{15} = \frac{1}{4m}\rho S C (C_{l_q} s_\alpha - C_{d_q} c_\alpha) q, c_{16} = \frac{1}{m}\rho S_P C_P k_m^2$
$d_A = \dot{V}_{a_y} s_\beta + \dot{V}_{a_z} s_\alpha c_\beta, d_{V_a} = \frac{d}{dt}(-g s_\theta + rv - qw - \dot{u}_w + \dot{d}_A), d_V = d_{V_a} + c_{14} V_a (\dot{V}_a - 1) + c_{16} U_4 (\dot{U}_4 - 1)$

Let $c_{14}x_7$, $c_{15}x_8$, and c_{16} be known nonlinear functions, $x_7 \in R^n$, $x_8 \in R$, $U_4 \in R$ and d_V unknown interference (until computed from the model) with magnitude $|d_V| \leq D_V$, $c_{16} > 0$. Defining the desired airspeed with V_d, systematic error by ($e = V_a - V_d$) and ($z_7 = e$, $z_8 = \dot{e}$), the error dynamics in state space will be;

$$\dot{z}_7 = z_8, \quad \dot{z}_8 = c_{14}x_7 + c_{15}x_8 + c_{16}U_4 + d_V - \ddot{V}_d \tag{4.40}$$

4.4.1 Twisting SMC to Airspeed

Using the state-space models from equ. 4.39 and 4.40, the sliding variable ξ_A and surface for SMC defined as $\xi_A = z_7$.

Now apply the reaching law of SMC design at the sliding manifold to find $U_{switching}$.

$$\begin{aligned} \dot{\xi}_A &= \dot{z}_7 = z_8 \\ \ddot{\xi}_A &= \dot{z}_8 = c_{14}x_7 + c_{15}x_8 + c_{16}U_4 + d_V - \ddot{V}_d \end{aligned} \tag{4.41}$$

The discontinuous controller $U_{switching} = -k_7 sgn(\xi_A) - k_8 sgn(\dot{\xi}_A)$ is selected to make the Lyapunove function $V_{\xi_A} = \frac{\xi_A^2 + \dot{\xi}_A^2}{2}$ asymptotically stable.

$$\begin{aligned} \dot{V}_{\xi_A} &= \xi_A\dot{\xi}_A + \dot{\xi}_A\ddot{\xi}_A = z_7 z_8 + z_8(c_{14}x_7 + c_{15}x_8 + c_{16}U_4 + d_V - \ddot{V}_d) \\ &= z_7 z_8 - k_7 c_{16} z_8 sgn(z_7) + (-k_8 c_{16} z_8 sgn(z_8) + z_8(c_{14}x_7 + c_{15}x_8 + d_V - \ddot{V}_d)) \\ &= z_7 z_8 - k_7 c_{16}|z_7| + (-k_8 c_{16}|z_8| + z_8(c_{14}x_7 + c_{15}x_8 + d_V - \ddot{V}_d)) \end{aligned} \tag{4.42}$$

For asymptotic stability $k_8 > |z_8(c_{14}x_7 + c_{15}x_8 + d_V - \ddot{V}_d)| > 0$ and $k_7 > k_8 + |z_7 z_8|$ must be satisfied, provided that c_{16} is positive. The equivalent controller solved from $\ddot{\xi}_A = 0$ and complete twisting-SMC, U_4 for airspeed written in equ. 4.43, and 4.44 respectively.

$$U_{equivalent} = \frac{1}{c_{16}}(\ddot{V}_d - c_{14}x_7 - c_{15}x_8 - d_V) \tag{4.43}$$

$$U_4 = U_{switching} + U_{equivalent} = -k_7 sgn(\xi_A) - k_8 sgn(\dot{\xi}_A) + \frac{1}{c_{16}}(\ddot{V}_d - c_{14}x_7 - c_{15}x_8 - d_V) \tag{4.44}$$

4.5 Inertial Position Controller Design

The translational accelerations for the state vector derived from Newton second law of motion in IF can be computed as in the equ. 4.45 below, using the equ. 3.17.

$$\begin{aligned} m * (\ddot{x}, \ddot{y}, \ddot{z})^T &= F_g^I + F_a^I + F_p^I \\ m * (\ddot{x}, \ddot{y}, \ddot{z})^T &= (0, 0, mg)^T + R_B^I \circledast F_a^B + R_B^I \circledast f_{p_x}^B \end{aligned} \tag{4.45}$$

On simplification with aerodynamic force components considered as uncertainty, the acceleration model in state space given by 4.46, where notations are defined in [8].

$$\begin{aligned} \ddot{x} &= c_\theta c_\psi \frac{f_{p_x}}{m} + d_x \\ \ddot{y} &= c_\theta s_\psi \frac{f_{p_x}}{m} + d_y \\ \ddot{z} &= -s_\theta \frac{f_{p_x}}{m} + g + d_z \end{aligned} \tag{4.46}$$

Virtual acceleration control is developed and used as outer-loop because the FW-UAV is under actuated system, it isn't possible to control all of the seven DOF directly. The inner loop directly controls states ϕ, θ, ψ, and V_a. Virtual controller outputs U_x, U_y, and U_z are used to determine the desired attitude angles. Defining ($x_9 = x$, $x_{10} = \dot{x}$, $x_{11} = y$, $x_{12} = \dot{y}$, $x_{13} = z$, $x_{14} = \dot{z}$, $U_x = c_\theta c_\psi \frac{f_{px}}{m}$, $U_y = c_\theta s_\psi \frac{f_{px}}{m}$, $U_z = -s_\theta \frac{f_{px}}{m}$), equ. 4.46 rewritten as in equ. 4.47.

$$\begin{aligned} \dot{x}_{10} &= U_x + d_x \\ \dot{x}_{12} &= U_y + d_y \\ \dot{x}_{14} &= U_z + g + d_z \end{aligned} \tag{4.47}$$

Defining the desired positions with (x_d, y_d, z_d) then systematic error dynamics in state space become ($z_9 = x - x_d$, $z_{10} = \dot{x} - \dot{x}_d$, $z_{11} = y - y_d$, $z_{12} = \dot{y} - \dot{y}_d$, $z_{13} = z - z_d$, $z_{14} = \dot{z} - \dot{z}_d$). To design twisting SMC for virtual control let's define the sliding surfaces for x, y, and z in respective sequences as $\xi_x = z_9$, $\xi_y = z_{11}$, and $\xi_z = z_{13}$. Apply the

[8] $f_{p_x} = \frac{1}{2}\rho S_P C_P (k_m^2 \delta_t^2 - V_a^2), F_a^B = (F_{a_x}, F_{a_y}, F_{a_z})^T, F_{a_x} = \frac{1}{2}\rho V_a^2 S(C_l s_\alpha - C_d c_\alpha), F_{a_y} = \frac{1}{2}\rho V_a^2 S C_Y, F_{a_z} = -\frac{1}{2}\rho V_a^2 S(C_l c_\alpha + C_d s_\alpha), d_x = \frac{1}{m}(c_\theta c_\psi F_{a_x} + (s_\phi s_\theta c_\psi - s_\phi s_\psi)F_{a_y} + (c_\phi s_\theta c_\psi + s_\phi s_\psi)F_{a_z}), d_y = \frac{1}{m}(c_\theta s_\psi F_{a_x} + (s_\phi s_\theta s_\psi + c_\phi c_\psi)F_{a_y} + (c_\phi s_\theta s_\psi - s_\phi c_\psi)F_{a_z}), d_z = \frac{1}{m}(-s_\theta F_{a_x} + s_\phi c_\theta F_{a_y} + c_\phi c_\theta F_{a_z})$

reaching law at the respective sliding manifold to find U_x, U_y, and U_z.

$$\begin{aligned}
\dot{\xi}_x &= z_{10} = \dot{x} - \dot{x}_d, \quad \ddot{\xi}_x = \dot{z}_{10} = \ddot{x} - \ddot{x}_d = U_x + d_x - \ddot{x}_d \\
\dot{\xi}_y &= z_{12} = \dot{y} - \dot{y}_d, \quad \ddot{\xi}_y = \dot{z}_{12} = \ddot{y} - \ddot{y}_d = U_y + d_y - \ddot{y}_d \\
\dot{\xi}_z &= z_{14} = \dot{z} - \dot{z}_d, \quad \ddot{\xi}_z = \dot{z}_{14} = \ddot{z} - \ddot{z}_d = U_z + g + d_z - \ddot{z}_d
\end{aligned} \tag{4.48}$$

The equivalent controller for x from $\ddot{\xi}_x = 0$ becomes $U_{equivalent} = \ddot{x}_d - d_x$. Where as the total twisting SMC for x can be combined as in equ. 4.49.

$$U_x = -k_9 sgn(\xi_x) - k_{10} sgn(\dot{\xi}_x) + \ddot{x}_d - d_x \tag{4.49}$$

With similar approaches the y and z position virtual controllers become;

$$\begin{aligned}
U_y &= -k_{11} sgn(\xi_y) - k_{12} sgn(\dot{\xi}_y) + \ddot{y}_d - d_y \\
U_z &= -k_{13} sgn(\xi_z) - k_{14} sgn(\dot{\xi}_z) + \ddot{z}_d - g - d_z
\end{aligned} \tag{4.50}$$

From the virtual controllers we derive the desired Euler angles to achieve this algorithms. Solving for $\frac{f_{px}}{m}$ from equ. 4.46 results;

$$\frac{f_{p_x}}{m} = \frac{U_x}{c_\psi c_\theta} = \frac{U_y}{s_\psi c_\theta} = -\frac{U_z}{s_\theta} \tag{4.51}$$

Taking the middle two equations of 4.51 solve for desired yaw angle, ψ_d.

$$\psi_d = tan^{-1}(\frac{U_y}{U_x}) \tag{4.52}$$

From the last two equations of 4.51 solve for desired pitch angle, θ_d.

$$\theta_d = tan^{-1}(-c_{\psi_d}\frac{U_z}{U_x}) = tan^{-1}(-s_{\psi_d}\frac{U_z}{U_y}) \tag{4.53}$$

The propeller force is projected on IF along x, y, and z-axis as in equ. 4.46, so its BF component along the main flight axis (x-axis) is given by equ. 4.54.

$$f_{p_x} = m\sqrt{U_x^2 + U_y^2 + U_z^2} \tag{4.54}$$

Using the sliding surfaces and their derivatives from equ. 4.48 and the Lyapunove functions $V_{\xi_x} = \frac{\xi_x^2+\dot{\xi}_x^2}{2}$, $V_{\xi_y} = \frac{\xi_y^2+\dot{\xi}_y^2}{2}$ and $V_{\xi_z} = \frac{\xi_z^2+\dot{\xi}_z^2}{2}$ for x, y, and z respectively, the stability of virtual controllers verified as follows.

$$\begin{aligned}
\dot{V}_{\xi_x} &= \xi_x\dot{\xi}_x + \dot{\xi}_x\ddot{\xi}_x = z_9 z_{10} + z_{10}(U_x + d_x - \ddot{x}_d) \\
&= z_9 z_{10} + z_{10}(-k_9 sgn(\xi_x) - k_{10} sgn(\dot{\xi}_x) + d_x - \ddot{x}_d) \\
&= z_9 z_{10} - k_9 z_{10} sgn(z_9) - k_{10} z_{10} sgn(z_{10}) + z_{10}(d_x - \ddot{x}_d) \\
&= z_9 z_{10} - k_9|z_9| + (-k_{10}|z_{10}| + z_{10}(d_x - \ddot{x}_d)
\end{aligned} \tag{4.55}$$

$$\begin{aligned}
\dot{V}_{\xi_y} &= \xi_y\dot{\xi}_y + \dot{\xi}_y\ddot{\xi}_y = z_{11} z_{12} + z_{12}(U_y + d_y - \ddot{y}_d) \\
&= z_{11} z_{12} + z_{12}(-k_{11} sgn(\xi_y) - k_{12} sgn(\dot{\xi}_y) + d_y - \ddot{y}_d) \\
&= z_{11} z_{12} - k_{11} z_{12} sgn(z_{11}) - k_{12} z_{12} sgn(z_{12}) + z_{12}(d_y - \ddot{y}_d) \\
&= z_{11} z_{12} - k_{11}|z_{11}| + (-k_{12}|z_{12}| + z_{12}(d_y - \ddot{y}_d)
\end{aligned} \tag{4.56}$$

$$\begin{aligned}
\dot{V}_{\xi_z} &= \xi_z\dot{\xi}_z + \dot{\xi}_z\ddot{\xi}_z = z_{13} z_{14} + z_{14}(U_z + g + d_z - \ddot{z}_d) \\
&= z_{13} z_{14} + z_{14}(-k_{13} sgn(\xi_z) - k_{14} sgn(\dot{\xi}_z) + g + d_z - \ddot{z}_d) \\
&= z_{13} z_{14} - k_{13} z_{14} sgn(z_{13}) - k_{14} z_{14} sgn(z_{14}) + z_{14}(g + d_z - \ddot{z}_d) \\
&= z_{13} z_{14} - k_{13}|z_{13}| + (-k_{14}|z_{14}| + z_{14}(g + d_z - \ddot{z}_d)
\end{aligned} \tag{4.57}$$

For asymptotic stability $k_{10} > |(d_x - \ddot{x}_d)| > 0$, $k_9 > k_{10} + |z_9 z_{10}|$, $k_{12} > |(d_y - \ddot{y}_d)| > 0$, $k_{11} > k_{12} + |z_{11} z_{12}|$, $k_{14} > |(g + d_z - \ddot{z}_d)| > 0$, and $k_{13} > k_{14} + |z_{13} z_{14}|$ must be satisfied, provided that the error dynamics has small positive values for x, y and z states.

4.6 Optimization Algorithms

Optimization algorithms are methods used to find the input parameters to some defined cost function which result the best value satisfying prescribed tolerance or precondition to the cost. There are different varieties of algorithms such as simulated annealing, genetic algorithm, particle swarm, deep learning, branch bound, and evolutionary algorithms. They are used in many areas of study to find solutions that maximize or minimize study parameters (input resources).

4.6.1 Particle Swarm Optimization (PSO)

In this thesis particle swarm optimization (PSO) is applied for parameter tuning of discontinuous controller gains of twisting SMC and normalizing gains of fuzzy switching. It's selected due to it's faster speed, cheaper way, and simplicity, [29]. PSO is a population based stochastic approach, [5] and doesn't guarantee global convergence, but achieved by increasing the number of iterations, [29]. It's influenced by the following parameters.

- Swarm size is the number of particles in the population. An increased number of particles enable increased area of search space to be covered but increases also computational complexity. In literatures 10 to 30 particles are recommended.
- Neighborhood size defines the extent of social interaction within the swarm. It's recommended that starting the search with smaller size and increase proportionally with the number of iterations. This is because the smaller the neighborhoods, the less interaction occurs and more reliable convergence to optimal solutions.
- Inertia weight determines the contribution rate of a particle's previous velocity to its present time step velocity.
- Dimension of the search space is determined and compatible to the number of parameters that are needed to-be optimized in the objective function.
- Number of iterations are problem dependent parameters. Too few iterations may terminate the search prematurely. Where as too large number of iterations may add computational complexity, so it's selected in accordance with the problem size.
- Acceleration coefficients control the stochastic influence of the cognitive (c_1) and social learning (c_2) components on the overall velocity equation of each particle. (c_1) express a particle's confidence in itself and (c_2) with it's neighbors.

The current position of each particle is used to calculate the fitness value at that location. Each particle has three parameters, namely, position x, velocity v and the previous best positions p. In addition, the position of a particle that has the best fitness value is called global best position denoted with G.

During the searching process, the current positions of all particles are evaluated using the fitness function. The fitness value of each particle is then compared with the current position and the best position is stored in the previous best positions $p_{(i)}$. The converging rate to the optimal solution is highly constrained with the velocity of the particles. So, mostly the velocity is limited within ranges of maximum and minimum values but in this thesis it's initially generated randomly.

The position and velocity of all particles are changed iteratively until it reaches a predefined stopping criterion, [3] which is the number of iterations in this thesis. The new positions of all particles are then calculated by adding the velocity and the current position of that particle as in equ. 4.58, where [9].

$$\begin{aligned} x_{(t+1)} &= x_{(t)} + v_{(t+1)} \\ v_{(t+1)} &= wv_{(t)} + c_1 r_1 (p_{(t)} - x_{(t)}) + c_2 r_2 (G - x_{(t)}) \end{aligned} \tag{4.58}$$

4.6.2 Cost Function used in PSO

In this thesis the main concern is how the desired trajectories are followed by the actual trajectories in FW-UAV flight control. So the cost function was designed to take error dynamics as an argument. Control Engineers found different sets of performance indexes which rely on the error dynamics in trajectory tracking, [9]; integral squared error, integral time squared error, integral absolute error and integral time absolute error (ITAE). ITAE penalize large initial error lightly and error occurring after heavily (penalize long settling time and error), which results small overshoot and minimum damped oscillations in control system design, [9]. In this thesis the overall sum of ITAE block was developed for all controlled state variables and used as the objective function. For each controlled state ITAE is defined by equ. 4.59, where [10].

$$ITAE = \int_{t_0}^{t_f} ||e|| t dt \tag{4.59}$$

[9] $x_{(t+1)}$ - new position of each particle, $x_{(t)}$ - present position of each particle, $v_{(t+1)}$ - new velocity of each particle, w - inertia weight, c_1 - cognition learning factor, c_2 - social learning factor, r_1, r_2 - uniformly generated random numbers and G - the best solution of the i^{th} particle.

[10] $||e||$ - tracking error magnitude, t_0 - initial simulation time, t_f - final simulation time, and t - integral time

Chapter 5

Trajectory Generation, Simulation Results and Analysis

5.1 Trajectory Generation

Numerous approaches to trajectory tracking discussed in the literatures. Trajectory is developed using dynamic nonlinear state space model of a FW-UAV. The specific flight dynamics model of FW-UAV is taken for trajectory tracking.

FW-UAVs pass through different trajectories to complete the desired flight. In long distance flights the UAVs need to attain the minimum altitude before level flight to generate lift and avoid possible obstacles (buildings, mountains, birds and etc) collision. So helical, bow-tie [33], elliptical and circular trajectories are some of the paths which are helpful for flight tests at the beginning of any FW-UAV flight control.

However, there is a constraint for FW-UAVs to track these trajectories called turning radius about the curvature. The tangential and centripetal forces of lift and weight must be balanced respectively to move around the curvature, [32]. The centripetal force acts on a FW-UAV moving in a curvature and directed towards the center of the circular path, and it's balance with the lift force is given by equ. 5.1.

$$f_{lift} * sin(\phi_{max}) = m\frac{v^2}{r_{min}} \tag{5.1}$$

The tangential force acts on a flying FW-UAV in the tangential direction to the curved path, and the tangential lift and weight balance given by equ. 5.2.

$$f_{lift} * cos(\phi_{max}) = mg \tag{5.2}$$

The minimum turning radius solved from combining the above two equations, expressed by equ. 5.3 and depends on the maximum roll angle and speed of the UAV,[32], [1].

$$r_{min} = \frac{v^2}{g * tan(\phi_{max})} \tag{5.3}$$

The other condition in helical, bow-tie, and circular trajectories to be considered is the frequency of the desired sinusoidal trajectory. This depends on the number of circular trajectories to be completed within a given time frame. In this thesis the UAV is set to complete 60 cycles of circular paths within an hour. So the frequency of the sinusoidal signal is calculated by dividing number of cycles completed with time needed, equ. 5.4. Therefore the helical and bow-tie trajectories frequency is set to 0.017 Hertz, in the subsequent numerical simulations.

$$f = \frac{60}{3600} cycle/sec = \frac{1}{60} cycle/sec \tag{5.4}$$

After completing the helical trajectories and reached on the required altitude for level flight, the FW-UAVs need the second phase of trajectory generation called level flight. This is developed with techniques of polynomial trajectory planning for real data way-points taken as the GPS information in section 5.1.1 and 5.1.2.

5.1.1 Way-Point Trajectory Generation

Paths can be generated from way-points through different path planning algorithms. But most paths have sharp corner turns and edges which are difficult to be followed by any stable dynamic system. The sharp corners need to be accessible possibly by the FW-UAV

[1] Where: f_{lift} - lift force, ϕ_{max} - maximum roll angle, m - mass, v - speed, r_{min} - minimum turning radius, g - acceleration due to gravity.

naturally. The way-points need feasibility to be kinematically reachable by the plant, so they must be taken at intervals of the minimum turning radius. In-order to tackle the problem of sharp corners different curve fitting methods of polynomial approximation are recommended in MATLAB environment.

Way-point data are samples of discrete values along a continuum. However, estimates of points between these discrete values is required. One way to do this is to formulate a function to fit these values approximately. This application is called curve fitting and performed with different approaches. The first is to derive a single curve that represents the general trend of the data, not necessarily pass through the points and known mostly as least-squares regression. The second approach is interpolation which is to fit a single curve or a series of curves that pass directly through each of the way-points. There are different polynomial spline methods available on MATLAB; linear, quadratic, cubic, B-splines, and minimum snap polynomial.

In this thesis the minimum snap polynomial trajectory is used in MATLAB to generate trajectories that pass through the way-points at respective specified time points, [7]. The desired trajectory is fixed to ninth order piece-wise polynomial, and the coefficients are extracted by solving the quadratic programming (QP) based optimization.

The trajectory designed to minimize the QP cost function, given by equ. 5.5, [2]. The necessary condition of optimality is that the tenth order derivative is zero. As it can be seen from the state space model in equ. 3.43, the fourth derivative of inertial positions is explicitly a function of all control commands, [19]. Therefore, reducing the snap $(x^{(4)}, y^{(4)}, z^{(4)})$ results that optimum control effort can be achieved.

$$p^*(t) = argmin \int_{t_0}^{t_f} ||p^{(4)}||^2 dt \tag{5.5}$$

The QP can either be constrained or unconstrained depending on the nature of way-points. Constrained QP requires the derivatives of the trajectory at each endpoint and mostly applied for low degree polynomial and small number of way-points. It's application in higher order results ill-conditioned system and numerical un-stability. However

[2] $p^*(t)$ - optimal polynomial, *argmin* - stand for minimizing argument, $||p^{(4)}||$ - 4th order derivative magnitude, t_0 - initial time and t_f - final time

the unconstrained form is optimization of free endpoint derivatives instead of polynomial coefficients. This is recommended that it solves the problems of constrained optimization.

The second case to-be considered in this optimal trajectory generation is the time allocated at each segment. Small time leads system saturation and large time results the UAV to move slowly, which makes practically inefficient. To overcome this problem the time allocated at each segment was calculated by considering desired navigation speed along the main flight direction.

5.1.2 Real Data-Point Trajectory Generation

Real geographical inertial positions (x, y, z) are extracted from GPS sensors in guidance and navigation of FW-UAVs. The need for real GPS data of border paths comes because the FW-UAV modelled in this thesis is featured to be applicable for border patrolling. However, Ethiopia have no clear geographical boundary lines with neighboring countries, rather there is areal boundary, which makes us take way-points within the country for simulation data preparation. Real GPS data are taken from google map using "Google Earth Pro", which is used from early 2015 till now. The tool used for viewing lots of information geographically such as routes from one place to the other, [26]. In this thesis place-marks (points of interest) are created and analysed for "Ayat to Torhyloch", and "Kality to Piazza", railway roads in Addis Ababa, Ethiopia.

Path created using "add path", feature of "Google Earth Pro", at specified interest points on the way to the desired routes. The direction tool is used to quickly and efficiently navigate from "Ayat to Torhyloch", and "Kality to Piazza", to create a flying route for the aircraft. The routes are created on the map through connecting all the place-marks along the paths of each route starting from their respective starting point to their corresponding destinations, explained with fig. 5.1 and 5.2.

The way points are taken randomly on the way manually for all routes. After creating the route there are different forms to save the required data like ".gpx", and ".kml", but for simplicity it's saved as ".kml", data for the respective paths. The ".kml", data is geodetic coordinate information in earth-centered-earth-fixed (ECEF) RF of each route with latitude and longitude in degrees, altitude in meters and the path-way creation time.

However, for FW-UAV trajectory control and guidance the inertial positions must be provided with Cartesian coordinates of (x, y, z) expressed with respect to NED frame to be applicable in MATLAB Simulink. So, first the geodetic latitudes and longitudes converted to (x, y, z) in ECEF frame and then the positions (x, y, z) transformed from ECEF to the NED frame using MATLAB.

Discrete data forms of positions (x, y, z) in units of meter is found in NED frame. From this data, way-points are taken and paths developed along x, y, and z positions with the help of minimum snap polynomial trajectory. Way-points in tables D.1, D.2 developed with their respective time of arrival using a navigation airspeed of 30m/s.

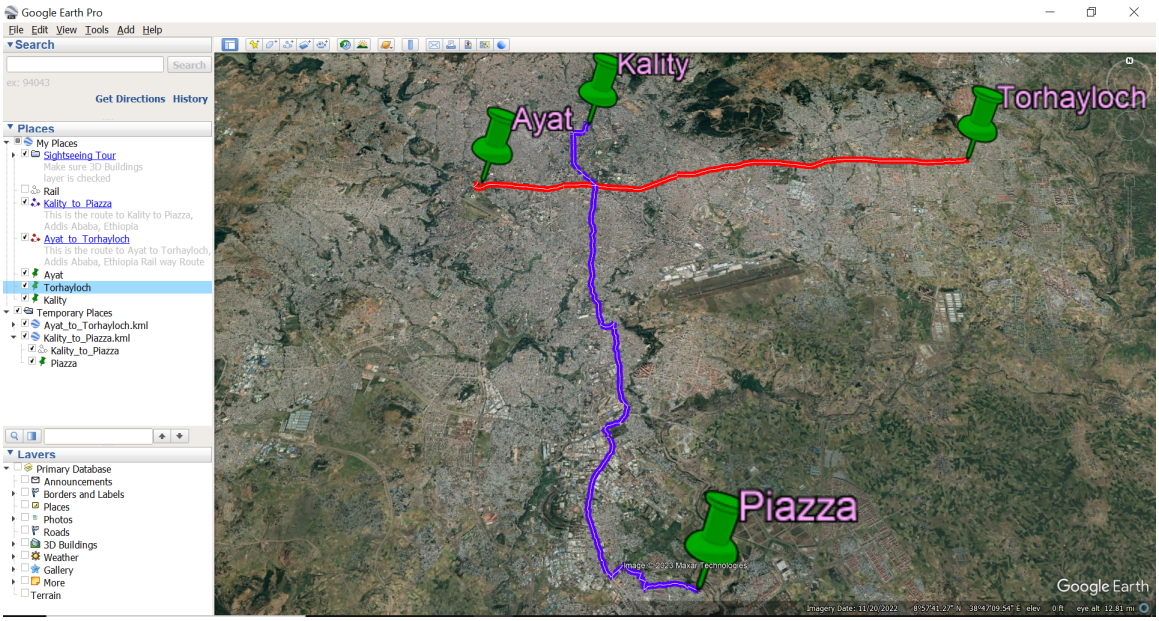

Figure 5.1: GPS Data Extraction for Railway Routes

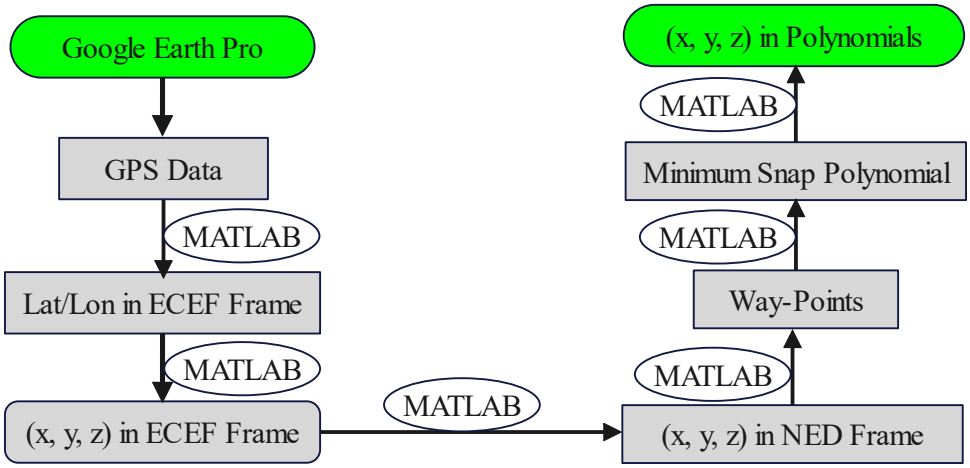

Figure 5.2: Steps in Way-Point Trajectory Generation

5.2 Simulation Results and Analysis

The complete mathematical model of the fixed wing unmanned aerial vehicle is developed in MATLAB Simulink. The desired states of interest to be controlled $(x, y, z, \phi, \theta, \psi, V_a)$ were decoupled and developed in state space. This state space model was used for twisting SMC design and then the controllers performance was evaluated on the overall coupled 12-state mathematical model.

The plant model parameters were adopted from literature survey, [4] for a typical Aerosonde aircraft, presented in tables A.1, A.2, and A.3. The plant was selected due to it's small size, long-endurance in extended missions and well-behaved open-loop dynamics, [4]. The plant has high endurance of flying for about 30 hours and over 150 kilometers within radio frequency communication system. It has the ability to-be used for patrolling border areas. This UAV has the capability to fly beyond 200 kilometers but needs other communication system for control.

The performance of designed controllers verified and validated for different trajectories with and without disturbance and uncertainty, with bounded magnitude input disturbances, parameter variation, matched uncertainties. And finally first order transfer function modeled actuator dynamics was included on the plant, to see the resilience of controllers response. Signals labelled as underscore 'd' are the desired signals, for respective state variables which are going to-be tracked by the actual state variables. The rest are signals which are found from sensor measurements, feedback or though performing algebraic operations from measuring devices.

In this thesis the FW-UAV is required to fly within a range of 15 m/s to 30 m/s speed. The maximum bank angle is also taken as 1.255 rad for turning radius calculations. The minimum turning radius for 15 m/s flight results 7.494 m whereas 30 m/s flight speed gives 30 m turn. So the amplitude of sinusoidal signals must be minimum of 7.494 m. Taking these preconditions, different flight paths are developed. The minimum amplitude of the sinusoidal trajectories taken to-be greater than the minimum turning radius as preference in the following simulations.

5.2.1 Helical Trajectory Tracking Simulation Results

In the absence of external disturbances and matched uncertainty, the performance of controllers were tested and results presented in fig. 5.3, 5.4, and 5.5. The desired guidance trajectories were set as x_d=10cos(2πft), y_d=10sin(2πft), z_d=$(-0.0001t^3 + 0.463t^2)10^{-3}$, V_d=15 m/s, and ϕ_d=0.25 rad, $\forall$t$\leq$3600, where z_d was developed by cubic polynomial. The initial states $(x_0, y_0, z_0, \phi_0, \theta_0, \psi_0, V_0)$ were (7,0,0,0.1,0,0,10) respectively.

The switching and normalizing controller gains were found from PSO and presented with tables 5.3, and 5.2. The ITAE table is also looked-up with table 5.1.

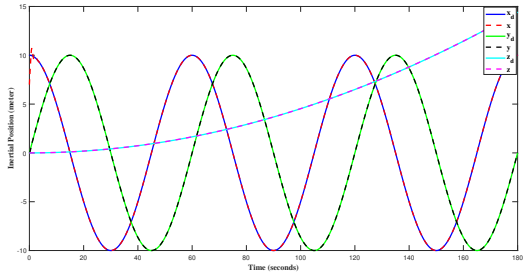

(a) Inertial position tracking

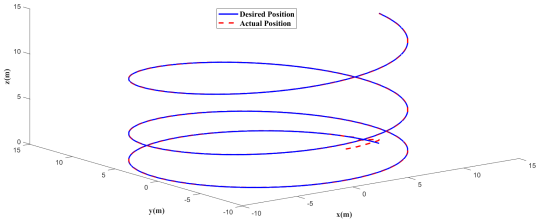

(b) 3D plot of inertial position

Figure 5.3: Helical Trajectory Tracking

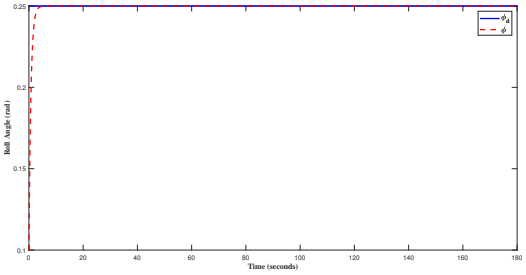

(a) Roll tracking

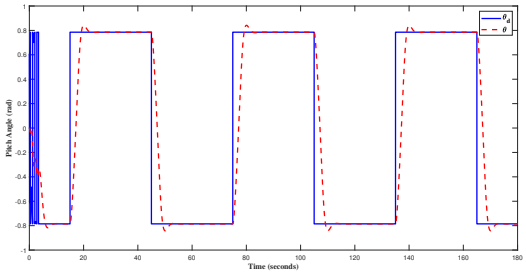

(b) Pitch tracking

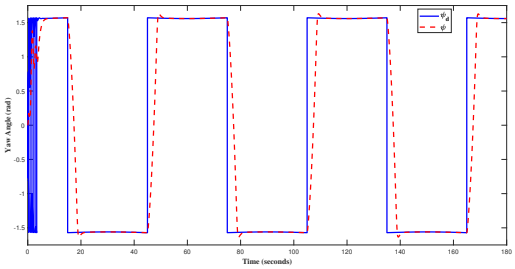

(c) Yaw tracking

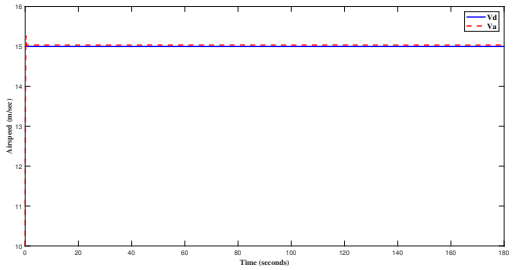

(d) Airspeed tracking

Figure 5.4: Attitude and Airspeed Tracking for Helical Trajectory

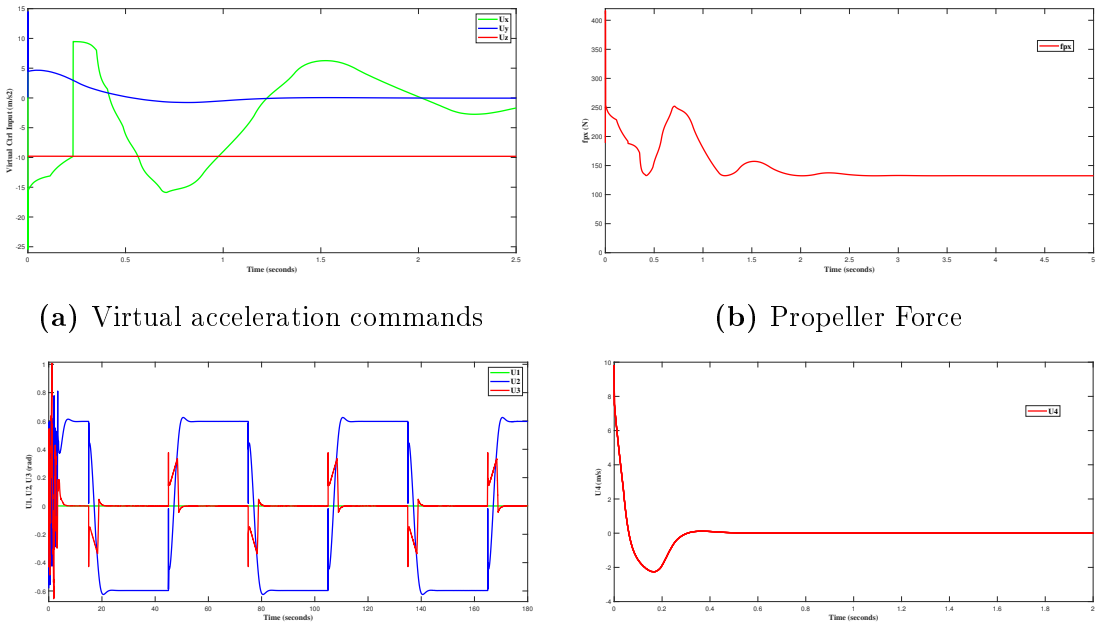

(a) Virtual acceleration commands

(b) Propeller Force

(c) Attitude commands

(d) Airspeed command

Figure 5.5: Control Signals and Force of Propeller for Helical Trajectory Tracking

Table 5.1: ITAE Performance Index for Helical Trajectory Control Against 20% Increased Parameter Variation (PV), Matched Uncertainty (MU), Input Disturbance (ID), and Actuator Dynamics (AC)

ITAE Item	ϕ	θ	ψ	x	y	z	V_a	**Total**
Nominal	0.08197	1910	3945	54.81	53.94	49.62	555	**6569**
PV	0.08149	2029	4196	54.81	53.94	49.62	555.6	**6939**
MU	0.08197	1910	3945	54.81	53.94	49.62	566.9	**6581**
ID	4.202	2096	3970	54.81	53.94	49.62	553	**6782**
AC	0.08175	1948	4046	54.81	53.94	49.62	553.2	**6706**

Table 5.2: Normalizing Gains for Helical Trajectory Obtained Through PSO

Gain:	n_1	n_2	n_3	n_4	n_5	n_6	n_7	n_8
Values:	0.77	0.1221	0.77	0.221	0.793	0.23	0.0812	0.00751

Table 5.3: Switching Gains for Helical Trajectory Obtained Through PSO

Gain:	k_1	k_2	k_3	k_4	k_5	k_6	k_7
Values:	4	3	-0.3927	-0.3927	0.3927	0.3604	25
Gain:	k_8	k_9	k_{10}	k_{11}	k_{12}	k_{13}	k_{14}
Values:	24	23	20	23	20	5	3.8628

5.2.1.1 Helical Trajectory with Parameter Variation

The performance of designed controllers evaluated against 20% parameter variations of mass and inertia. All the initial conditions and desired trajectories are kept with the same as in section 5.2.1. The ITAE sum of all controlled states increased from 6569 to 6939 which is 5.6325% from the nominal value within 180 seconds, it can be seen and compared from table 5.1.

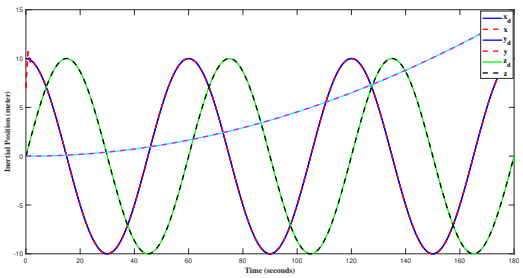

(a) Inertial position tracking

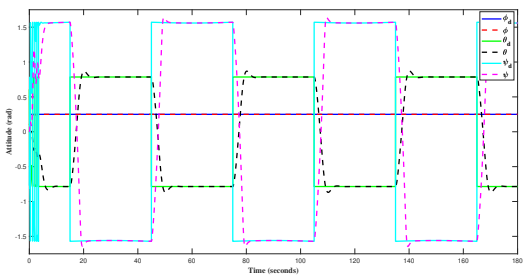

(b) Attitude tracking

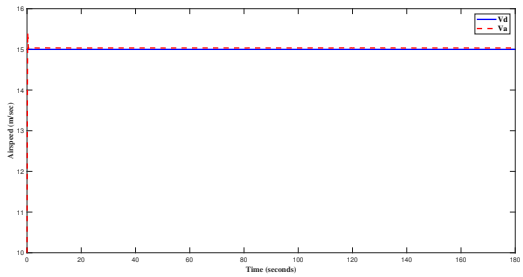

(c) Airspeed tracking

Figure 5.6: Helical Trajectory Tracking with 20% Increased Mass and Inertia

5.2.1.2 Helical Trajectory with Matched Uncertainty

The effect of attitude uncertainties d_ϕ, d_θ and d_ψ defined in chapter 4 analysed in the absence of external input and wind disturbances. The total ITAE increased by 0.1827% from the nominal value within 180 seconds, see table 5.1.

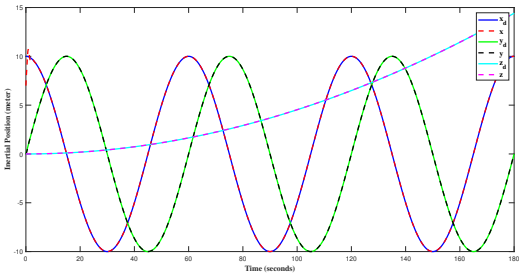

(a) Position tracking

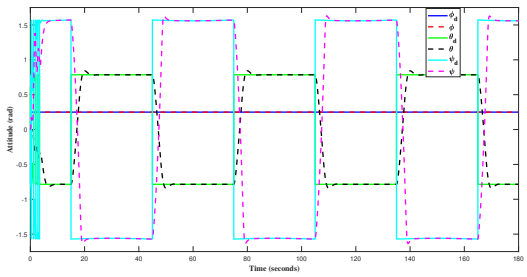

(b) Attitude tracking

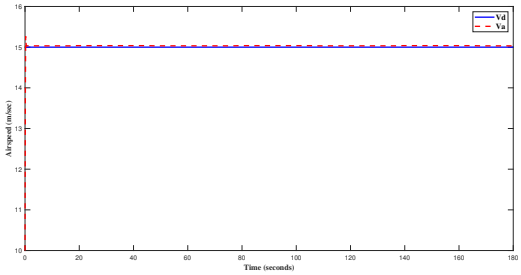

(c) Airspeed tracking

Figure 5.7: Helical Trajectory Tracking with Matched Uncertainty

5.2.1.3 Helical Trajectory with Input Disturbance

In this section the controllers performance was evaluated against input and wind disturbances of known magnitude. It's considered that input disturbances were evolved into the system algebraically as additive form of $U = U_{nominal} + d_U$, with control signals (U_1, U_2, U_3) due to actuator imperfections. So the effect of input disturbances of attitude control having a magnitude of 20% the nominal deflection angle of 1 rad have been verified. These were d_{U_1}=0.2sin(0.001t), d_{U_2}=0.2sin(0.001t), and d_{U_3}=0.2sin(0.001t) along U_1, U_2, and U_3 respectively.

Wind is the main source of disturbance in UAVs, [33] and it's effect incorporated into the model as seen in section 3.5.3.7. The wind components taken from [33] in which they

have been estimated in the kinematic analysis during their path-following developments. These were u_w=2sin(0.1t), v_w=2sin(0.1t) and w_w=0.5sin(0.1t) + 1. The ITAE increased from 6569 to 6782 which is 3.2425%, see table 5.1.

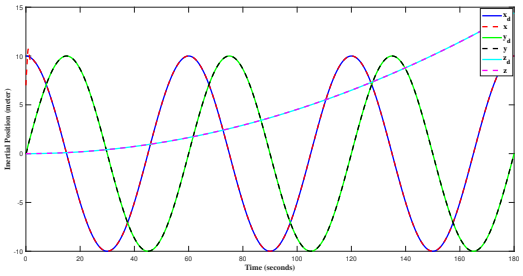

(a) Position tracking

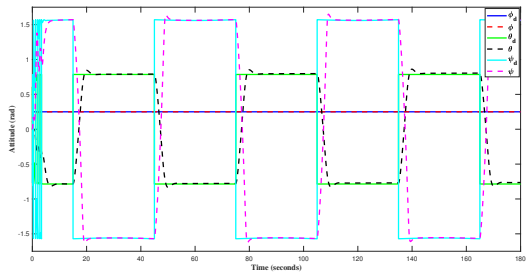

(b) Attitude tracking

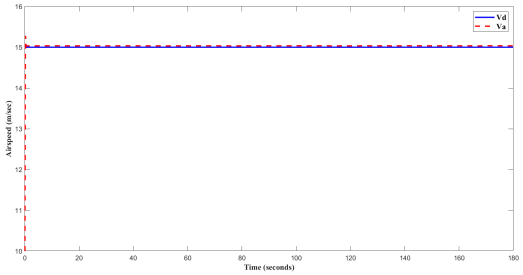

(c) Airspeed tracking

Figure 5.8: Helical Trajectory Tracking with Input Disturbances

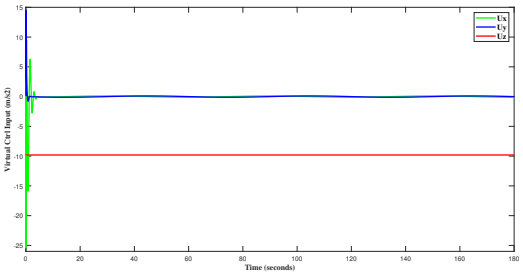

(a) Position commands

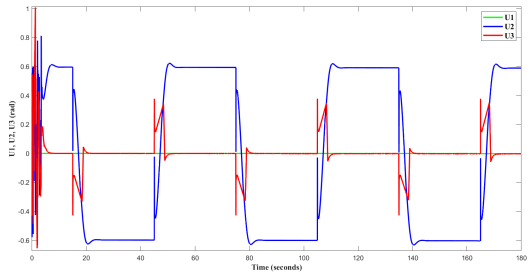

(b) Attitude commands

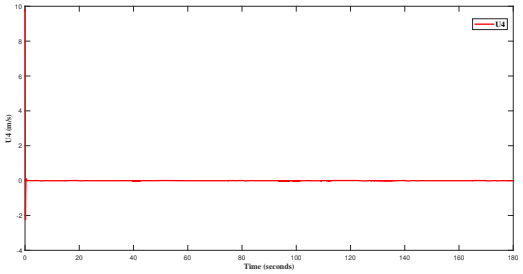

(c) Airspeed command

Figure 5.9: Control Commands for Helical Trajectory with Input Disturbances

5.2.1.4 Helical Trajectory Tracking with Actuator Dynamics

In FW-UAV control the surface deflections (U_1, U_2, U_3) and propeller command (U_4) of engines are limited to their maximum allowable practical ranges. These control commands are generated by the controllers designed earlier and they are given to the actuators as input. So the performance of the actuators is the main determining factor in generating the maximum allowable energy by motors. And then the output of the actuators given to the actual FW-UAV model for driving it in the desired conditions.

The actuators for motors in FW-UAV are mostly modelled with first order transfer functions, $G(s)$ as in equ. 5.6, [10]. The dynamic response of the plant, FW-UAV is very slow compared to the response speed of actuators, and motors. It's assumed that actuators have relative time constants with motors, [10] i.e. motors and actuators have nearly similar time constants. In this simulation all actuator dynamics are considered to have the same time constants and gain, equ. 5.6. The total ITAE increased from 6569 to 6706 which is 2.0855%, see table 5.1.

$$G(s) = \frac{O(s)}{U(s)} = \frac{1}{\tau s + 1} \tag{5.6}$$

Where:

- $O(s)$ = actual control signal given to the states from actuator
- $U(s)$ = control signal given to the actuators from control design
- s = the Laplace domain variable
- τ = 0.0222 second, is the time constant for the actuator dynamics

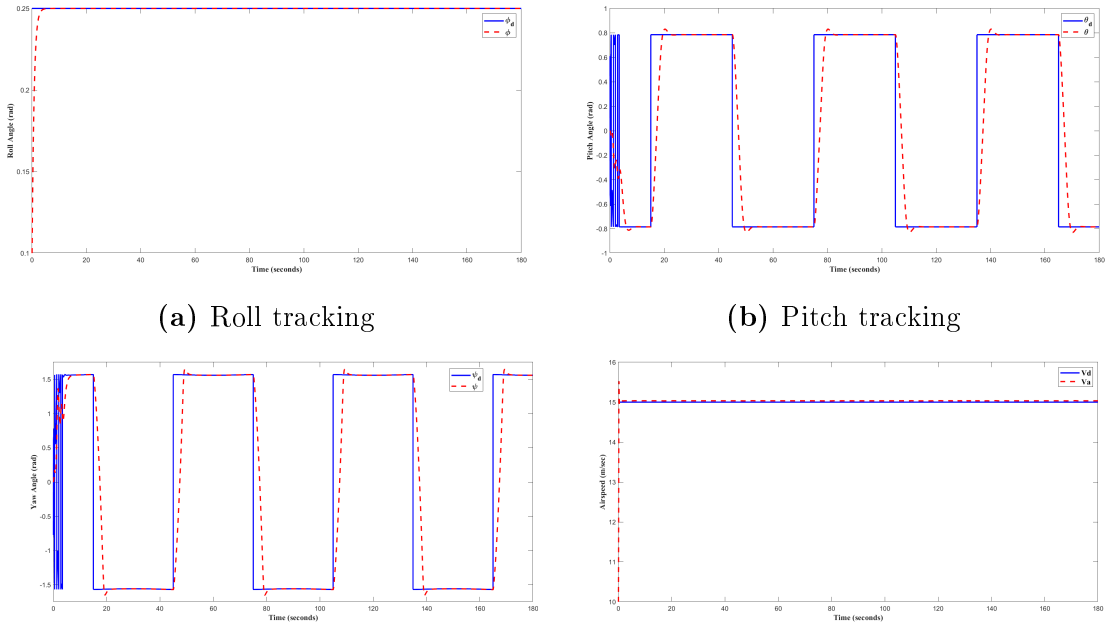

(a) Roll tracking **(b)** Pitch tracking

(c) Yaw tracking **(d)** Airspeed tracking

Figure 5.10: Helical Trajectory Tracking with Actuator Dynamics

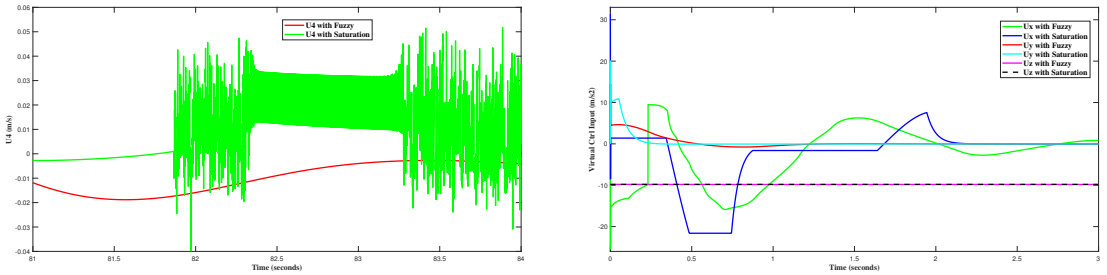

(a) Airspeed control input **(b)** Virtual acceleration commands

Figure 5.11: Chattering in Control Signals for Helical Trajectory Tracking

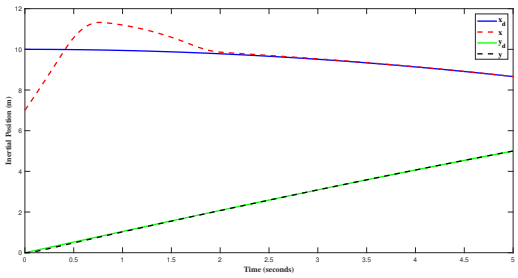

(a) Position tracking along x and y-axis

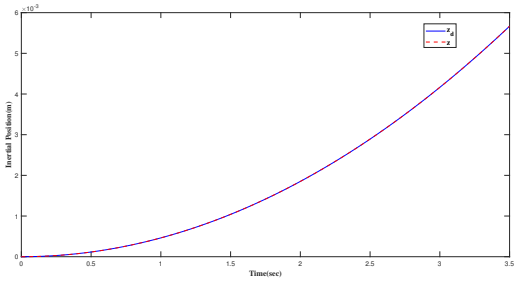

(b) Position tracking along z-axis

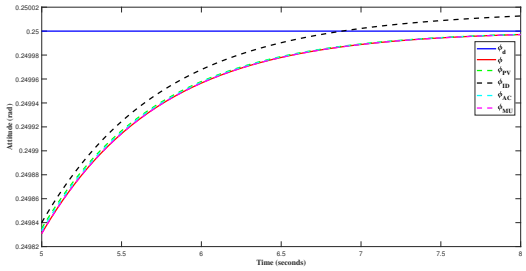

(c) Roll tracking

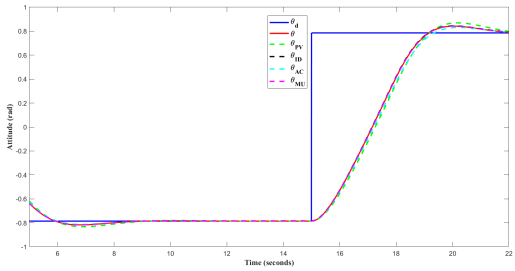

(d) Pitch tracking

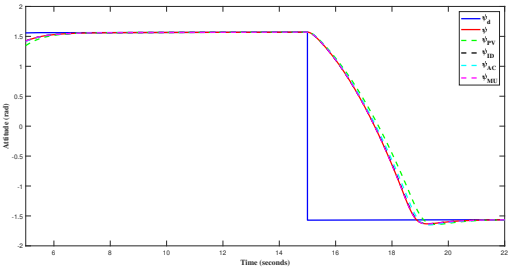

(e) Yaw tracking

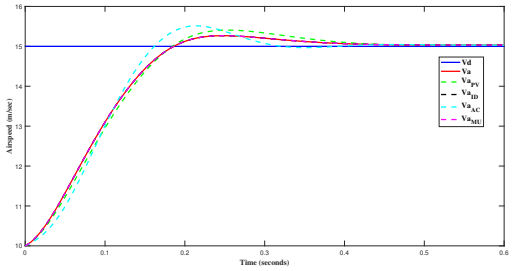

(f) Airspeed tracking

Figure 5.12: Partially Zoomed-in Views in Helical Trajectory Tracking

Where: ϕ, θ, ψ, and V_a in fig. 5.12 are considered as nominal values.

A yaw angle of 1.5708 rad in the attitude simulations presented earlier is an indicator of the FW-UAV complete rotation around its vertical axis. It's essentially a signifying result for the turning of the FW-UAV sideways through the x-y plane. It's commonly known as "knife-edge flight" and is generally not feasible in FW-UAV control during normal flight operations. Rather, it's sometimes used in research and development for testing and demonstrating the FW-UAV's flight capabilities and stability.

5.2.2 Bow-Tie Trajectory Tracking Simulation Results

Bow-Tie trajectory is one of the most challenging paths (benchmark) to-be followed by UAVs, [33]. This trajectory was studied, [33] for small FW-UAVs in wind disturbed environment. The controllers performance tested in the absence of uncertainty, and disturbances and illustrated in the following figures.

The initial conditions for $(x_0, y_0, z_0, \phi_0, \theta_0, \psi_0, V_0)$ were $(7, 0, 10, 0.1, 0, 0, 10)$ in their respective SI units. The desired trajectories were x_d=8cos(2πft), y_d=8sin(4πft), and z_d=22+8cos(2πft), $\forall t \geq 0$. The desired airspeed and roll angle were also taken as V_d=15 m/s, ϕ_d=0.25 rad, $\forall t \geq 0$ respectively. The switching control gains were tuned with PSO tuning algorithm and presented in table 5.4 in which the respective ITAE indexes are also tabulated in table 5.5.

Table 5.4: Switching Gains for BowTie Trajectory Obtained Though PSO

Gain:	k_1	k_2	k_3	k_4	k_5	k_6	k_7
Values:	4	3.5	-0.3927	-0.3885	0.3927	0.3627	25
Gain:	k_8	k_9	k_{10}	k_{11}	k_{12}	k_{13}	k_{14}
Values:	24	23	20	16	15	25.5	23.8628

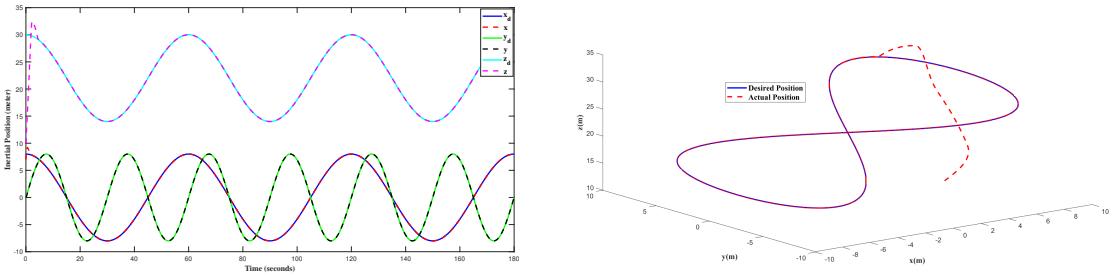

(a) Position tracking **(b)** 3D plot of positions

Figure 5.13: Inertial Position Tracking with Bow-Tie Trajectory

Table 5.5: ITAE Performance Index for BowTie Trajectory Control Against 20% Increased Parameter Variation (PV), Matched Uncertainty (MU), Input Disturbance (ID), and Actuator Dynamics (AC)

ITAE Item	ϕ	θ	ψ	x	y	z	V_a	**Total**
Nominal	0.1123	1898	3991	1.049	0.2418	25.1	2.612	**5918**
PV	0.1118	2018	4239	1.049	0.2418	25.1	2.781	**6286**
MU	0.1123	1898	3991	1.049	0.2418	25.1	4.417	**5920**
ID	7.346	1944	4029	1.049	0.2418	25.1	2.307	**6009**
AC	0.1121	1935	4090	1.049	0.2418	25.1	2.961	**6055**

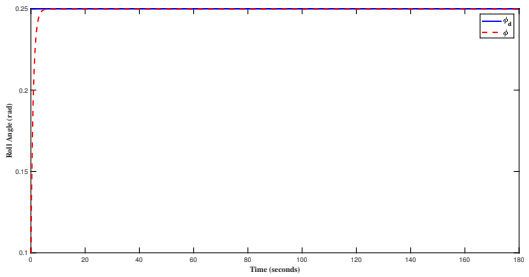

(a) Roll tracking

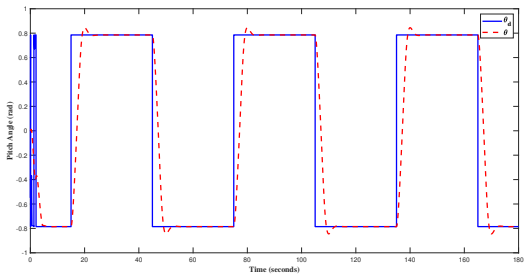

(b) Pitch tracking

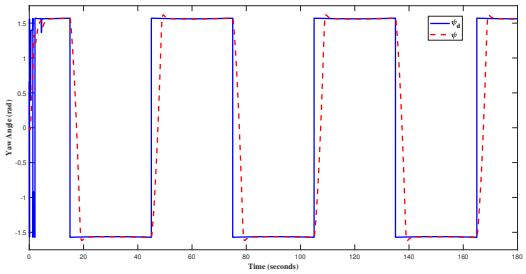

(c) Yaw tracking

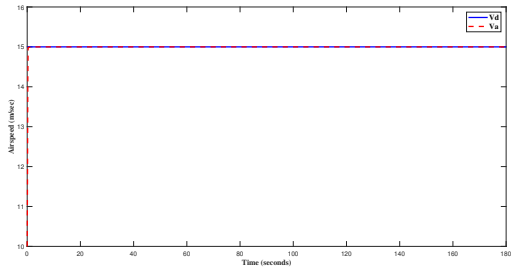

(d) Airspeed tracking

Figure 5.14: Attitude and Airspeed Tracking with Bow-Tie Trajectory

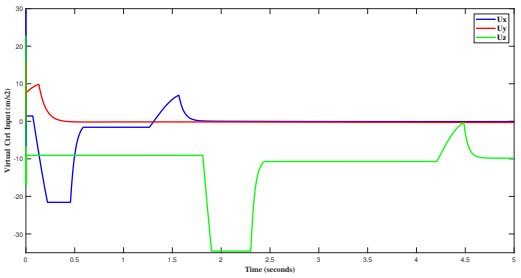

(a) Virtual acceleration commands (Zoomed)

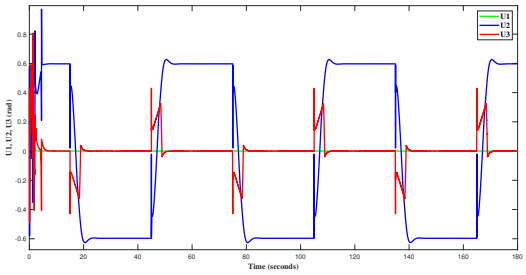

(b) Attitude commands

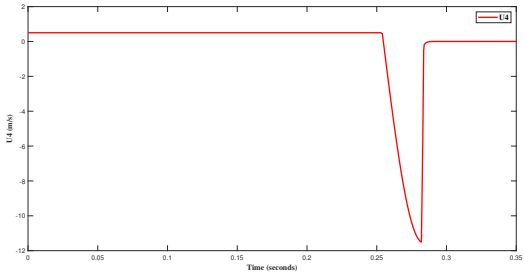

(c) Airspeed command (Zoomed view)

Figure 5.15: Control Signals for Bow-Tie Trajectory Tracking

5.2.2.1 BowTie Trajectory with Parameter Variation

Keeping all the conditions as in section 5.2.2 the performance of controllers evaluated against 20% increased variations of mass and inertia. Total ITAE increased by 6.2183%.

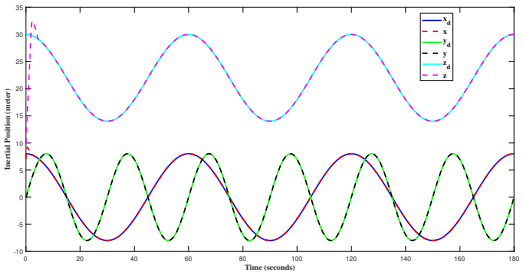

(a) Position tracking

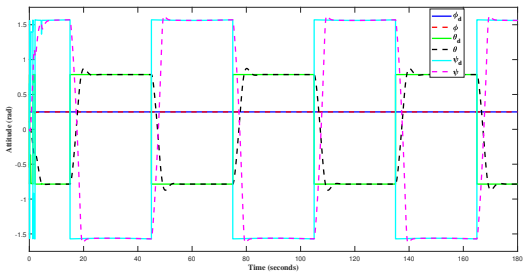

(b) Attitude tracking

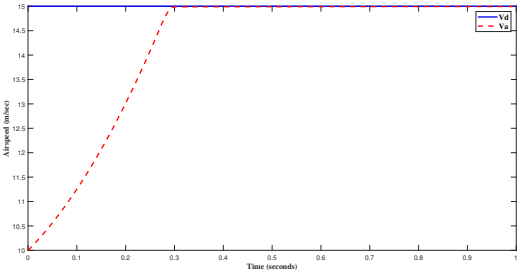

(c) Airspeed tracking (Zoomed view)

Figure 5.16: BowTie Trajectory Tracking with Parameter Variation

5.2.2.2 BowTie Trajectory with Matched Uncertainty

The effect of attitude uncertainties (unknown interference until computed from the model) d_ϕ, d_θ and d_ψ in bowtie trajectory was analysed and verified. The total ITAE increases by 0.03379%, table 5.5.

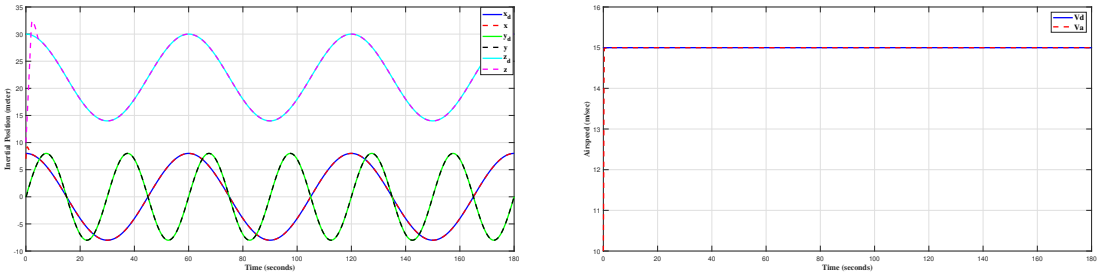

(a) Position tracking **(b)** Airspeed tracking

Figure 5.17: BowTie Trajectory Tracking with Matched Uncertainty

5.2.2.3 BowTie Trajectory with Actuator Dynamics

The actuators dynamic model as in section 5.2.1.4 was used in this trajectory to check the response of the controller against the first order actuator delay. The total ITAE increased by 2.3149%, see table 5.5.

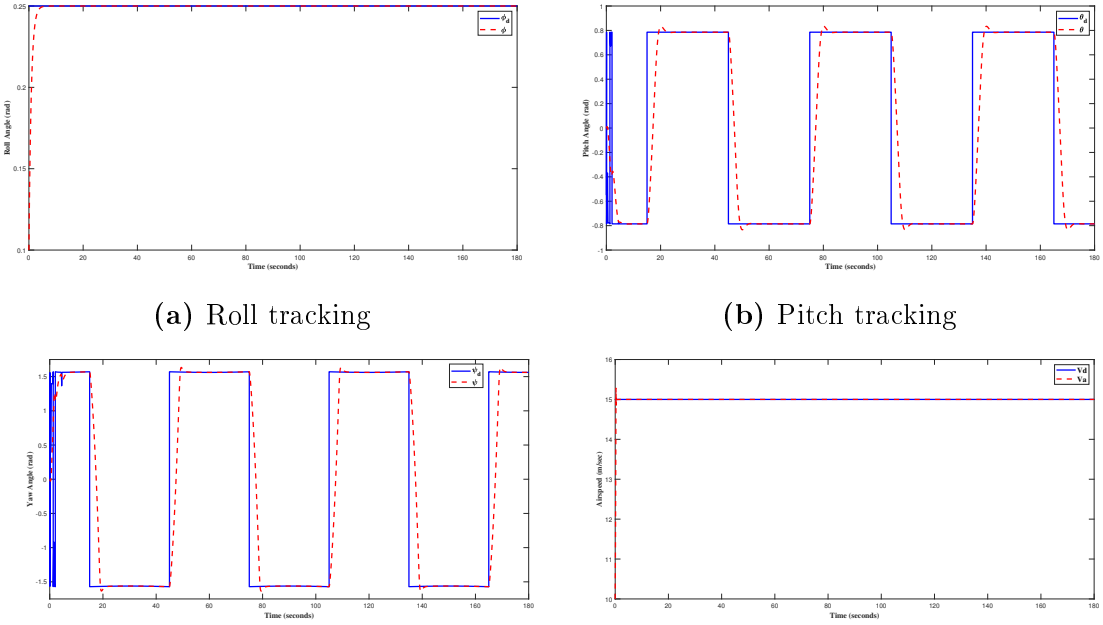

(a) Roll tracking **(b)** Pitch tracking

(c) Yaw tracking **(d)** Airspeed tracking

Figure 5.18: Attitude and Airspeed Tracking with Actuators in BowTie Trajectory

5.2.2.4 BowTie Trajectory with Input Disturbance

As in section 5.2.1.3, algebraically additive input disturbances of d_{U_1}=0.15sin(0.0001t), d_{U_2}=0.15sin(0.0001t), and d_{U_3}=0.15sin(0.0001t) along U_1, U_2, and U_3 respectively and wind disturbances u_w=2sin(0.1t), v_w=2sin(0.1t), and w_w=0.5sin(0.1t) + 1 were added on the model for checking disturbance rejection ability in bowtie trajectory. The total ITAE of all controlled states increased from 5918 to 6009 i.e. 1.5377%, in table 5.5.

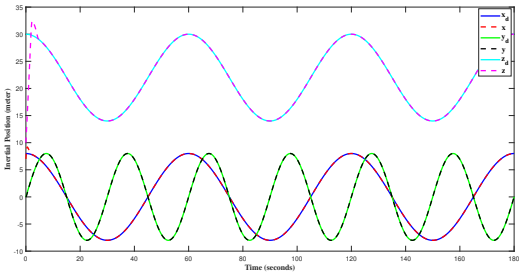

(a) Position tracking

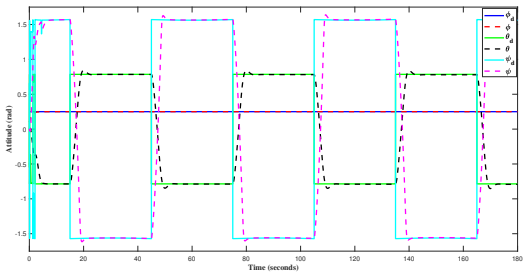

(b) Attitude tracking

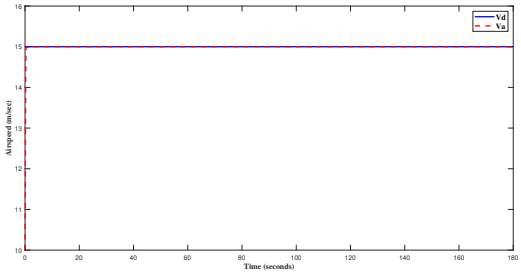

(c) Airspeed tracking

Figure 5.19: BowTie Trajectory Tracking with Input Disturbance

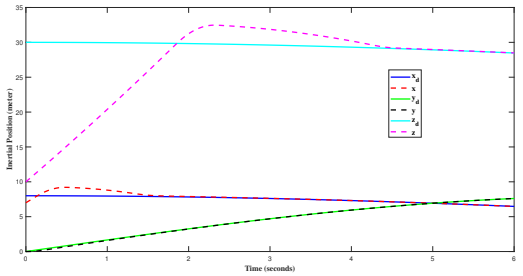

(a) Position tracking

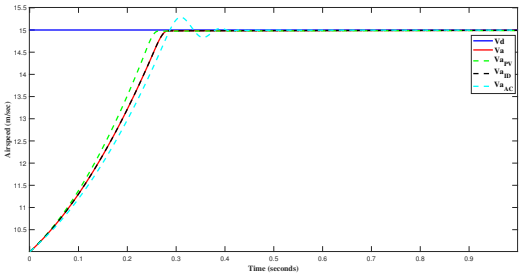

(b) Airspeed tracking

Figure 5.20: Zoomed-in Views of Position and Airspeed in BowTie Trajectory Tracking

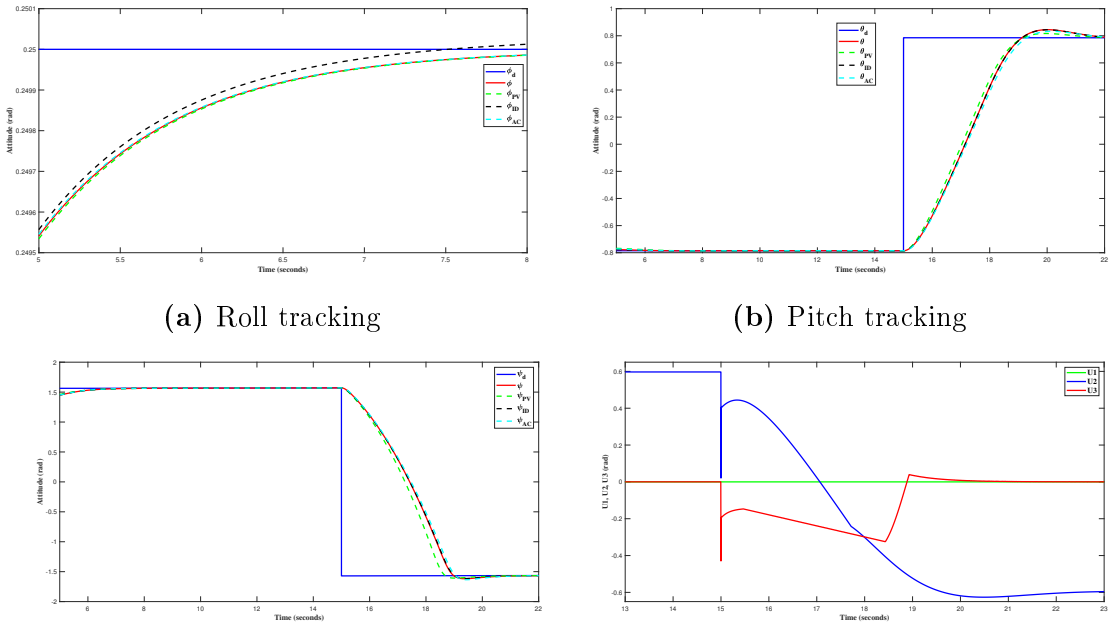

(a) Roll tracking

(b) Pitch tracking

(c) Yaw tracking

(d) Attitude commands

Figure 5.21: Partially Zoomed-in Views of Attitudes and Attitude Control Inputs in BowTie Trajectory Tracking

Where: ϕ, θ, ψ, and V_a in fig. 5.20 and 5.21 are taken as nominal values.

In the simulations above there are 45° and 90° turns of pitch (θ) and yaw (ψ) angles respectively. This is explained with similar scenario as in the last part of section 5.2.1. These type of kinematics exists indicating the swing of values between positive and negative angles alternatively. This happens because the FW-UAV is brought to fly about it's central axis of rotation, side-way flight. It is evident that there are corner turns on figures 5.21b, 5.21c and 5.21d. This is one of the draw-back of Newton-Euler modeling approach, which can be solved by Quaternion approach modeling.

5.2.3 Real Data Trajectory Tracking Simulation Results

Applying minimum snap polynomial trajectory on the data presented in section 5.1.2 the following simulation results found. In this scenario the simulation started at t=3600 second, because it's assumed that level flight starts after the FW-UAV achieved a desired altitude with helical trajectories. So the conversion of data from lat/lon→ECEF→NED frame have been performed with reference to the level point at initial way-points.

5.2.3.1 Ayat-Torhyloch Way-Point Trajectory Simulation Results

Way-points were extracted starting from Ayat on the way to Torhyloch along the railway road. The whole path needs several flight minutes to be completed for simulation purpose only, way-points which can be accessed within 152.2 seconds were considered, see table D.1.

The desired trajectories of inertial positions (x_d, y_d, z_d) measured with reference to Ayat at an altitude of 2 kilometer. Ayat is referred as a coordinate of (0, 0, 2000), where 2000 indicates altitude in meter. Where as V_d=30 m/s and ϕ_d=0.25 rad , $\forall t \geq 3600$.

So the initial conditions were properly selected from helical trajectory outputs, considering initial point of real data points which were from helical trajectory at t=3600 seconds x_0=10cos(120π) m, y_0=10sin(120π) m, z_0=2000 m, ϕ_0=0.1 rad, θ_0=0 rad, ψ_0=0 rad and V_0=15 m/s.

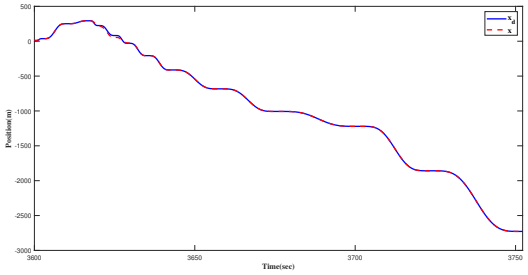

(a) Position tracking along x axis

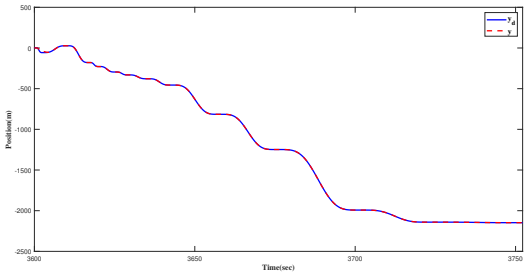

(b) Position tracking along y axis

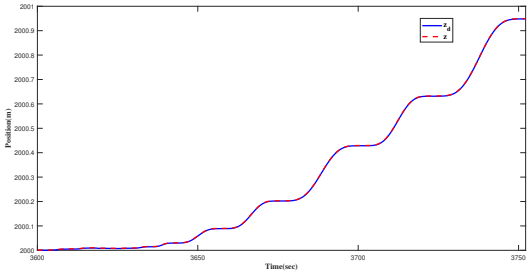

(c) Position tracking along z axis

Figure 5.22: Ayat-Torhyloch Way-Point Trajectory Tracking (Ayat Reference Position)

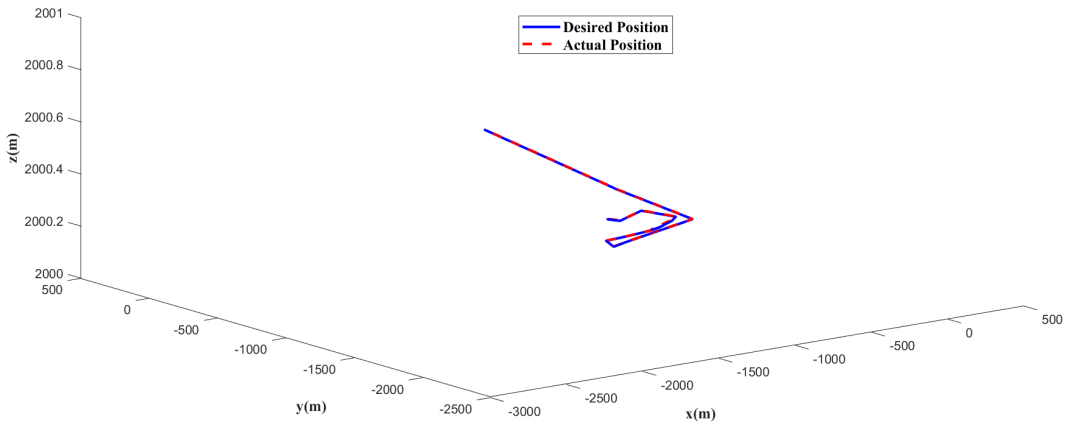

Figure 5.23: 3D Plot of Positions in Ayat-Torhyloch Way-Point Trajectory Tracking

Table 5.6: ITAE Performance Index for Ayat-Torhyloch Way-Point Trajectory Control Against 20% Increased Parameter Variation (PV), Matched Uncertainty (MU), Input Disturbance (ID), and Actuator Dynamics (AC)

ITAE (10^4)	ϕ	θ	ψ	x	y	z	V_a	**Total**
Nominal	0.0048	11.5	31.6	84.3	18.11	0.05	2.424	**148**
PV	0.0053	12.33	33.82	84.3	18.11	0.005	2.451	**151.1**
MU	0.0048	11.5	31.6	84.3	18.11	0.05	2.431	**148**
ID	0.025	11.71	31.76	84.3	18.11	0.05	2.42	**148.4**
AC	0.0069	11.49	33.75	84.3	18.11	0.05	2.417	**150.1**

Table 5.7: Normalizing Gains for Ayat-Torhyloch Way-Point Trajectory

Gain:	n_1	n_2	n_3	n_4	n_5	n_6	n_7	n_8
Values:	0.0875	0.1827	0.0860	0.0729	2.983	0.8963	0.0812	0.00751

Table 5.8: Switching Gains for Ayat-Torhyloch Way-Point Trajectory

Gain:	k_1	k_2	k_3	k_4	k_5	k_6	k_7
Values:	3	0.4716	-0.7854	-0.5007	0.3927	0.3404	40
Gain:	k_8	k_9	k_{10}	k_{11}	k_{12}	k_{13}	k_{14}
Values:	38	22.195	21.15	25.15	24.14	23.75	22.545

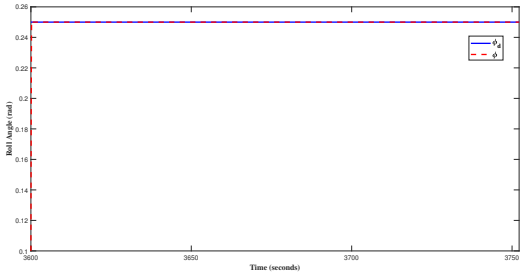

(a) Roll tracking

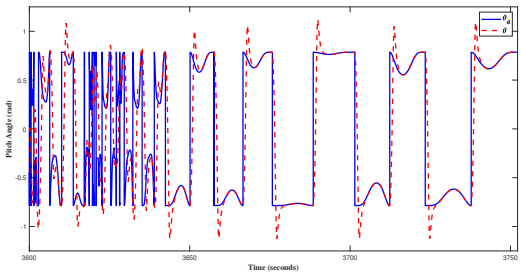

(b) Pitch tracking

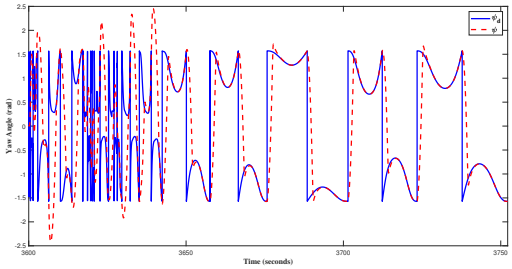

(c) Yaw tracking

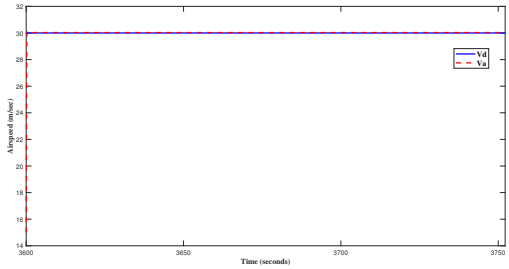

(d) Airspeed tracking

Figure 5.24: Attitude and Airspeed Tracking for Ayat-Torhyloch Way-Point Trajectory

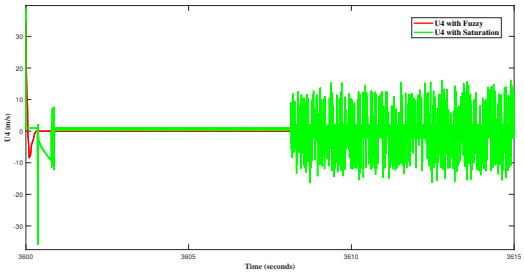

(a) Airspeed control input

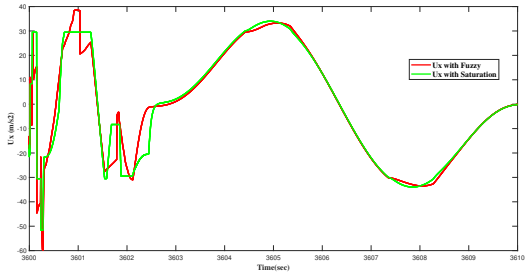

(b) Virtual acceleration commands

Figure 5.25: Chattering in Control Signals for Ayat-Torhyloch Trajectory Tracking

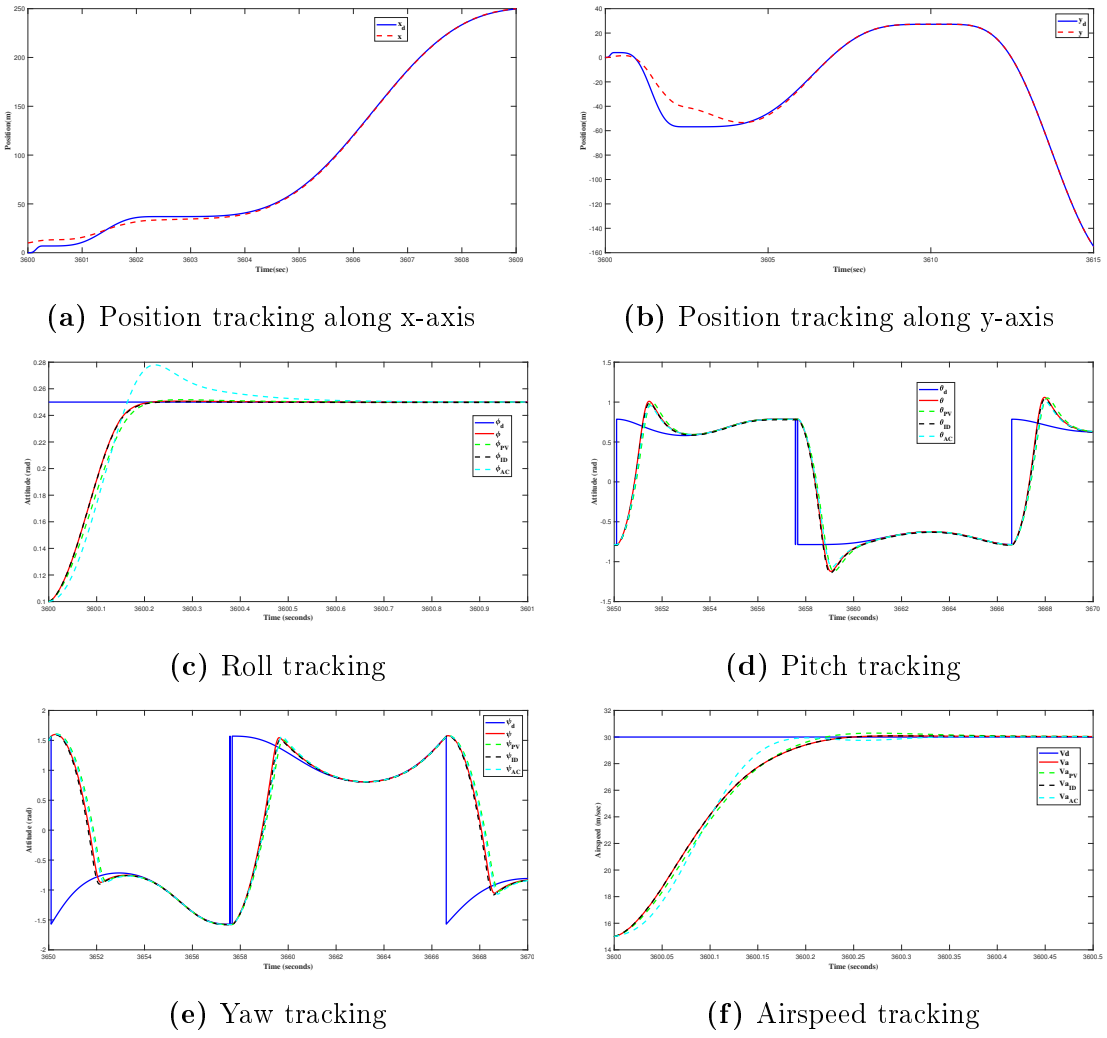

(a) Position tracking along x-axis

(b) Position tracking along y-axis

(c) Roll tracking

(d) Pitch tracking

(e) Yaw tracking

(f) Airspeed tracking

Figure 5.26: Enlargement Views in Ayat-Torhyloch Way-Point Trajectory Tracking (Ayat Reference Position and ϕ, θ, ψ, V_a are nominal values)

To test the performance of the controllers in Ayat-Torhyloch way-point trajectory tracking the model was subjected to ↑20% parameter variation, attitude uncertainty, input disturbances, and actuator dynamics. The total ITAE increased from nominal value by 2.0946%, 1.456%, 0.2703%, and 1.4189% respectively.

From Ayat-Torhyloch simulation results control system saturation is exhibited as expected in fig. 5.24b, and 5.24c in the first four way-points tracking. This is the result of small time allocation for each segment of way-points as discussed in section 5.1.1.

5.2.3.2 Kality-Piazza Simulation Results

The starting reference location is Kality at 2 kilometer altitude with destination Piazza however, only 9 way-points which can be reached within 132.2634 seconds were considered, table D.2. All conditions except (x_d, y_d, z_d) were used as in section 5.2.3.1. Kality was taken as initial location of reference and it's considered that, Kality expressed with coordinate point of (0, 0, 2000), where 2000 indicates the altitude in units of meter.

Table 5.9: ITAE Performance Index for Kality-Piazza Way-Point Trajectory Control Against 20% Increased Parameter Variation (PV), Matched Uncertainty (MU), Input Disturbance (ID), and Actuator Dynamics (AC)

ITAE (10^4)	ϕ	θ	ψ	x	y	z	V_a	**Total**
Nominal	0.0048	7.071	18.5	27.02	8.196	0.0433	2.175	**63.01**
PV	0.0053	7.768	19.75	27.02	8.196	0.0433	2.191	**64.97**
MU	0.0048	7.071	18.5	27.02	8.196	0.0433	2.175	**63.01**
ID	0.0022	7.279	18.62	27.02	8.196	0.0433	2.164	**63.34**
AC	0.0089	7.051	19.46	27.02	8.196	0.0433	2.169	**63.94**

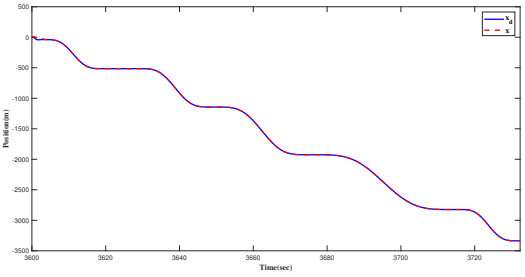

(a) Position along x-axis

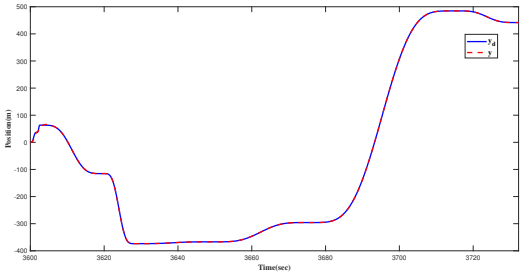

(b) Position along y-axis

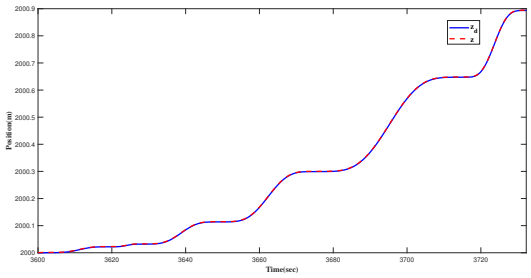

(c) Position along z-axis

Figure 5.27: Kality-Piazza Way-Points Trajectory Tracking (Kality Reference Position)

Table 5.10: Normalizing Gains Kality-Piazza Way-Point Trajectory

Gain:	n_1	n_2	n_3	n_4	n_5	n_6	n_7	n_8
Values:	0.0875	0.03827	0.0860	0.0729	2.983	0.8963	0.0812	0.00751

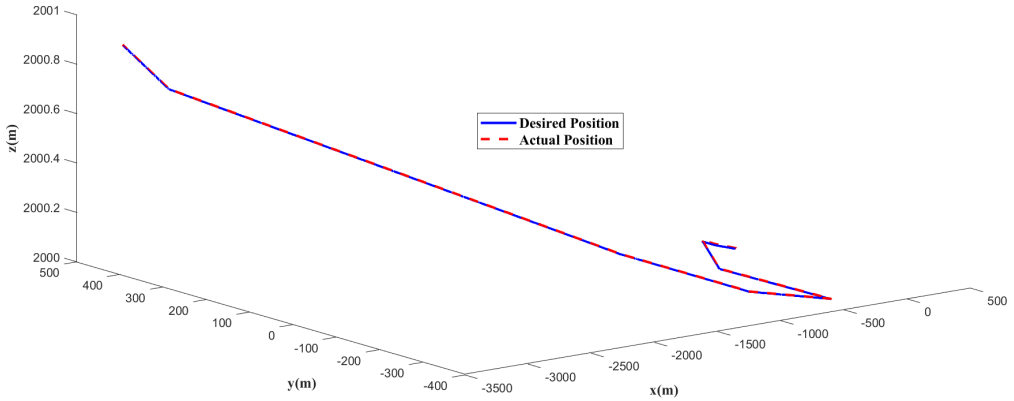

Figure 5.28: 3D Plot of Positions in Kality-Piazza Way-Point Trajectory Tracking

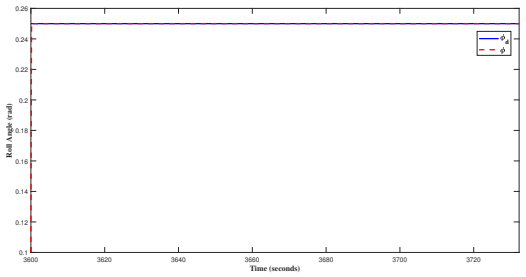

(a) Roll tracking

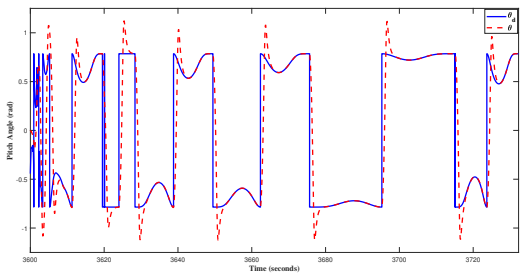

(b) Pitch tracking

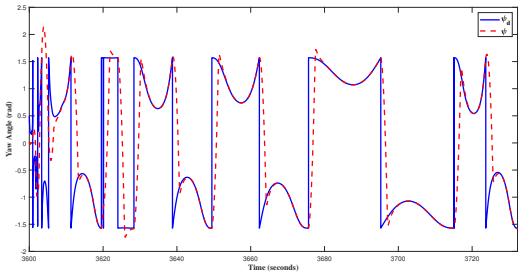

(c) Yaw tracking

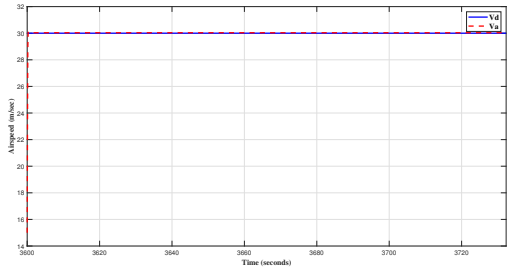

(d) Airspeed tracking

Figure 5.29: Attitude and Airspeed Tracking for Kality-Piazza Way-Point Trajectory

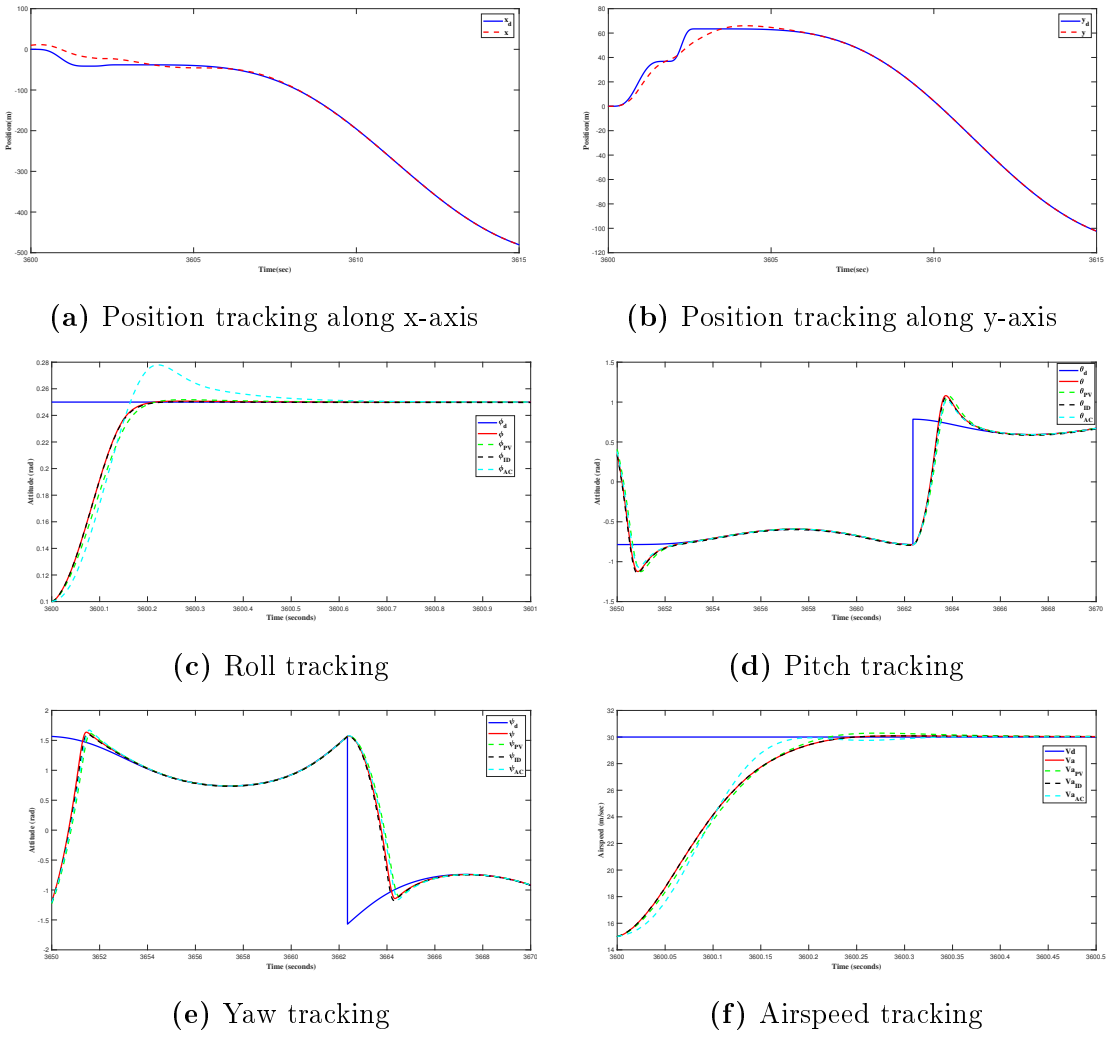

(a) Position tracking along x-axis

(b) Position tracking along y-axis

(c) Roll tracking

(d) Pitch tracking

(e) Yaw tracking

(f) Airspeed tracking

Figure 5.30: Zoomed-in Views in Kality-Piazza Way-Point Trajectory Tracking (Kality as Reference Position of (0, 0, 2000))

5.3 Quantitative Analysis and Description About the Level of Chattering in Control Commands

The level of chattering in SMC can be quantified statistically for different types of control signals. It can be expressed using root mean square (RMS) value as an index. The RMS value of a continuous time signal or a set of values is defined as the square root of the arithmetic mean of the squares of the values. It represents the average power of such a signal over some predefined time. So, RMS is directly related to the energy content of

the chattering or vibration profile of a signal. Keeping this in mind the signal with high value of RMS is expected to have high chattering for the respective signal.

Table 5.11: Chattering performance Index in Helical Trajectory

Control Command	Fuzzy Switching (RMS)	Saturation Switching (RMS)
U_4	0.1058	0.1591
U_x	0.9367	0.9725
U_y	0.185	0.2383
U_z	9.809	9.809

Table 5.12: Chattering performance Index in Ayat-Torhyloch Trajectory

Control Command	Fuzzy Switching (RMS)	Saturation Switching (RMS)
U_4	0.4435	2.075
U_x	13.19	13.42
U_y	11.14	11.43
U_z	9.81	9.81

As it can be seen from tables 5.11, and 5.12 the RMS value in saturation switching is higher than fuzzy switching for the respective control signal. This indicates that chattering is reduced with applying fuzzy switching in SMC. The chattering in altitude control signal, U_z are nearly the same, this is due to the fact that the cubic polynomial in helical trajectory and very small variation of real data along z-axis need relatively low mathematical computation.

Chapter 6

Conclusion and Recommendation

6.1 Conclusion

In this thesis the Newton-Euler based mathematical modeling for FW-UAV and twisting SMC design for tracking desired states were buried effectively. The model exploits high complexity, non-linearity, and coupling between different states. This attribute of the model highly influences the control system. To overcome this muddle twisting SMC was designed relaying on the hypothesis: SMC handles non-linearity, complexity, matched uncertainty, and external disturbances hence, it's robust. And was verified in simulations.

Twisting SMC was outlined to the seven states; $(x, y, z, \phi, \theta, \psi, V_a)$, for tracking the respective desired states. Control system stability was insured through Lyapunove's direct method of stability analysis. PSO was pivot to get the appropriate switching gains of SMC and normalizing gains in fuzzy switching. The algorithm tried to reduce the total ITAE of controlled states based on the initial boundary and it's effective. The fuzzy switching for inertial position and airspeed control were essential for accommodating the robustness and chattering reduction in twisting SMC.

The controllers performance was examined with different set of numerical simulations in different trajectory tracking problems; helical, infinity and real data based minimum snap polynomial. The simulation results in chapter 5 show that the controllers respond well against coupling, non-linearity, 20% parameter variation, matched uncertainty, actuator dynamics, and external input and wind disturbances of limited magnitude.

Tables of ITAE for each state during every set of the simulation indicate that the index was used for reducing the steady state error, overshoot, settling and rise time. The ITAE with no disturbance, uncertainty, parameter variation, and actuator dynamics was taken as the nominal value for each trajectory. And in all cases; uncertainty, parameter variation, disturbance, and actuator dynamics the total ITAE for the controlled states increased within less than 7% as per the respective simulation time for all trajectories.

The FW-UAV control was achieved significantly within practically accepted ranges of values (finite control effort). As it has been seen from fig. 5.5 nominal deflection angles of control surface of aileron(14°), elevator(34°), and rudder(22°) were required, which are in the working ranges of practical control, unity rad. The thrust force generated by the propeller in BF along x-axis was within accepted range. It has an average value of 133 N, which is nearly equivalent to the weight of the FW-UAV 132.5 N. The propeller engine acceleration was also in accepted range. It had maximum values of 10 m/s (376 revolutions per minute) and 30 m/s (1128 revolutions per minute) in helical and level flights respectively.

6.2 Recommendation

The speed of response, reduced steady state error and robustness indicates that the control methodology can be used for other complex and coupled systems. Furthermore; the recommended future works are:

- The FW-UAV was guided on pre-defined trajectories, trajectory preparation was offline assuming existing GPS data of way-point paths. So dynamic path generation is a possible future work for autonomous control.
- Trajectory control wasn't fully autonomous so much of high level control analysis is possible in the future.
- Energy optimal control can be extended for climbing phase trajectories.
- Dynamic gain scheduling between different flight phases could be done.
- Hardware implementation of the designed control system could be done.

References

[1] Elevator (aeronautics). Fixed-wing aircraft flight control surfaces. URL: `https://en.wikipedia.org/wiki/Elevator_(aeronautics)`.

[2] Aileron. Fixed-wing aircraft flight control surfaces. URL: `https://en.wikipedia.org/wiki/Aileron`.

[3] Qinghai Bai. Analysis of particle swarm optimization algorithm. *Computer and information science*, 3(1):180, 2010.

[4] Randal W Beard and Timothy W McLain. *Small unmanned aircraft: Theory and practice*. Princeton university press, 2012.

[5] James Blondin. Particle swarm optimization: A tutorial. *Availaible from: http://cs. armstrong. edu/saad/csci8100/pso tutorial. pdf*, 34, 2009.

[6] Peter Burt and Jo Frew. Crossing a line: The use of drones to control borders. *Drone Wars UK*, 2020.

[7] Luca Carlone, Kasra Khosoussi, Vasileios Tzoumas, Golnaz Habibi, Markus Ryll, Rajat Talak, Jingnan Shi, and Pasquale Antonante. Visual navigation for autonomous vehicles: An open-source hands-on robotics course at mit. *arXiv preprint arXiv:2206.00777*, 2022.

[8] Herman Castaneda, Oscar S Salas-Pena, and Jesús de León Morales. Adaptive super twisting flight control-observer for a fixed wing uav. In *2013 International Conference on Unmanned Aircraft Systems (ICUAS)*, pages 1004–1013. IEEE, 2013.

[9] Belsty Derseh. Particle swarm optimization tuned fractional order sliding mode controller for altitude stabilization and trajectory tracking of agricultural monitoring quadcopter.

[10] STEFANO FARI. Guidance and control for a fixed-wing uav. 2017.

[11] Yufei Guo, Leru Luo, and Changchun Bao. Design of a fixed-wing uav controller combined fuzzy adaptive method and sliding mode control. *Mathematical Problems in Engineering*, 2022, 2022.

[12] Yang Han, Peng Li, and Zhiqiang Zheng. A non-decoupled backstepping control for fixed-wing uavs with multivariable fixed-time sliding mode disturbance observer. *Transactions of the Institute of Measurement and Control*, 41(4):963–974, 2019.

[13] KS Holkar and LM Waghmare. Sliding mode control with predictive pid sliding surface for improved performance. *International Journal of Computer Applications*, 78(4), 2013.

[14] Myung Hwangbo and Takeo Kanade. Maneuver-based autonomous navigation of a small fixed-wing uav. In *2013 IEEE International Conference on Robotics and Automation*, pages 3961–3968. IEEE, 2013.

[15] Aline Ingabire and Andrey A Sklyarov. Control of longitudinal flight dynamics of a fixedwing uav using lqr, lqg and nonlinear control. In *E3S Web of Conferences*, volume 104, page 02001. EDP Sciences, 2019.

[16] Amber Israr, Eman H Alkhammash, and Myriam Hadjouni. Guidance, navigation, and control for fixed-wing uav. *Mathematical Problems in Engineering*, 2021:1–18, 2021.

[17] Yeonsik Kang and J Karl Hedrick. Linear tracking for a fixed-wing uav using nonlinear model predictive control. *IEEE Transactions on Control Systems Technology*, 17(5):1202–1210, 2009.

[18] Mohammad Khalid Khan. *Design and application of second order sliding mode control algorithms*. University of Leicester (United Kingdom), 2003.

[19] Mihret Kochito. Mrac design for a surveillance uav for the detection of water hyacinth.

[20] Jinkun Liu. *Sliding mode control using MATLAB*. Academic Press, 2017.

[21] Roland Siegwart Marco Hutter and Thomas Stastny. Fixed-wing uavs: Dynamic modeling and control. *Autonomous Systems Lab, ETH zurich*, 2, 2017.

[22] JOUAV Product News and Use Cases. Different types of drones. URL: `https://www.jouav.com/blog/drone-types.html`.

[23] A Noth, Samir Bouabdallah, and R Siegwart. Dynamic modeling of fixed-wing uavs. *Swiss Federal institute of technology, version*, 2, 2006.

[24] Wilfrid Perruquetti and Jean Pierre Barbot. *Sliding mode control in engineering*, volume 11. Marcel Dekker New York, 2002.

[25] Abid Raza, Nigar Ahmed, Rameez Khan, and Fahad Mumtaz. Sampled-data higher order sliding mode control of fixed wing uav. In *The Fifth International Academic Conference for Graduates, NUAA*, 2017.

[26] Alex Rocateli and Laura Goodman. Using google earth for mapping and assessing grazeable land. Technical report, Oklahoma Cooperative Extension Service, 2016.

[27] Rudder. Fixed-wing aircraft flight control surfaces. URL: `https://en.wikipedia.org/wiki/Rudder`.

[28] Andra Saicharan Sagar, PD Shendge, and SM Vaitheeswaran. Attitude control of fixed wing uav using multiple sliding surface. In *2016 IEEE 1st International Conference on Power Electronics, Intelligent Control and Energy Systems (ICPEICES)*, pages 1–6. IEEE, 2016.

[29] Joan Serra and Josep Lluis Arcos. Particle swarm optimization for time series motif discovery. *Knowledge-Based Systems*, 92:127–137, 2016.

[30] Thomas J Stastny, Adyasha Dash, and Roland Siegwart. Nonlinear mpc for fixed-wing uav trajectory tracking: Implementation and flight experiments. In *AIAA guidance, navigation, and control conference*, page 1512, 2017.

[31] Vadim Utkin. Discussion aspects of high-order sliding mode control. *IEEE Transactions on Automatic Control*, 61(3):829–833, 2015.

[32] Peng Yan, Zhuo Yan, Hongxing Zheng, and Jifeng Guo. A fixed wing uav path planning algorithm based on genetic algorithm and dubins curve theory. In *MATEC Web of Conferences*, volume 179, page 03003. EDP Sciences, 2018.

[33] Jun Yang, Cunjia Liu, Matthew Coombes, Yunda Yan, and Wen-Hua Chen. Optimal path following for small fixed-wing uavs under wind disturbances. *IEEE Transactions on Control Systems Technology*, 29(3):996–1008, 2020.

[34] Yu-Xin Zhao, Tian Wu, and Gang Li. A second-order sliding mode controller design for spacecraft tracking control. *Mathematical Problems in Engineering*, 2013, 2013.

Appendix A

Plant Model Parameters

Table A.1: Aerosonde UAV Physical Characteristics, [4]

Parameter	**Symbol**	**Value**	**SI unit**
Wing area	S	0.55	m2
Wing span	B	2.8956	m
Aerodynamic chord	C	0.18994	m
Weight	m	13.5	Kg
Payload	-	2	Kg
Inertia along xx	Jx	0.8244	Kg- m2
Inertia along yy	Jy	1.759	Kg- m2
Inertia along zz	Jz	1.8244	Kg- m2
Inertia along xz	Jxz	0.1204	Kg- m2
Max speed	-	40	m/sec
Cruise speed	-	[20,30]	m/sec
Stall speed	-	20	m/sec
Travel range	-	3000	Km
Radio Communication	-	150	Km
Flight Duration	-	30	hr
Propeller swept area	S_P	0.2027	m2
Propeller radius	-	0.254	m
Air density	ρ	1.2682	Kg/m3
Linear speed constant	k_m	80	-
Angular speed constant	k_Ω	0	-
Torque speed constant	K_T	0	-
Force pressure proportionality	C_P	1	-

Table A.2: Table of Longitudinal Aerodynamic coefficients to Aerosonde UAV, [4]

Longitudinal Coeff.	**Value**
C_{l_0}	0.28
C_{d_0}	0.03
C_{y_0}	-0.02338
C_{l_α}	3.45
C_{d_α}	0.30
C_{y_α}	-0.38
C_{l_q}	0
C_{d_q}	0
C_{y_q}	-3.6
$C_{l_{\gamma_e}}$	-0.36
$C_{d_{\gamma_e}}$	0
$C_{y_{\gamma_e}}$	-0.5

Table A.3: Table of Lateral Aerodynamic coefficients to Aerosonde UAV, [4]

Lateral Coeff.	**Value**
C_{Y_0}	0
C_{Y_β}	-0.98
C_{x_β}	-0.12
C_{z_β}	0.25
C_{x_p}	-0.26
C_{z_p}	0.022
C_{x_r}	0.14
C_{z_r}	-0.35
$C_{x_{\gamma_a}}$	0.08
$C_{z_{\gamma_a}}$	0.06
$C_{Y_{\gamma_r}}$	-0.17
$C_{x_{\gamma_r}}$	0.105
C_{Y_p}	0
C_{Y_r}	0
$C_{Y_{\gamma_a}}$	0
C_{x_0}	0
C_{z_0}	0

Appendix B

Rotation Matrices

The rotation sequences from inertial to body frame discussed in chapter 3 are:

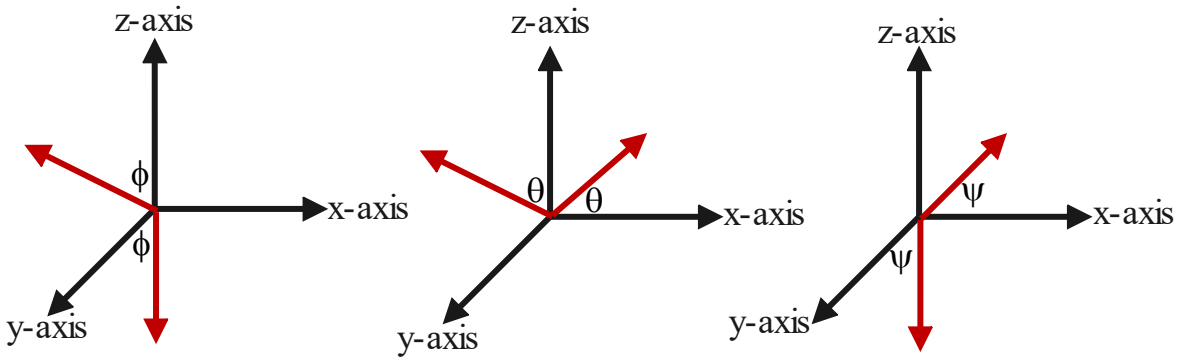

Figure B.1: Right-Handed Rotations in 3D

$$R(\psi) = \begin{pmatrix} c_\psi & s_\psi & 0 \\ -s_\psi & c_\psi & 0 \\ 0 & 0 & 1 \end{pmatrix} \quad R(\theta) = \begin{pmatrix} c_\theta & 0 & -s_\theta \\ 0 & 1 & 0 \\ s_\theta & 0 & c_\theta \end{pmatrix} \quad R(\phi) = \begin{pmatrix} 1 & 0 & 0 \\ 0 & c_\phi & s_\phi \\ 0 & -s_\phi & c_\phi \end{pmatrix} \tag{B.1}$$

$$R_B^I = \begin{bmatrix} c(\psi)c(\theta) & c(\psi)s(\theta)s(\phi) - s(\psi)c(\phi) & c(\psi)s(\theta)c(\phi) + s(\psi)s(\phi) \\ s(\psi)c(\theta) & s(\psi)s(\theta)s(\phi) + c(\psi)c(\phi) & s(\psi)s(\theta)c(\phi) - c(\psi)s(\phi) \\ -s(\theta) & c(\theta)s(\phi) & c(\theta)c(\phi) \end{bmatrix} \tag{B.2}$$

Euler→body rates conversion (vertical line indicates the concatenation of vector).

$$T_I{}^B(\phi, \theta) = ((1,0,0)^T | R(\phi) \circledast (0,1,0)^T | R(\phi) \circledast R(\theta) \circledast (0,0,1)^T) \tag{B.3}$$

$$T_B{}^I(\phi, \theta) = \begin{bmatrix} 1 & s(\phi)t(\theta) & c(\phi)t(\theta) \\ 0 & c(\phi) & -s(\phi) \\ 0 & s(\phi)sec(\theta) & c(\phi)sec(\theta) \end{bmatrix} \tag{B.4}$$

Appendix C

Vector Differential, Force and Moment Equivalents

The time differential in the analysis of aircraft flight motion involves different reference frames. Here the differential of a vector that moves in rotating frame is derived at the other fixed frame, no translation between frames, [10]. Let's define the angular velocity of frame F^B as seen in frame F^B by $\omega_{B/I}$ and take a vector V in F^B by $V^B = V_x i^B + V_y j^B + V_z k^B$, then the vector $\dot{V}$ w.r.t the IF is given by, chain rule, [1].

$$\begin{aligned}\frac{d}{dt}V^I &= \dot{V}_x i^B + \dot{V}_y j^B + \dot{V}_z k^B + V_x \frac{d}{dt} i^B + V_y \frac{d}{dt} j^B + V_z \frac{d}{dt} k^B \\ &= \dot{V}_x i^B + \dot{V}_y j^B + \dot{V}_z k^B + V_x * \omega_{B/I} \otimes i^B + V_y * \omega_{B/I} \otimes j^B + V_z * \omega_{B/I} \otimes k^B \\ &= (\dot{V}_x, \dot{V}_y, \dot{V}_z)^T + \omega_{B/I} \otimes (V_y, V_y, V_z)^T \\ &= \frac{d}{dt}V^B + \omega_{B/I} \otimes V^B\end{aligned} \tag{C.1}$$

The equivalent forces and moments on FW-UAV expressed with equ. C.2 and C.3.

$$\begin{aligned}F_x^B &= \frac{1}{2}\rho V_a^2 S(C_l s_\alpha - C_d c_\alpha) + \frac{1}{2}\rho S_P C_P (k_m^2 \delta_t^2 - V_a^2) - mg s_\theta \\ F_y^B &= \frac{1}{2}\rho V_a^2 S C_Y + mg s_\phi c_\theta \\ F_z^B &= -\frac{1}{2}\rho V_a^2 S(C_l c_\alpha + C_d s_\alpha) + mg c_\phi c_\theta\end{aligned} \tag{C.2}$$

$$\begin{aligned}M_x^B &= \frac{1}{2}\rho V_a^2 S B C_x - K_M k_\Omega^2 \delta_t^2 \\ M_y^B &= \frac{1}{2}\rho V_a^2 C S C_y \\ M_z^B &= \frac{1}{2}\rho V_a^2 S B C_z\end{aligned} \tag{C.3}$$

[1] Symbols are: $*$ - scalar multiplier from the left, $\circledast$ - matrix multiplication, $\otimes$ - vector cross product, V^T - Transpose of the matrix/vector V. ...

Appendix D

Real Data Way-Points

Table D.1: Ayat-Torhyloch Route Way-Points

Way Point	x(m)	y(m)	z(m)	Time(sec)
1	0	0	2000	3600
2	6.9	4	2000	3600.3
3	37	-57	2000.0004	3602.5
4	251.1	27	2000.005	3610.2
5	293.2	-179	2000.0093	3617.2
6	224.7	-228	2000.008	3620
7	81.5	-295	2000.0074	3625.3
8	-29.5	-331	2000.0086	3629.2
9	-206.7	-378	2000.0146	3635.3
10	-412	-456	2000.0297	3642.6
11	-683	-815	2000.0889	3657.6
12	-1007	-1248	2000.2021	3675.6
13	-1220.9	-1992	2000.4286	3701.4
14	-1858.1	-2141	2000.6315	3723.3
15	-2727.7	-2147	2000.9482	3752.2

Table D.2: Kality-Piazza Route Way-Points

Way Point	x(m)	y(m)	z(m)	Time(sec)
1	0	0	2000	3600
2	-41	36.8	2000.0002	3601.8
3	-38	63.4	2000.0004	3602.7
4	-515	-115.3	2000.0220	3619.7
5	-515.3	-373.6	2000.0319	3628.3
6	-1144	-367	2000.1138	3649.3
7	-1926	-295.8	2000.2993	3675.4
8	-2824	484.7	2000.6474	3715.1
9	-3337	441.7	2000.8935	3732.3